

# POLITECNICO DI TORINO

Master's Degree in Electronic Engineering

Master's Degree Thesis

## De-embedding procedure for multi-port networks using thru-reflect-line and thru-reflect-match calibration



**Politecnico  
di Torino**

**Supervisor**

Professor Franco FIORI

*Supervisor's signature*

.....  
.....

**Candidate**

Ivan PORCELLI

*Candidate's signature*

.....

Academic year 2021-2022



*To my family*

# Summary

The context of the present thesis is the measurement of the scattering parameters of a device-under-test (DUT) employing vector network analyzers (VNA).

The de-embedding of the DUT S-parameters from the total measurements that include the test-fixture contribution is investigated in detail. The fixtures are required to physically connect the DUT to the instrument and make the data acquisition possible, but their presence is making the measured S-parameters look completely different from the actual DUT ones. The scope of the present work is to provide a strategy to de-embed the DUT from the total, or fixture-DUT-fixture, measurements. In literature, the techniques to pursue this goal are many and are considering most of the time the two-port case. In this thesis, a simple and effective de-embedding strategy for multi-port measurements is developed.

The most general topic of VNA calibration in S-parameters measurements is investigated first from a mathematical perspective. Then, the most classical state-of-the-art de-embedding strategies are reviewed. These strategies are considering two-port networks, such as filters or amplifiers. An environment able to perform the de-embedding in this classical way is implemented with a MATLAB<sup>®</sup> script, that takes in input the measurements on the calibration structures and provides the DUT S-parameters. These methods are validated in a SPICE environment and by measurements on real devices. The advantages, disadvantages as well as limitations concerning other de-embedding strategies are studied. A criterion for the definition of the calibration structures is developed, considering the working bandwidth and the available reference impedances.

The core of this work is on the extension of the state-of-the-art de-embedding strategies for a more general case. The proposed solution can be applied to a multi-port DUT with an even or odd number of ports. The DUT can be embedded within test-fixtures for which no hypothesis is made on their symmetry or type. The overall strategy can be used in a bandwidth that extends from the ultra-low frequency (ULF) to the GHz range.

After the validation of this de-embedding technique, another one that minimizes the number of built calibration structures and following associated measurements is proposed.



# Acknowledgements

Il candidato desidera ringraziare il relatore di tesi Professore Franco Fiori, anzitutto per aver fornito la possibilità di lavorare su questo problema, oltre che per la sua disponibilità e la sua preziosa guida durante tutto questo percorso. Un ulteriore ringraziamento è dedicato a Michele, Erica e specialmente a Mark, per la sua pazienza infinita, per aver condiviso la sua conoscenza e per la sua illimitata disponibilità quando del supporto si rendeva necessario. Un ringraziamento va alla famiglia, senza il cui sostegno arrivare al termine di questo percorso non sarebbe stato possibile.

# Contents

<b>List of Tables</b>	8
<b>List of Figures</b>	9
<b>0 Introduction</b>	13
0.1 Subject of the thesis work	13
0.2 State of the art	15
0.2.1 Motivation	15
0.2.2 Literature review	18
0.2.3 Position of the work among the literature	24
<b>1 Test fixture de-embedding</b>	27
1.1 Summary	27
1.2 Introduction	27
1.2.1 Microwave circuits	28
1.2.2 Vector network analyzers	33
1.2.3 Removing fixture contribution	44
1.2.4 Port-extension	45
1.3 TRL de-embedding for two-port networks	46
1.3.1 In-fixture calibration	46
1.3.2 Theoretical derivation	47
1.3.3 Limitations of the TRL de-embedding	51
1.3.4 Line standard impedance correction	52
1.3.5 Calculation of the TRL line standard lengths	54
1.3.6 Thru reflect match (TRM) de-embedding for two-port networks	54
1.3.7 Validation of the method	55
1.4 Multi-port de-embedding	71
1.4.1 Theoretical derivation	72
1.4.2 Multi-port TRL	75
1.4.3 Validation of the method: de-embedding of an op-amp S-parameters	76
<b>2 De-embedding on real devices</b>	91
2.1 Introduction	91
2.2 Measurement on a 20 dB attenuator	91

2.2.1	Strategy 1 . . . . .	95
2.2.2	Strategy 2 . . . . .	97
2.3	De-embedding of a low return loss fixture . . . . .	103
2.4	Voltage follower test circuit . . . . .	107
<b>3</b>	<b>Conclusions and future work</b>	<b>115</b>
<b>A</b>	<b>Derivation of the de-embedding algorithms</b>	<b>117</b>
A.1	TRL line length computation . . . . .	117
A.1.1	Three lines . . . . .	119
A.1.2	Four lines . . . . .	119
A.1.3	Use of a higher number of line standards . . . . .	119
A.1.4	Some numeric examples . . . . .	120
A.2	TRL for 2-port networks . . . . .	121
A.3	TRM for 2-port networks . . . . .	126
A.4	multi-port de-embedding . . . . .	129
<b>B</b>	<b>Matlab Code</b>	<b>131</b>

# List of Tables

1.1	Name of the terms of the twelve-term error model [14]. . . . .	41
1.2	Name of the terms of the eight-term error model [14]. . . . .	43
1.3	Error terms of the twelve-error model in function of the eight-term one. . .	44
1.4	Required number of line standard for the TRL de-embedding as the band- width increases. . . . .	51
1.5	Required line standards, computed with equations of appendix A.1. . . . .	62
2.1	Description of the measurements made for the TRM application. . . . .	92
2.2	List of the measurements required for each strategy. . . . .	93
A.1	Line standards required by the TRL. . . . .	120
A.2	Line standards required by the TRL, $\epsilon_{eff} = 3.3$ . . . . .	120
A.3	Line standards required by the TRL, $\epsilon_{eff} = 10.2$ . . . . .	120
A.4	Effect of an additional line standard. . . . .	121

# List of Figures

1	Steps of two-tier calibration. . . . .	18
1.1	N-port representation of a microwave circuit [31]. . . . .	28
1.2	Generator providing power to a load. . . . .	32
1.3	Schematic of a directional coupler. . . . .	34
1.4	Architecture of a one-port VNA. . . . .	36
1.5	Architecture of a VNA for unidirectional two-port measurement. . . . .	36
1.6	VNA with a complete reflectometer on port 1 and port 2. . . . .	37
1.7	VNA with a reference channel put before the switch. . . . .	37
1.8	VNA architectures with four (a) and three (b) ideal reflectometers cascaded with an error network. . . . .	39
1.9	Error model for one-port measurements [14]. . . . .	39
1.10	VNA error adapter terms for the forward (a) and reverse (b) operation [14].	41
1.11	Normalized VNA error adapter terms for the forward (a) and reverse (b) operation [14]. . . . .	42
1.12	Signal flow graph of the eight-term error model [14]. . . . .	42
1.13	Illustration of the de-embedding of a DUT: test fixture effects are removed by moving the reference planes [35]. . . . .	45
1.14	Moving the reference planes for eliminating the fixture contribution. . . . .	46
1.15	Block diagram of a network analyzer measurement of a two-port device [2].	47
1.16	Block diagram and signal flow graph for the Thru connection [2]. . . . .	48
1.17	Block diagram and signal flow graph for the Reflect connection [2]. . . . .	48
1.18	Block diagram and signal flow graph for the Line connection [2]. . . . .	49
1.19	Block diagram and signal flow graph for the Match connection. . . . .	55
1.20	Total, or fix-DUT-fix, simulated structure (symmetric error networks case).	56
1.21	Connection required by TRL algorithm. . . . .	57
1.22	Comparison of the DUT de-embedded scattering matrix and the actual one.	58
1.23	Comparison of the test fixture de-embedded scattering matrix and the actual one. . . . .	59
1.24	Error on the DUT (dashed traces are for no re-normalization). . . . .	60
1.25	Error on the fixture (dashed traces are for no re-normalization). . . . .	61
1.26	Match connection . . . . .	62
1.27	De-embedding effect on measured data. . . . .	63
1.28	Cross-section of the line standard. . . . .	64
1.29	"Thru" standard realized with a physical line. . . . .	65

1.30	Error on the magnitude for DUT and error network. . . . .	66
1.31	Error on the phase for DUT and error network. . . . .	67
1.32	Fix-dut-fix simulated structure (asymmetric error networks). . . . .	68
1.33	Comparison of the DUT de-embedded scattering matrix and the simulated one. . . . .	69
1.34	Error on the DUT. . . . .	70
1.35	De-embedding effect on measured data. . . . .	71
1.36	Cascade of 2N scattering matrices. . . . .	72
1.37	First step of the multi-port de-embedding. . . . .	73
1.38	Second step of the multi-port de-embedding. . . . .	74
1.39	Dut with four ports. . . . .	75
1.40	Schematic representation of multi-port TRL calibration kit. . . . .	76
1.41	Complete system made up of the DUT and three asymmetric fixtures. . . . .	76
1.42	Schematic of a bias tee with idealized elements. . . . .	77
1.43	Schematic of a real inductor. Impedance ( $\Omega$ ) for $L = 1 \mu H$ , $C = 1 pF$ , $R = 100 m\Omega$ . The SRF results around 157 MHz. . . . .	78
1.44	Schematic of a real capacitor. Impedance ( $\Omega$ ) for $L = 100 pH$ , $C = 1 nF$ , $R = 100 m\Omega$ . The SRF results around 500 MHz. . . . .	79
1.45	S-parameters for the initial design of the bias-T. The right one accounts for the inductor parasitics. . . . .	80
1.46	Final design of the bias-T. . . . .	81
1.47	S-parameters when tuning the values of the elements in the bias-T design. . . . .	81
1.48	Schematic for the DUT measurements. On the right, the high frequency network used to model the parasitic elements between the terminals [46]. . . . .	82
1.49	Standards required to obtain the S-matrix of the fixture "2". In the characterization of this fixture, the "reflect" and "match" are one-port measurements. . . . .	83
1.50	"Thru" standards required to obtain the S-matrix of the fixture "1" and "3". . . . .	83
1.51	S-parameters of the fixture "2" compared with directly simulated. . . . .	84
1.52	S-parameters of the fixture "3", obtained by left de-embedding the fixture "2" from the "thru" of them, compared with directly simulated. . . . .	85
1.53	S-parameters of the DUT(1). . . . .	86
1.54	S-parameters of the DUT(2). . . . .	87
1.55	S-parameters of the DUT(3). . . . .	88
1.56	Error on the magnitude and phase for the fixture "2". . . . .	89
2.1	Measured S-parameters of the 20 dB attenuator. . . . .	92
2.2	Schematic representation of the performed measurements. . . . .	93
2.3	Total ( <b>A</b> ) and DUT only S-parameters. . . . .	94
2.4	Comparison between de-embedded DUT and actual one. . . . .	96
2.5	Difference between measured, de-embedded and actual fixtures. . . . .	97
2.6	Fixture 2 de-embedded compared with the measurement. . . . .	98
2.7	Schematic representation of the measurements for fixture 1. . . . .	99
2.8	Fixture 1 de-embedded compared with the measurement. . . . .	100
2.9	S-parameters of the thru connection between the fixtures <b>D</b> . . . . .	101
2.10	Magnitude and phase for the de-embedded DUT S-parameters compared to the actual ones. . . . .	102

2.11	Table 3 from the datasheet of the VNA used. In the bandwidth up to 1 GHz the directivity is of 41 dB. . . . .	103
2.12	Measure of the I-SMA scattering parameters (left) and phase error on the $s_{12}$ parameter between the measured and de-embedded DUT (right). The error is corresponding to the phase shift introduced by the I-SMA in the non-ideal thru connection. . . . .	103
2.13	Capacitor soldered between two female SMA connectors. . . . .	104
2.14	Schematic representation of the thru between fixture "1" and the capacitor. . . . .	104
2.15	Capacitor (blue) and thru (red) scattering parameters. . . . .	104
2.16	Comparison between actual and de-embedded capacitor scattering parameters. . . . .	105
2.17	Error on the magnitude (a) and phase (b) on the de-embedded S-parameters of the capacitor. . . . .	106
2.18	Schematic of the built prototype. . . . .	107
2.19	Second scenario. . . . .	107
2.20	Comparison between de-embedded S-parameters (solid line) and measured one (circles). . . . .	108
2.21	Plot of the acquisition of the S-parameters. . . . .	109
2.22	Comparison of the DUT s-parameters with the fix-dut-fix ones. . . . .	109
2.23	Third scenario. . . . .	110
2.24	Comparison between de-embedded S-parameters (solid line) and measured one (circles). . . . .	111
2.25	Plot of the acquisition of the S-parameters. . . . .	112
2.26	Comparison of the DUT s-parameters with the fix-dut-fix ones. . . . .	112
2.27	Error for the first scenario. . . . .	113
2.28	Error for the second scenario. . . . .	113
A.1	Match standard (a) and set up for $s_{11}$ computation (b). . . . .	126





# Chapter 0

## Introduction

### 0.1 Subject of the thesis work

At the time of writing, different paid software solutions are available on the market for de-embedding the scattering matrix of a device-under-test (DUT) from the fixture-DUT-fixture measurement. As far as the candidate knows, there is no a ready-to-use procedure to perform de-embedding of a multi-port DUT in a coaxial or planar environment, when the S-parameters of the fixtures are not available or cannot be directly measured. A calibration procedure, with the description of how to build a calibration board for the de-embedding of multi-port networks, will be introduced. The algorithm to post-process the measurements acquired with a vector network analyzer will be presented. The goal of this work is to address the problem of de-embedding of the S-parameters of the DUT from its test fixtures, with the following characteristics: *wide bandwidth* (kHz to GHz range), DUT with *even* or *odd* number of ports, *asymmetric* test-fixtures, *minimum number* of required calibration structures. This goal is pursued by extending the algorithms that provide the foundation of the de-embedding problems solution to work in a more general case.

A brief background information to frame the context of this work is now provided. The topic of the de-embedding, which is the subject of this thesis, is of extreme importance during S-parameters acquisition using a vector network analyzer (VNA). In fact, VNAs are measuring RF devices when they are mounted on test fixtures. Test fixtures are most of the times required to connect the DUT to the measurement system. The most classical case is when the network analyzer has a coaxial interface and the DUT is mounted on a printed circuit board (PCB). In this case the PCB traces from the coaxial connector to the DUT pins are representing the test fixtures. Another example of fixture could be an on-board bias tee used to provide an RF and DC path to the input of an amplifier mounted on a PCB. In this case, the amplifier S-parameters needs to be de-embedded from the contribution of the non-ideal bias tee. Test fixtures are then expensive, difficult to design, and cloud the performance of the DUT. Due to their inevitable presence, the measured S-parameters look nothing like the DUT ones. Even if it might sound easy, de-embedding hides difficulties which are related to the techniques to make it done, which

can be difficult to understand and implement.

Recently, the topic of the de-embedding has gained importance. The recent (2020) *IEEE Standard for Electrical Characterization of Printed Circuit Board and Related Interconnects at Frequencies up to 50 GHz* [1] describes the requirements for designing test fixtures and removing test fixture effects, to ensure the quality of the DUTs measured data. The standard provides the rigorous definitions of the most important terms that will be used in this thesis. The *test fixture* is the "structure used to connect test equipment cables, typically coaxial, to a non-coaxial DUT. The fixture is in many cases constructed using a PCB". The *de-embedding* is the "process by which the characteristics of the test fixture are mathematically removed from the measured data, leaving the characteristics of the DUT" [1]. To isolate the DUT the de-embedding requires extra measurements of devices called standards. Another term which in this field is often used interchangeably with the de-embedding is the *calibration*, defined as "The process of characterizing the systematic errors of the instrument by measuring known devices (calibration standards)". The following chapters will intend these terms exactly as described above, to avoid confusion as can easily happen for this topic.

This thesis is organized as follows. In the next paragraph, a literature review on the de-embedding and calibration topic is provided, acknowledging the previous work on which this thesis is building. At this point, it will be clear when the contribution provided by the thesis begins. The thesis goal concerning the solutions found in literature is then better explained, along with what will and will not be included. Chapter 1 will mainly provide the description of the theory and the mathematical foundations for the de-embedding. First, the concept of microwave circuits and scattering parameters are recalled. Then, the VNAs are described, with an emphasis on their calibration. The short-open-load-thru (SOLT) calibration technique is studied, as it is the one most used nowadays by VNAs. The reasons for this focus are two: first, in any case, calibration has to be performed before making any measurement with the instrument; second, de-embedding theory is based on the common concepts that calibration uses. For instance, both calibration and de-embedding use standards to calculate a model of the test fixture called an error box. The error box or fixture model is then mathematically used to de-embed the DUT. The theory, procedure, and calculations of the main methods available in the literature to perform de-embedding are described. An important focus is made on how to choose the standards. The advantages and limitations of these techniques are investigated. It will be shown that de-embedding algorithms are mathematically perfect, and in a simulation environment can remove complex test fixtures without errors. After this prior analysis, it begins the new contribution of this thesis. It is described a de-embedding procedure that can be applied for multi-port networks, extending the basic literature de-embedding techniques. First, the basic idea and mathematical foundations are provided, then this procedure is validated in a simulation environment. Also, one practical example of fixture design is provided. It is considered the design of a bias tee made with discrete off-the-shelf components that will be used to measure the S-parameters of an active device. Chapter 2 is dedicated to the measurements on real devices, to validate the theory. This is a very important part, as it will be shown that in the real world, de-embedding without error is not achievable. This is often due to poor measurements and standards that are different from the fixtures that are actually connected to the DUT. In any case, measurements will confirm a good accuracy

provided by the de-embedding methods defined in the previous section. Appendix A presents the mathematical derivation of the expressions that are described in chapter 1. Appendix B is instead providing the MATLAB<sup>®</sup> codes corresponding to the de-embedding strategies described in this thesis.

## 0.2 State of the art

Before the acknowledgment of the previous work on which this thesis is built and the review of the state-of-the-art solutions, it is first described of the context in which this work is framed.

### 0.2.1 Motivation

The field of radio frequency (RF) and microwave engineering is fast-growing nowadays, due to the diffusion of wireless communication systems. The RF system bandwidth is covering frequencies between the range going from 30 MHz to 3 GHz, while the microwave range is extending from 3 GHz to 300 GHz [2]. Microwave technologies are indispensable in a good part of areas of electronics. Cellular systems work with microwave transceivers and digital systems have clock frequencies in the GHz range, requiring distributed circuit concepts for their design. The components (lumped or distributed) involved in the design of these systems, and many others working at microwaves, are characterized by measurement instruments that are functioning at these frequencies, and in particular by vector network analyzers. Microwave measurements are not only important for design applications, but also for the electromagnetic interference (EMI) and compatibility (EMC) fields. The EMC field is of growing importance. Electromagnetic pollution has increased over the last decades, due to the diffusion of wireless communication systems, in which are working modules such as BlueTooth, GSM, wifi, etc. that need to coexist in the same system without causing interference. Moreover, integrated circuits are used in any given electronic system. Due to the growing complexity and scaling, they are becoming directly affected by radiated disturbances themselves since they can work as effective antennas. PCB tracks used to interconnect them can also collect EMI disturbances and conduct the resulting voltages and currents which can be of amplitude comparable to the nominal signals. To comply with regulations, ICs must be able to not generate too much emission while keeping the immunity to disturbances. The trend is to pursue a PCB design oriented to minimize EMC problems, along with the design of analog IC which achieve a higher degree of immunity against EMI. For measurements in this field, handled spectrum analyzers and VNAs have been used extensively in the past few years.

A traditional electrical measurements laboratory includes instruments like oscilloscopes, multimeters, and signal generators. At high frequencies, where the wavelength is no more very large with respect to the system dimensions, the measurement procedures change drastically. The lumped elements approximation of classical circuit theory is no more valid: microwave components will act as distributed elements, where the voltages and currents will change along their physical dimensions. This makes it impossible to measure (or even define) voltage or current at a particular point. At these frequencies, it

results in easier to sample forward and backward power waves that are propagating along a transmission line. For linear networks, the DUT is viewed as an N-port, where a port is defined as "a structure by which a test signal is applied to or observed at the interface of the DUT" [1]. The DUT can then be described by relating forward and reflected power waves at the ports through the scattering matrix: a matrix of complex quantities that quantifies how RF energy propagates through a multi-port network, at specified frequencies. Each component of the matrix is corresponding to the ratio of the reflected power wave to the incident power wave for a given pair of input ports and output port, and at a given frequency. The instrument that makes this measurement is the VNA.

### Vector network analyzer

The vector network analyzer is the most important instrument in microwave measurements today. Regarding this thesis work, it will be used to measure the S-parameters that are used to perform the de-embedding of the DUT from its test fixtures.

The VNA revolutionized the design of high-frequency components, allowing the measurement of the properties of transmission, reflection, and impedance. In the 1940s and 1950s, the construction of a Smith Chart required hours of hand-tuned measurements to be done one frequency at a time. The network analysis, that is the measurement of amplitude and phase of power waves, was made by combining a swept scalar analyzer for magnitude measurements with a manual point-by-point reconstruction of the phase [3]. By the 1960s, thanks to the advantages of semiconductor technology, samplers based on semiconductor diodes allowed the sampling of waveforms enabling relative amplitude and phase measurements on signals. In 1967 HP introduced the 8410 network analyzer, consisting of a benchtop system based on multiple boxes, which allowed the comparison of amplitude and phase of two waveforms up to 12 GHz. The first VNA including error-correction mathematics was the HP 8542 (1970). In 1984, the 26 GHz HP 8510 VNA was introduced. It included error correction, time domain, and pulse measurements. It allowed to choose the frequency range (down to 45 MHz) and the number of points, with an IF fixed to 20 MHz. The S-parameters were already popular and the VNA was provided by a display able to put transmission, reflection, and impedance into a single representation that could be in the format of a rectangular graph or smith-chart. This instrument became the metrology standard for microwave systems measurements. In the 1990s, wireless device deployments had a boom due to the diffusion of communication networks, and VNAs (once an R&D tool) start becoming a device used in industry. In 2001 came out the first four-port network analyzer (E5071A). In successive years an effort was put into developing systems with higher port counts ( $N$ ), with a particular eye on calibration. As will be explained in chapter 1, traditional calibration requires more than  $N^2$  connection steps. Eventually, the required connection steps became  $N$  [3]. New systems can ensure a broader dynamic range. The dynamic range is the range of power that the system can measure, which is limited by  $P_{max}$  (the highest input power level the system can measure) and  $P_{min}$  (the minimum input power level measurable, which depends on the noise floor of the system). The dynamic range can be improved by reducing the IF system bandwidth. Since 2010, new trends are going towards the measurement of multi-port devices in less time without sacrificing accuracy. Recently, nonlinear vector network analyzers (NVNA)

are being developed, bringing the VNA evolution moving into the measurement of non-linear features of the components. The biggest disadvantage of traditional S-parameters is that they are only defined for linear networks [2]. Nonlinear component characterization is important to describe active devices. Nonlinear X-parameters are the extension of S-parameters to work into large-signal conditions and can be measured by NVNA.

The vector network analyzer is the most important test equipment in today's microwave measurements, and it is probably the most advanced one. In this thesis, the emphasis is given on the VNA calibration (or error correction), which concept is now briefly described.

## Calibration

As reported in [4], the calibration procedure is mandatory to obtain correct measurements from the VNA. Strictly speaking, calibration means to shift the reference planes at which the S-parameters are measured up to the intended location (i.e. the DUT interface). If a coaxial cable is connecting the VNA ports to the DUT interface, its presence will have an impact on the magnitude and phase making the measurement quality unacceptable. By calibration, the measurement system is characterized to remove the systematic error from the measurement result. From the 1980s on, with the introduction of computer-controlled VNAs, calibration algorithms were included in the firmware for one or two-port cases. The most popular calibration routines are the thru-reflect-line (TRL), short-open-load-thru (SOLT) and line-reflect-match (LRM). These routines consist of two steps: in the first one known standards are measured. The second step uses these measurements to make computations from this acquisition to correct the result. The meaning of the term *calibration* in the VNA measurement context is different from the usual meaning. Typically, most electronic measurement equipment is calibrated by measuring with other equipment with lower uncertainty, typically once a year. The calibration of the equipment is certificated by the application of a calibration label. In the context of VNAs, there is at least another meaning for the term *calibration*. The calibration concept in its traditional meaning is still valid, as the VNA can be sent for calibration every year. For VNAs, another form of calibration that is performed in-site each time the system is set up for making measurements is referred to with a more proper term: *vector error correction*. This process is used to characterize systematic error which is present when making measurements using the VNA. This calibration is needed because of two reasons:

- Imperfections of the VNA hardware (for example the finite directivity of the internal directional coupler).
- Presence of cables connected externally to which reference planes shall move past. For example, the cables that have to be connected to the front-panel VNA connectors before making the measurements possible.

The calibration will remove the effect of these impairments, to obtain high quality DUT measurements. The *vector* prefix is used as the error correction is both for amplitude and phase response of the data acquired from the VNA. [5].

## De-embedding

De-embedding and calibration are similar concepts, but their scope is different. Consider figure 1.

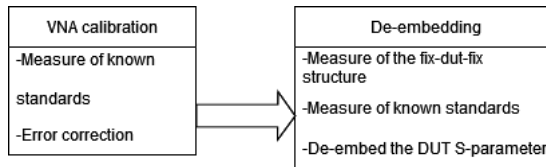


Figure 1: Steps of two-tier calibration.

To obtain the DUT S-parameters, it is possible *first* to calibrate in a common coaxial-SMA environment and *second* to measure the combination of the fixture and DUT (fix-DUT-fix) [6]. If the fixture can be characterized, its effect can be removed and the DUT response is de-embedded from the measurements. This process consisting of two steps is referred to as two-tier calibration [7]. Each step moves the reference planes of the measurements closer to the DUT. This requires two sets of calibration standards: the first one is made by high accuracy and repeatable typically coaxial standards, the second one instead uses insitu calibration standards (that provide more precise characterization in a particular environment). The fixture characterization can be accomplished in different ways as will be discussed in later sections. The best possible way to de-embed the fixture is to determine the exact s-parameters of the fixture [6]. Usually, direct measurement is not possible. The approaches for the second-tier could be to model the fixture in an EM structure simulator to estimate the S-parameters, port-extension techniques to characterize loss or fixture delay, or time-domain gating applied to a 2x-thru back-to-back connection of the fixtures [1].

### 0.2.2 Literature review

#### Early VNA calibration

At the end of the 1960s, it was introduced the first calibration techniques for automated vector network analyzers measurements. These techniques worked for two-ports measurement systems, and were already introducing the concept of "error network" [8]. The concept of "error network" is still used in recent works to gather the imperfections of the VNA and the effect of test cables in two fictitious two-port networks in the front of the DUT. This work [8] and those available at that time (like [9, 10]) were developed to remove the test-set errors occurring in the measurements of linear two-ports. The systematic measurement errors were represented using imaginary two-port error networks, described by their S-parameters. These parts have to be removed from the measured quantities as they are not related to the DUT. These deviations stems from stochastic (like noise) and drift (like environment variations) causes but also from the instrument itself. Random uncertainties cannot be removed but can be estimated. The latter contribution (from the instrument effects) is repeatable and thus corresponds to a systematic error that can be

removed by calibration, which is made by measuring known standards and applying the correction. In [9] the calibration standards for two-port network calibration were a sliding load (which reflection is measured in three different positions), a short, an offset-short (a shorted coaxial line one-quarter wavelength long at mid band), and a thru (a direct connection of the two-ports). Then, reflection and transmission measurements are made on the DUT and an iterative process solves for its scattering parameters  $s_{11}$ ,  $s_{12}$ ,  $s_{21}$ ,  $s_{22}$  using the coefficients acquired during calibration standard measurements. These solutions were using numerical and iterative computations, making the calibration of a VNA a long process. The sliding load was used to simulate a match termination. It is difficult to realize a perfect matched load. A sliding load is a transmission line with a load that can slide along it: this provides a constant magnitude reflection coefficient and the slider can change the phase angle according to a  $2\beta l$  variation. By measuring the device for different load positions it is obtained a circle on the complex plane, which center point is the coefficient to be used in the calibration process.

In [11] a simpler technique for directly solving for the scattering parameters of a two-port DUT was developed. This method used the calibration standards of an open, a short, a match (each at both VNA ports), and a thru. The "error network" was still the same as [8], containing eight terms (the four S-parameters for each fictitious error network), but the expressions of the two-port DUT S-parameters were obtained for the first time in an explicit form. This has proven to save a lot of computer time, as the DUT S-parameters have to be determined at every frequency.

The following works provided a variation on the calibration standard used and on the error network model. In [12] closed-form formulas and procedures were provided for two cases: two known standards and a sliding termination and one known standard and two sliding terminations. For the calibration, the magnitude and the initial phase angle needed not to be known but were required to be constant. Closed-form expressions were derived to calibrate the VNA for one-port measurements, requiring in this case just only one error network [5] described originally as a matrix of four S-parameters. In [9] turned out that for one-port reflection measurements the error correction required only three terms from the error network:  $s_{11}$ ,  $s_{22}$  and the product  $s_{12}s_{21}$ . This three-term error model is still nowadays the most common representation of one-port calibration for reflection measurements [5]. For one port devices, the reflection measurement can be performed without having a complete two-port calibration.

While one-port calibration uses the three-term error model, regarding two-port measurements the situation is different. There are alternative error adapter models which were developed, that mainly depends on the VNA internal architecture. Nowadays, the most used calibration routines use the twelve-terms or the eight-terms error model.

In [13] it was considered a two-port error model that included leakage paths: this contribution, that increases the number of error terms in the error model, is nowadays typically neglected (as the crosstalk of modern VNAs is lower than the noise floor of the instrument) but in the earlier VNA systems it was shown to improve the measurement accuracy. It is proven that an increased measurement accuracy from the VNA can be acquired by improving the hardware or the calibration standards, but also by increasing the number of error coefficients included in the error model [5]. This number depends on the hardware topology of the VNA, in particular the number of measurement receivers,



the number of ports, and the required accuracy. Nevertheless, this work proposed for the first time a twelve terms error model that is still used today. Two different VNA architectures represented with different flow-graph models were considered. The first is the one considered in [9], where the reverse measurements of the DUT S-parameters are made by manually reversing the DUT to allow measurements in both directions. The error model for the forward ( $s_{11}$ ,  $s_{12}$ ) and reverse ( $s_{21}$ ,  $s_{22}$ ) direction measurements were considered. For each direction, the error model includes six terms, reducing to only five if the leakage term (also called crosstalk one) representing the signal leakage between the measurement ports is not considered.

The 12 error terms are computed using the expressions of [9], but the DUT S-parameters are now found by a direct (non-iterative) computation according to the expressions in [13]. The second one considers the presence of a coaxial switch that automatically allows the reverse measurement of the DUT S-parameters, as in modern VNAs. Again, the calibration standards were a short, an offset-short, and a match termination simulated by a sliding load. The error terms included in the model are ten if the leakage in both directions is considered, or eight if it is neglected (like [8]). The DUT S-parameters are obtained directly from formulas accounting for the 8(10) error terms.

Summing up, at this point the models used for calibration were the following. For one-port measurements, a three-term error model still used today was introduced. For two-port measurements, it was not initially provided a unified error model for different test sets. It was available an eight-term one, ten if crosstalk is included, that modeled the bidirectional measurement of two-port devices. It required the knowledge of all four S-parameters for each fictitious error adapter put in front of the DUT. For unidirectional DUT measurements, a five error term (six when considering crosstalk) model was developed. Other models made a distinction between the presence of a coaxial switch inside the VNA architecture or not. The twelve terms error model [13] unified the description of the measurement system and became the standard model for the description of two-port VNA [5], being independent of the test set configuration. This model is still in use today to calibrate modern VNAs, under the name of SOLT (short-open-load-thru) or TOSM (thru-open-short-match) calibration.

In general, the calibration procedures developed so far are using two categories of models. The ones employing twelve error terms (made with two separate six terms models in forward and reverse measurements), aim to model the error network according to the internal architecture of the VNA. As will be described, the error terms are directly linked to the characteristics of the reflectometers (or directional coupler) that made up the VNA. This model can be adapted to different VNA architectures providing in this way a unified error model. The models employing eight error terms were initially based on a purely mathematical approach, as they are represented by two imaginary error boxes with their respective  $\mathbf{S}$  matrices. These models can be used directly only on VNAs with a complete reflectometer on each port. Each model needs different calibration measurements. The calibration based on the twelve terms error model requires six independent measurements for each direction [13] (or five each if crosstalk is neglected). As seen from the cited works, the most common one-port standard used are the open, the short, and the load (for each port), and a thru for the two-port connection. Those one-port standards were the most commonly used as they provide good separation of variables. For the eight-term



error model, it will be seen now that they rely more on two-port standards rather than requiring precise open, short, or load reflection coefficients.

In general, the eight-term and the twelve-term model can be both applied and be interchangeable only for the VNA architectures with a reflectometer on each port [4]. For VNA with only one reference coupler, the twelve-term model can be used.

### **Calibration with the seven-term error model: self-calibration**

The equations that represent the link between the DUT and measured S-parameters of a DUT embedded in the twelve terms error model are particularly complicated. The eight terms error model can provide advantages in the calibration procedure. The big advantage of this representation is that the system can be modeled as a cascade of three two-port networks, the DUT and the two error boxes representing the instrument imperfections. In this way, the vector error correction can be applied using *transmission parameters* [14]. Another advantage is that to perform a full two-port calibration, only seven out of eight error terms are required [5]. To distinguish these new approaches from the old eight-term error models, these are called seven-terms models. The basis of this new approach was first proposed in 1975, when a work carried in the "Analog Techniques Department" of *Tektronix* [15] described a new procedure for system calibration in automated S-parameters measurements, employing this concept. This procedure used only three standards, the "through", the "short" and the "delay". A closed-form mathematical expression for calibration was found. "Through" indicates the "thru" connection, the "short" an ideally perfect short termination at both ports, and the "delay" a 50  $\Omega$  line of arbitrary length and unknown propagation constant connected between the two instrument ports. An algorithm to obtain directly the S-parameters of these networks was provided. For the first time, the procedure employed the conversion of the scattering parameters into transmission parameters. With respect to previous works, the standards do not include mechanical parts as the sliding loads, but it requires a good accuracy in the "delay" standard characteristic impedance and on the short quality. In any case, the most important feature of the standards is that for the first time they were not required to be fully known. In fact, in this work, the knowledge of the "delay" standard propagation constant is not required. The techniques that use the seven terms error model to calibrate the VNA with standards only partly known are called *self-calibration* techniques.

### **Thru - reflect - line calibration**

Probably the most important self-calibration technique is the TRL (thru-reflect-line) calibration, first introduced by G.F. Engen and C.A. Hoer in 1974 [16]. It used the seven-term error model to calibrate the VNA. The only one-port standard used is the "reflect" one, which can be only partially known. The two-port standards are the "line" one (a transmission line of known impedance and partially known propagation constant) and the "thru". This feature is possible thanks to the redundancy of measurement results. Another peculiarity of the TRL is that it is the only technique that employs a distributed standard (the line) to fix the characteristic impedance of the system. This fact made it possible to achieve measurement traceability using well-defined air-isolated line standards [5]. The

TRL calibration is used when classical standards like open, short, load cannot be realized (for example when measuring devices with non-coaxial interfaces). The TRL can work for higher frequencies than the SOLT, as the accuracy of the SOLT calibration depends on the accuracy of its standards, which inevitably degrades when the frequency increases. After the TRL was introduced, many other self-calibration techniques came out, in particular the TRM (thru-reflect-match). This strategy replaces the line standard, which is a two-port one, with two measurements of one-port standards, the "match". This and other self-calibration techniques, using the seven-term error model, such as the LRM (line-reflect-match), SOLR (short-open-load-thru), LRRM (line-reflect-reflect-match), QSOLT (quick-short-open-load-thru) are providing flexibility regarding the type of standards (e.g. coaxial or wafer-level, known or partially known), the frequency range, speed, cost, and accuracy.

The TRL calibration (and all the other self-calibration techniques) can be applied for VNAs that have four reflectometers, described with the seven-terms error model. However, the TRL provides flexibility, as it can still be used on cheaper VNAs with only three reflectometers under the variation of "TRL\*" [17]. In the same way, also the LRM\* is available. The TRL\* calibration results in the same twelve-terms error model as the SOLT. This allows the extension of the TRL to the three reflectometers VNA, however, it cannot correct for the change in the impedance of the switch when it is thrown between the forward and reverse directions. The result is that the source and load match get averaged for each port. All the self-calibration techniques can work for a twelve-term model description (three reflectometers) assuming that the VNA port matches are the same when making measurements in the forward or the reverse direction. This fact is never true, as the match of the source and load changes when the switch is thrown. Since the source and load match are not corrected, SOLT can provide the most accurate calibration since it can perform a full twelve-term error correction for three receivers VNA, and the TRL\* is used when the SOLT standards are not available [17]. Instead, for VNA with four receivers, the TRL technique can correct this changing port match [18]. The TRL\* assumes a perfectly balanced test set architecture. The TRL\* is used in VNAs that have three measurement receivers, instead of the SOLT calibration, when it's difficult to have precise one-port standards.

In conclusion, the TRL\* determines the parameters of the seven-term model, but they can be transformed into the error terms of the twelve error model. The source match and load match, however, cannot be computed.

### **Multi-port calibration**

More recently have been developed VNAs with four, eight, and even twelve ports. The need for VNAs with a greater number of ports is due to the benefits in terms of measurement time and data post-processing time that is gained when making a single measurement per DUT. It is possible to measure multi-port DUTs with a two-port VNA, but this requires to make multiple measurements to be combined to produce the desired result. Of course, the calibration of a multi-port VNA has to be addressed. The most important techniques are described in [19]. The multi-port calibration techniques are still based on the TRL and SOLT for two-port systems.

## De-embedding of the DUT S-parameters

A different topic from the calibration is the de-embedding. The need for de-embedding is having growing importance nowadays. Traditionally, RF and microwave components have been designed with a coaxial interfaces. Their direct measurement is possible once the VNA, which has a coaxial interface, gets calibrated with one of the state-of-the-art techniques. Modern systems are providing higher component integration and lower manufacturing cost [20]. Expensive coaxial interfaces are being replaced with designs that use PCB and surface mount technologies (SMT). The problem is then to measure the performance of these components with the coaxial interface measurement system. A test fixture is required to interface the DUT placed on a PCB with the VNA. As a consequence, the DUT characterization requires removing the test fixture contribution from the measurements.

The problem of de-embedding is different from the calibration, as the latter aims to correct for the systematic error introduced by the imperfections of the test equipment. Nevertheless, they are strictly linked, and it's possible to find a mathematical equivalent between these two topics. A DUT embedded in a test fixture can be represented as the cascade between three networks [20]: the left fixture, the DUT itself, and the right fixture. This representation is equivalent to the eight-term error model used for VNA calibration. In the same way, the VNA calibration can be viewed as a de-embedding of the correct measurement from the error boxes. The model can contain also two additional terms, the crosstalk ones. They are usually not included in the fixture model as they are not a source of an error, unless when measuring DUT with very large insertion loss (on the order of the test fixture isolation).

The de-embedding techniques found in the literature fall into different categories [21, 22]: *modeling*, *direct measurement*, and *in-fixture calibration* (also called two-tier calibration). The mathematics used to de-embed the fixture is common to each of these techniques, instead, the difficult part of the problem is to determine the scattering parameters that describe the test fixture. The object of this thesis work is the last technique.

Modeling-based de-embedding is based on creating a model of the test fixture S-parameters. The approach to this problem strongly depends on the type of the test fixture. The simplest case is when the fixture can be modeled as a lossless transmission line, of matched impedance and electrical length. In this case, de-embedding is made by shifting the reference planes [2] after the VNA has been calibrated at the ends of the test cables, correcting the phase of the measured S-parameters. Modern VNAs can make this correction real-time, using the *port extension* feature [20]. If the test fixture is more complicated, the port extension leads to inaccurate results. Usually, this is the case, as at least the coaxial transition to the PCB is part of the test fixture to model. In this situation, 2D or 3D electromagnetic simulators can be employed, but the accuracy of the results will depend on the accurate modeling and description of the fixture (material and physical dimensions). This approach is better applied for test fixtures that are quite simple, due to the cost and complexity of electromagnetic modeling.

The de-embedding based on direct measurement requires test equipment able to measure the fixture on which the DUT is mounted. In practice, it requires expensive and dedicated test equipment (such as an RF probe). This is the strategy that provides the

highest accuracy [6].

The approach of in-fixture calibration, or two-tier calibration, is employed in this work. The in-fixture calibration, or calibration on board, requires to realize calibration standards on the test board. It uses the conventional SOLT or TRL calibration approach. While this solution implies a more complex test board, it has the advantage to remove the test fixture effect using a more accurate method than the modeling. To apply an in-fixture calibration, it is required a PCB that is used as a calibration board, where the standards of the SOLT or TRL are fabricated. This de-embedding strategy requires the creation of an in-fixture calibration kit. Then, the calibration algorithms used for VNA calibration can be adapted for the de-embedding of the DUT measurements. The most effective solution for SMT components is to realize a TRL-TRM calibration kit [6]. The reason is that the standards need not to be characterized, unlike SOLT, fitting better for on-board calibration. The kit consists of a PCB on which the standards of the thru, reflect, match, and line are realized. This set of standard is measured and the data is used to compute the scattering parameters of the fixture. Then, the measurements made at the plane where the VNA is calibrated are exported and processed, to de-embed the DUT. To examine the de-embedding response in real-time, it has been proved that is possible to include the test fixture S-parameters in the error terms (twelve or eight) used by the VNA for calibration [20]. In this case, is the VNA that performs all the de-embedding computations.

### 0.2.3 Position of the work among the literature

The procedure to perform a de-embedding with in-fixture calibration is available in the literature for two-port networks. Some examples can be found in [23, 24, 25]. These two works show the implementation of the TRL calibration on a PCB on which SMD components are mounted. The interface with the VNA is possible thanks to female SMA connectors that are soldered on the board. The first work considers two symmetrical fixtures (or error networks), consisting of a microstrip transmission line with a series SMD capacitor. The error networks connected to the correct calibration standards are replicated on a second board. Due to their symmetry, the open short and load standards are just created for one error network. The calibration standards are measured and the correction is applied in real-time by the VNA, through the correction of the error terms of the calibration. The S-parameters of a two-port DUT, a low pass filter, are extracted from the total measurement. In [24], the calibration structure to de-embed a bandpass DUT is placed on the same board of the DUT, to have a better accuracy. In [25], a solution is proposed to account for the finite length of the thru standard. Another work [26] is performing the de-embedding realizing the SOLT standard onboard. In this case, the calibration is improved by providing to the VNA software the model of the open termination, the most critical one, providing a fringe capacitance value.

Other than the SOLT and TRL, other techniques have been developed for the de-embedding [1]. For two-port DUTs, a new technique is the "2x-thru" [27]. The most important advantage consists in the fact that de-embedding is performed using just one standard made up by the back-to-back connection of the two fixtures: this structure

is called "2x-thru". The technique allows the computation of the complete fixture S-parameters, unlike the de-embedding with the normalization technique. However, the "2x-thru" de-embedding has some disadvantages. First, it requires the acquisition of the S-parameters of the calibration structure with a large frequency span, starting close to DC, and high resolution to achieve better results since it performs time-domain computations to characterize the fixture. Second, this technique provides accurate de-embedding only when the test fixtures are transmission lines, without discontinuities [28]. A similar de-embedding strategy is known as the "1x-Reflect" [1]: this does not require a separate de-embedding calibration structure as it uses DUT test fixture itself to compute the error model. To apply this technique, it's required that the DUT is removable. In any case, it has the same limitations as the "2x-thru" method.

Considering the available research, the most accurate method for de-embedding a DUT from a general error network is the TRL/TRM. This strategy is the chosen one for this thesis.

Regarding multi-port de-embedding, in literature are not available many research papers. The most general one is [29]: it is provided a strategy to de-embed a DUT from  $N$  fixtures. The considered case is taking a DUT embedded within three identical fixtures made by a microstrip line. The technique requires the knowledge of the scattering parameters of the fixtures, which were obtained using a "2x-thru" calibration. However, there is no indication on how to realize a calibration board if the error networks are asymmetrical or are not consisting of simple transmission lines. This is showing a research gap that this work is trying to fill. The point is to determine which calibration structures to realize, which measurements to make and which math to apply when the DUT is embedded in more than two different error networks.

The work presented in this thesis will describe how to realize a calibration board to de-embed  $N$ -ports DUTs from its test fixture, starting from the classical TRL and TRM strategies.



# Chapter 1

## Test fixture de-embedding

### 1.1 Summary

This chapter is dedicated to providing a rigorous and complete description of the calibration procedure that will be used for the de-embedding of multi-port DUTs. First, it will provide a short description on the characterization of microwave circuits with the scattering parameters. Then, it will be provided a detailed description of the error models used for VNA calibration. After describing the need for the de-embedding for in-fixture measurements, the strategies of modeling and direct measurement are quickly reviewed. Then it will be described the two in-fixture calibration techniques proposed in this work, the TRL and the TRM. They are first analyzed for the case of two-ports DUT, in the case of symmetric and unsymmetric test fixtures. A mathematical, as well as a simulation (SPICE) approach, is used to investigate on their characteristics. After this, the concept of multi-port de-embedding is introduced by extending the two-port de-embedding to work for  $2N$  and  $2N + 1$  networks. It will be described the calibration structure used to apply TRL and TRM to an  $N$ -port DUT. This approach is validated in a simulation environment. At the end of this chapter, it is provided a step-by-step procedure required to de-embed the DUT.

### 1.2 Introduction

Nowadays vector network analyzers (VNA) are one of the most advanced measurement systems that are used at microwaves. They are primarily used to measure the scattering parameters of microwave circuits. The scattering parameters are used to characterize microwave circuits using the concept of traveling waves [30]. A review of the description of  $N$  port networks with scattering parameters is now provided.

### 1.2.1 Microwave circuits

#### N-port analysis

Considering an electrical network, made up by the interconnection of electric elements connected to a generator, the surrounding space internally or externally these elements is home to electromagnetic fields. Maxwell's equations and constitutive relationship of mediums are describing the distribution of the electric and magnetic fields. In principle, to fully describe a circuit, the solution of these equations to determine the field distribution is required. However, to determine the current and voltage of the individual circuit elements it is sufficient to work with a lumped-parameter model. Circuit theory employs this model to provide the equations of N-pole elements without taking into account the electromagnetic field in space. The lumped-parameter model can simplify the description of the spatially distributed physical elements that made up the electrical network. The assumption under which this model is valid is that the physical dimension of the electrical network has negligible size compared to the wavelength of the electric signals that interest it. These circuits operating at low frequency are described using Kirchoff voltage and current laws and the impedance concept of circuit theory. As the operating frequency increases, these techniques can't be applied as they are for microwave circuits. As explained in [2], basic circuit concepts can be adapted to describe microwave problems of practical interest. This operation is welcome since it is much easier to describe a microwave network employing the familiar concepts of lumped-element analysis than to solve Maxwell's equation: this solution is made possible by adopting the concept of microwave circuit. In addition, usually, the knowledge of the electromagnetic field in all the points in space is way more information than needed for the design or analysis of a microwave circuit. Most of the time, we are only interested in how the voltage, current, and power at the externally available terminals of the network are related. As reported in [31], we define a microwave circuit as a "region of space confined by perfectly conducting walls, enclosing an EM field and connected to the external space by N transmission lines", as depicted in figure 1.1. At each line, we define a reference plane  $T_i$  sufficiently distant from the circuit such that only the dominant propagation mode is present, which can be described in terms of equivalent voltages and currents. The volume that encloses the distributed-element circuit can be represented as an N-port network.

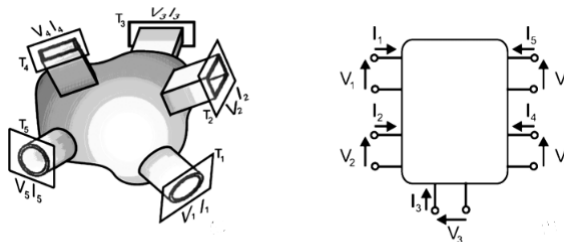


Figure 1.1: N-port representation of a microwave circuit [31].



### Matrix representation

A microwave circuit with  $N$  apertures can be represented as an  $N$ -port network [31]. To completely characterize a linear circuit, the relationships between the  $2N$  voltages and currents at each port are employed and linked to each other by parameters that are extracted by measurements under specific conditions. This procedure will lead to a matrix description of the network. These parameters are then used to completely describe the electrical behavior of the network even when the source and load conditions change with respect to the ones used for the measurements. The most employed parameters are briefly described in the following sections.

**The impedance matrix** The impedance matrix  $\mathbf{Z}$  of the  $N$ -port network relates the voltages and currents:

$$\begin{bmatrix} V_1 \\ V_2 \\ \vdots \\ V_N \end{bmatrix} = \begin{bmatrix} Z_{11} & Z_{12} & \cdots & Z_{1N} \\ Z_{21} & Z_{22} & \cdots & Z_{2N} \\ \vdots & & & \vdots \\ Z_{N1} & \cdots & \cdots & Z_{NN} \end{bmatrix} \begin{bmatrix} I_1 \\ I_2 \\ \vdots \\ I_N \end{bmatrix} \quad (1.1)$$

Each element  $Z_{ij}$  can be found as:

$$Z_{ij} = \left. \frac{V_i}{I_j} \right|_{I_k=0 \text{ for } k \neq j} \quad (1.2)$$

The  $Z_{ij}$  element is found by driving the port  $j$  with a current source  $I_j$  and computing the ratio  $V_i/I_j$  with other ports loaded with an open circuit.

**The admittance matrix** The admittance matrix  $\mathbf{Y}$  of the  $N$ -port network relates the voltages and currents:

$$\begin{bmatrix} I_1 \\ I_2 \\ \vdots \\ I_N \end{bmatrix} = \begin{bmatrix} Y_{11} & Y_{12} & \cdots & Y_{1N} \\ Y_{21} & Y_{22} & \cdots & Y_{2N} \\ \vdots & & & \vdots \\ Y_{N1} & \cdots & \cdots & Y_{NN} \end{bmatrix} \begin{bmatrix} V_1 \\ V_2 \\ \vdots \\ V_N \end{bmatrix} \quad (1.3)$$

Each element  $Y_{ij}$  can be found as:

$$Y_{ij} = \left. \frac{I_i}{V_j} \right|_{V_k=0 \text{ for } k \neq j} \quad (1.4)$$

The  $Y_{ij}$  element is found by driving the port  $j$  with a voltage source  $V_j$  and computing the ratio  $I_i/V_j$  with other ports loaded with a short circuit.

**The scattering matrix** The main problem of  $\mathbf{Y}$ ,  $\mathbf{Z}$ , and other similar representations such as  $ABCD$  and  $h$  parameters is that at microwave frequencies it is difficult to measure total current or voltage. Open-circuit and short-circuit conditions are difficult to

be created above 300 MHz, since after a displacement of  $\frac{\lambda}{4}$  an open becomes a short. Furthermore, active devices employed in amplifiers have to deliver power to avoid oscillations (instability), and this can't happen when the load is an open or a short. At high frequency, power, reflection coefficient, gain, and loss are easy measured, so a matrix representation that employs these familiar quantities is desirable. S-parameters deal with incoming and outgoing waves at the network ports. While voltages and current can't be measured directly, this is not true for the amplitude and phases of the waves that travel along the transmission lines connected to the N ports, which can easily be measured [31]. Forward waves are the ones traveling towards the network, while the ones coming from the network are called reflected waves. Considering the microwave circuits in figure 1.1, the forward and reflected waves at each reference plane  $T_i$  are defined as:

$$a_i = \frac{V_i + Z_{0i}I_i}{2\sqrt{Z_{0i}}} = \frac{V_i^+}{2\sqrt{Z_{0i}}} \quad (1.5)$$

$$b_i = \frac{V_i - Z_{0i}I_i}{2\sqrt{Z_{0i}}} = \frac{V_i^-}{2\sqrt{Z_{0i}}} \quad (1.6)$$

The scattering matrix expresses the outgoing power waves  $b_i$  as linear functions of the incoming ones  $a_i$  [31]. In this way, they provide a complete description of the N-port network (and can be converted to other matrix parameters, if needed):

$$\begin{cases} b_1 = s_{11}a_1 + s_{12}a_2 + \dots + s_{1N}a_N \\ b_2 = s_{21}a_1 + s_{22}a_2 + \dots + s_{2N}a_N \\ \vdots \\ b_N = s_{N1}a_1 + s_{N2}a_2 + \dots + s_{NN}a_N \end{cases}$$

The S-parameters are defined when the characteristic impedances of the lines connected to the ports are determined: the set of values  $Z_{0i}$  (all considered to be real <sup>1</sup>) is also called the reference impedance, and the value of the S-parameters depend on the choice of it. Usually, the reference impedances are chosen to be all equal to 50  $\Omega$ . Each term of the matrix is computed in the following way:

$$s_{ij} = \left. \frac{b_i}{a_j} \right|_{\substack{a_1=a_2=\dots=a_n=0 \\ a_j \neq 0}} \quad (1.7)$$

---

<sup>1</sup>In the most general case the reference impedance can be complex (as in the case of lossy lines or lumped elements circuits), resulting into  $Z_R = R_R + jX_R$ . In this case,  $a = \frac{V + Z_R I}{2\sqrt{R_R}}$  while  $b = \frac{V - Z_R^* I}{2\sqrt{R_R}}$  [2]. The reflection coefficient can be found as:  $\Gamma_L = \frac{b}{a} = \frac{V - Z_R^* I}{V + Z_R I} = \frac{Z_L - Z_R^*}{Z_L + Z_R}$ . With this definition of the forward and reflected power waves, the concept of scattering matrix can be applied also to lumped-elements circuits, when no transmission lines are present. However, only in the latter case  $a$  and  $b$  are quantities representing the actual waves that are propagating along the lines.

So  $s_{ij}$  is computed by evaluating the ratio between the power wave coming out of port  $i$  and the one going into port  $j$ , when no other wave is incident on the remaining ports, condition that is met by closing them on a termination equal to the respective characteristic impedance  $Z_{0i}$ . This is the only conditions that guarantees that no power is reflected from each port towards the network, making  $a_i = 0$ .

**Physical meaning of the scattering parameters and incident and reflected waves** . The scattering parameters  $s_{ij}$  are related to power traveling through the network. The incident and reflected waves  $b_i$  and  $a_i$  have the dimensions of  $\sqrt{W}$ , and they are defined such that their square of the magnitude ( $|a_i|^2, |b_i|^2$ ) is representing power ( $W$ ) that is traveling in the forward or backward direction.

To show this concept, the power delivered to the load connected at the end of a transmission line is considered. In particular, the total voltage and current on a transmission line with characteristic impedance  $Z_0$  can be written in terms of forward and backward voltage waves as:

$$V = V_0^+ + V_0^- \quad (1.8)$$

$$I = \frac{1}{Z_0}(V_0^+ - V_0^-) \quad (1.9)$$

Where the net power delivered to a load is written as:

$$\begin{aligned} P_L &= \frac{1}{2} \Re(VI^*) = \frac{1}{2Z_0} \Re(|V_0^+|^2 - V_0^+V_0^{-*} + V_0^{+*}V_0^- - |V_0^-|^2) = \\ &= \frac{1}{2Z_0} (|V_0^+|^2 - |V_0^-|^2) = P^+ - P^- \end{aligned} \quad (1.10)$$

So  $P_L$ , the average power delivered to the load, is obtained as the difference between the incident and reflected powers [2]. This result can also be applied when  $Z_0$  is complex (lossy line) or when does not exist a transmission line between a generator and a load<sup>2</sup> by the definition of the incident and reflected power waves  $a$  and  $b$ , linked through a generalized reflection coefficient, the scattering matrix. In fact, the voltage and current are expressed in terms of power waves amplitude  $a_i$  and  $b_i$ :

$$V_i = (a_i + b_i)\sqrt{Z_{0i}} \quad (1.11)$$

$$I_i = \frac{(a_i - b_i)}{\sqrt{Z_{0i}}} \quad (1.12)$$

Considering the power transfer between a source  $E$  with internal impedance  $Z_0$  that is chosen as the reference impedance for the scattering parameters and a load  $Z_L$  (as depicted in figure 1.2):

---

<sup>2</sup>In this case  $a$  and  $b$  waves are not representing physical traveling power waves.

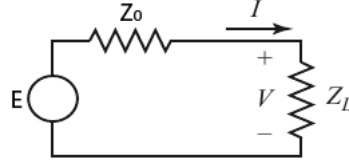


Figure 1.2: Generator providing power to a load.

$$\begin{aligned}
 P_L &= \frac{1}{2} \Re(VI^*) = \frac{1}{2} |V|^2 \Re\left(\frac{1}{Z_L^*}\right) = \frac{1}{2} \frac{|Z_L|^2}{|Z_0 + Z_L|^2} |E|^2 \frac{R_L}{(R_L^2 + X_L^2)} \frac{2Z_0}{2Z_0} = \\
 &= \frac{|E|^2}{4Z_0} \frac{2Z_0 R_L}{(R_L^2 + X_L^2) + X_L^2} = |a|^2 \frac{2Z_0 R_L}{(R_L^2 + X_L^2) + X_L^2}
 \end{aligned} \tag{1.13}$$

Where the last equality comes from:

$$a = \frac{1}{2\sqrt{Z_0}} (V + Z_0 I) = \frac{1}{2\sqrt{Z_0}} E \tag{1.14}$$

In maximum power transfer condition  $Z_L = Z_0^*$ :

$$P_L \Big|_{Z_L=Z_0^*} = P_{Av} = \frac{1}{2} |a|^2 \tag{1.15}$$

So the available power of the generator connected to port  $i$  is expressed as  $P_{Av,i} = \frac{1}{2} |a_i|^2$ .

Now, considering the difference between  $|a_i|^2$  and  $|b_i|^2$ :

$$\begin{aligned}
 \frac{1}{2} (|a_i|^2 - |b_i|^2) &= \\
 &= \frac{1}{2 \cdot 4Z_0} (|V|^2 + Z_0 V I^* + Z_0 I V^* + Z_0^2 |I|^2 - |V|^2 + Z_0 V I^* + Z_0 I V^* - Z_0^2 |I|^2) = \\
 &= \frac{1}{4Z_0} (Z_0 V I^* + Z_0 I V^*) = \frac{1}{4} (V I^* + I V^*) = \frac{1}{2} \Re(V I^*) = P_L = P_i^+ - P_i^-
 \end{aligned} \tag{1.16}$$

The equation above is representing the net power delivered to the load as the difference between the incident and reflected powers [2], and the quantities  $a_i$  and  $b_i$  can be regarded as *power waves*. The average power delivered to the load is the difference between the powers of the incident and reflected power waves. When  $Z_L = Z_0^*$  there is no reflected wave ( $b_i = 0$ ), and the power delivered to the load is the generator's available power.

The physical meaning of the scattering parameters can be investigated by applying the definition of them.

Considering the diagonal elements of the matrix:

$$s_{ii} = \frac{b_i}{a_i} \Big|_{a_1=a_2=\dots=a_n=0, a_i \neq 0} = \frac{V_i - Z_0 I_i}{V_i + Z_0 I_i} \Big|_{a_1=a_2=\dots=a_n=0, a_i \neq 0} = \frac{Z_i - Z_0}{Z_i + Z_0} \Big|_{a_1=a_2=\dots=a_n=0, a_i \neq 0} \tag{1.17}$$

So the term  $s_{ii}$  is the reflection coefficient seen looking into port  $i$  with all the other ports closed on their reference impedance, to make  $a_j = 0$ . Considering that  $|a|^2$  and  $|b|^2$  have the meaning of forward and backward power waves,  $|s_{ii}|^2 = \left. \frac{|b_i|^2}{|a_i|^2} \right|_{a_1=a_2=\dots=a_n=0, a_i \neq 0}$  is representing the ratio of the power reflected from port  $i$  to the power available at port  $i$ .

For the elements outside the diagonal:

$$s_{ij} = \left. \frac{b_i}{a_j} \right|_{a_1=a_2=\dots=a_n=0, a_j \neq 0} = \left. \frac{V_i - Z_0 I_i}{V_j + Z_0 I_j} \right|_{a_1=a_2=\dots=a_n=0, a_j \neq 0} = \left. \frac{2V_i}{E_j} \right|_{a_1=a_2=\dots=a_n=0, a_j \neq 0} \quad (1.18)$$

So the term  $s_{ij}$  is the transmission coefficient between port  $j$  (input) and  $i$  (output), with all the other ports closed on their reference impedance.  $|s_{ij}|^2 = \left. \frac{|b_i|^2}{|a_j|^2} \right|_{a_1=a_2=\dots=a_n=0, a_j \neq 0}$  is representing the ratio of the power delivered to the load on port  $i$  to the available power of the source connected at port  $j$ , also called the transducer power gain.

## 1.2.2 Vector network analyzers

The vector network analyzer (VNA) is the instrument that can measure the S-parameters of microwave devices, both in magnitude and phase. This is done by measuring the incident and reflected waves at each port of the device under test (DUT) while providing the required input signal at the different ports. It is a stimulus and response system, with one RF source and multiple measurement receivers. A very simple description of the components that made up a VNA is reported in [4]:

- One (or more) continuous wave sources with controllable frequency. It is implemented as a continuous wave synthesizer (CW): a pure sinusoidal tone that is swept over a broadband.
- Directional couplers for discriminating between the incident and reflected waves at the ports are representing a key component of a VNA. They are three-port devices that separate the incident wave from the reflected wave while a small portion of the forward wave is coupled out.
- One or more receivers to take the incident and reflected waves, performing down-conversion to IF for processing.
- An IF section and digitizer to process the converted wave amplitudes into a form useful for display.

### Directional coupler

The directional coupler is the most important passive component in the microwave measurement field: it is the device that can separate the incident and reflected waves [4]. The four-port directional coupler is schematized in figure 1.3.

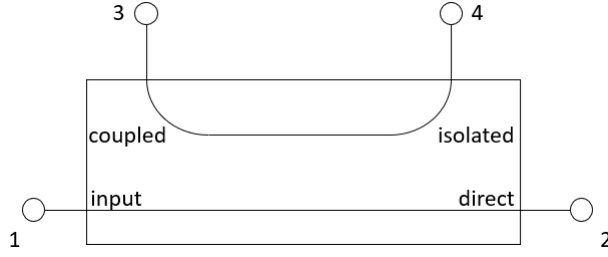


Figure 1.3: Schematic of a directional coupler.

The scattering matrix of a *reciprocal* and *symmetrical* directional coupler is the following [4]:

$$\begin{bmatrix} s_{11} & s_{12} & s_{13} & s_{14} \\ s_{21} & s_{22} & s_{23} & s_{24} \\ s_{31} & s_{32} & s_{33} & s_{34} \\ s_{41} & s_{42} & s_{43} & s_{44} \end{bmatrix} = \begin{bmatrix} \rho_1 & l_1 & k & \iota \\ l_1 & \rho_1 & \iota & k \\ k & \iota & \rho_2 & l_2 \\ \iota & k & l_2 & \rho_2 \end{bmatrix} \quad (1.19)$$

The diagonal terms represent the matching ( $\rho_1 \simeq \rho_2 \simeq 0$ ) and the terms  $l_1$  and  $l_2$  are the losses of the *main line* (between ports 1 and 2) and the *coupled line* (between ports 3 and 4). For simplicity it's possible to consider  $l_1 \simeq l_2 \simeq l$ . The scattering matrix of the directional coupler becomes the following:

$$\begin{bmatrix} s_{11} & s_{12} & s_{13} & s_{14} \\ s_{21} & s_{22} & s_{23} & s_{24} \\ s_{31} & s_{32} & s_{33} & s_{34} \\ s_{41} & s_{42} & s_{43} & s_{44} \end{bmatrix} = \begin{bmatrix} 0 & l & k & \iota \\ l & 0 & \iota & k \\ k & \iota & 0 & l \\ \iota & k & l & 0 \end{bmatrix} \quad (1.20)$$

The term  $k$  is called the *coupling factor* and  $\iota$  is the *isolation factor*.

The most important use of a directional coupler is when it works as a **reflectometer**, a device capable of separating the incident and the reflected waves on a device under test. Let's consider a load with reflection coefficient  $\Gamma = \frac{a_2}{b_2}$  connected to the direct port, the isolated port connected to a matched termination  $Z_0$ , a power meter with the same impedance connected to the coupled port, and the input port connected to a source  $E_0$  with internal impedance  $Z_0$ . It's possible to write:

$$\begin{cases} b_3 = ka_1 + \iota a_2 \simeq ka_1 \\ b_4 = \iota a_1 + ka_2 \simeq ka_2 \end{cases} \quad (1.21)$$

The last equality stems from considering  $\iota \simeq 0$ . Since  $b_2 = la_1$  it results:

$$\begin{cases} b_3 = ka_1 = \frac{k}{l}b_2 \\ b_4 = ka_2 = k\Gamma b_2 \end{cases} \quad (1.22)$$

The reflected waves at ports 3 and 4 are proportional to the reflected and incident waves at port 2. This can be used to measure the reflection coefficient  $\Gamma$ . In fact:

$$a_1 = \frac{V_1 + Z_0 I_1}{2} = \frac{E_0}{2} \quad (1.23)$$

$$P_{meter} = \frac{Z_0 |I_4|^2}{2} = \frac{|b_4|^2}{2Z_0} = \frac{|k|^2 |\Gamma|^2 |b_2|^2}{2Z_0} = \frac{|k|^2 |\Gamma|^2 |l|^2 |a_1|^2}{2Z_0} = \frac{|k|^2 |\Gamma|^2 |l|^2 |E_0|^2}{8Z_0} = P_{max} |\Gamma|^2 \quad (1.24)$$

The power  $P_{max}$  is the power measured by the power meter when a load with  $|\Gamma| = 1$  (short or open) is connected. After  $P_{max}$  is measured, the magnitude of the reflection coefficient of the load connected to the direct port can be obtained as:

$$|\Gamma| = \sqrt{\frac{P_{meter}}{P_{max}}} \quad (1.25)$$

It is noted that even if the directional coupler is ideal and only the magnitude of the load reflection coefficient is being measured, a calibration by connecting a one-port standard is already required. Real reflectometers have a source and isolated impedances different from  $Z_0$  (mismatch error) and are asymmetrical (the s-parameters are not close to the ideal ones). This system can be extended for the measurement of the phase of the reflection coefficient. The phase measurement can be theoretically done in the analog domain, but the best results are obtained when this operation is done digitally [32]. The goal is to measure the phase shift between two signals at microwave frequencies,  $x_1 = A_1 \cos(\omega_R t + \theta_1)$  and  $x_2 = A_2 \cos(\omega_R t + \theta_2)$ . Since they can't be directly digitized, they first need to be downconverted by a mixing operation with a local oscillator ( $\omega_{LO}$ ) to an intermediate frequency (IF). The phase shift between two signals is kept after this operation.

$$\begin{aligned} y_1 &= A_1 \cos(\omega_R t + \theta_1) A_{LO} \cos(\omega_{LO} t) = \\ &= \frac{A_1 A_{LO}}{2} (\cos((\omega_R + \omega_{LO})t + \theta_1) + \cos((\omega_R - \omega_{LO})t + \theta_1)) \end{aligned} \quad (1.26)$$

$$\begin{aligned} y_2 &= A_2 \cos(\omega_R t + \theta_2) A_{LO} \cos(\omega_{LO} t) = \\ &= \frac{A_2 A_{LO}}{2} (\cos((\omega_R + \omega_{LO})t + \theta_2) + \cos((\omega_R - \omega_{LO})t + \theta_2)) \end{aligned} \quad (1.27)$$

These signals have an high-frequency component and a low-frequency one (at the frequency difference). The latter is called the *downconverted* signal. The important point is that the phase difference between these two ( $\theta_1 - \theta_2$ ) is the same as the original signals  $x_1$  and  $x_2$ , even if they are now at a very low frequency (kHz range) suitable to be digitized. The phase difference is determined by digital processing [32].

A one-port VNA is realized by combining a directional coupler used as a reflectometer, an RF source, the down-converter, and the ADC for the digitalization. This structure is reported in figure 1.4.

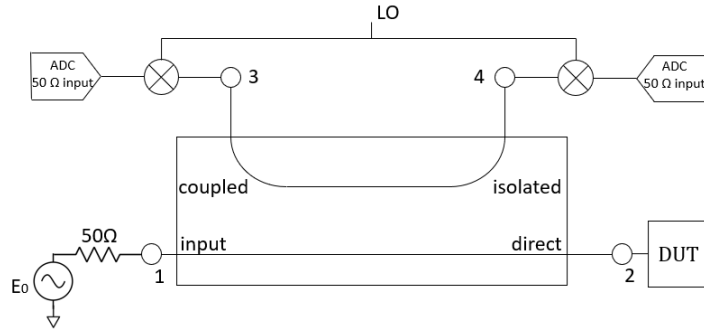


Figure 1.4: Architecture of a one-port VNA.

This arrangement is able to measure the magnitude and phase of the DUT reflection coefficient. In fact  $b_3 = ka_1$ ,  $b_4 = ka_2 = k\iota\Gamma a_1$  from which:

$$\begin{cases} \left| \frac{b_4}{b_3} \right| = |\Gamma\iota| \\ \angle \frac{b_4}{b_3} = \angle b_4 - \angle b_3 = \angle \Gamma - \angle \iota \end{cases} \quad (1.28)$$

Knowing  $\iota$ , again by calibrating the system with a known  $\Gamma$ , it's possible to obtain the DUT reflection coefficient in both magnitude and phase. To allow for transmission and reflection measurements, the system is arranged as in figure 1.5.

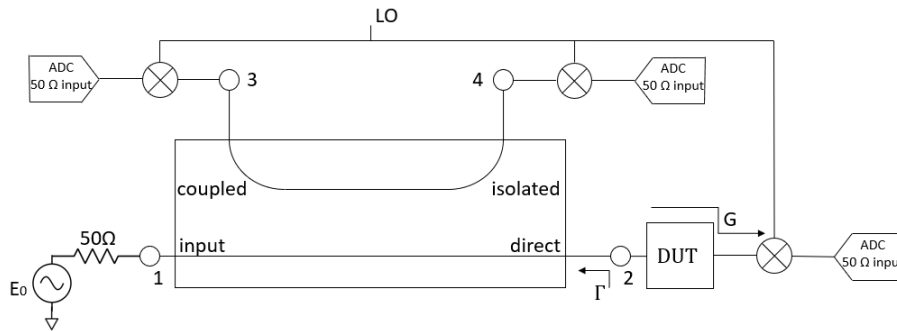


Figure 1.5: Architecture of a VNA for unidirectional two-port measurement.

This arrangement can provide the measurement of the  $s_{11}$  and the  $s_{21}$  of the DUT. These measurements are referred as *forward* diirection. To measure  $s_{12}$  and  $s_{22}$  (*reverse* direction) the DUT has to be manually turned. Early VNAs used this structure, as there are research papers describing their calibration [13].

### VNA architecture for vector error correction

In this section, it is presented the architecture of nowadays two-port VNAs, from the point of view of vector error correction (or calibration). To measure the S-parameters of



the DUT without manually reversing it, two reflectometers along with an RF switch are used. The most common architectures are the following (figure 1.6 and figure 1.7).

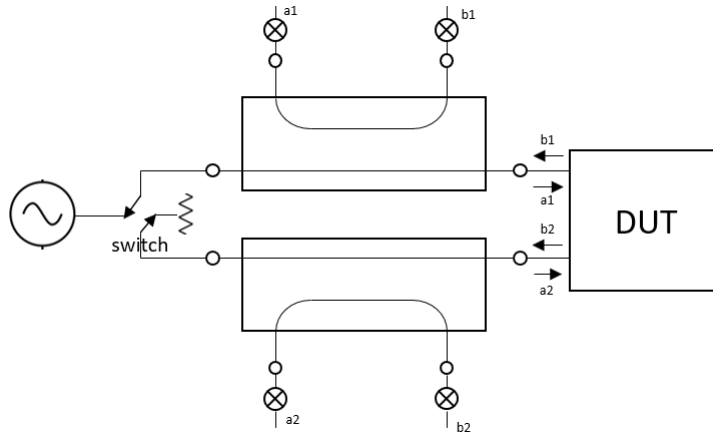


Figure 1.6: VNA with a complete reflectometer on port 1 and port 2.

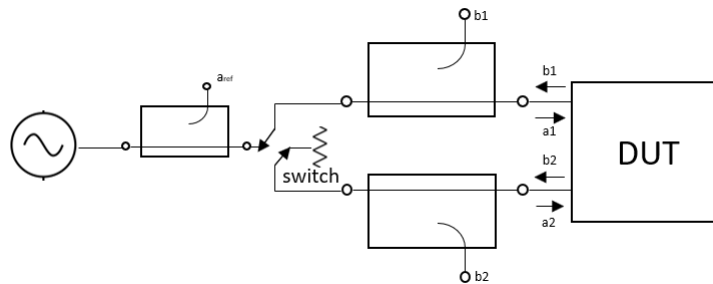


Figure 1.7: VNA with a reference channel put before the switch.

The error models used for calibration are different according to the VNA architecture. The first one (figure 1.6) has a complete reflectometer on both ports. This architecture can be calibrated using a seven-term error model, with a self-calibration technique. The second one (figure 1.7) is a less expensive configuration: it uses fewer components by putting the reflectometer for the reference signal before the RF source switch [14]. This model does not allow the use of modern calibration techniques, and it is calibrated using a twelve-term error model. Self-calibration techniques are possible but do not correct for the switch imperfections, as will be described.

### VNA calibration

Today VNAs are used to capture S-parameters over a broad frequency range starting from KHz up to millimeter waves. To provide meaningful measurements, a VNA requires a calibration procedure which is mandatory due to the enormous systematic error caused by working at microwave frequencies, where the components into play are distributed.

For example, test coaxial cables used to probe the DUT will introduce a systematic phase shift and attenuation that greatly affect the measurements: this error has to be corrected to avoid jeopardizing the accuracy of the results. For performing accurate measurements, there's the need to calibrate the test system. By calibration is intended the mathematical procedure that quantifies imperfections in the test systems applying the correction to move the reference plane of the test system. Network analyzer vector error correction, or calibration, is based on the measurement of known electrical standards, such as through, open circuit, short circuit, and precision load impedance [33].

Calibration means removing imperfections from the test system [34]. Imperfections include systematic errors that are caused by the non-idealities of test equipment and test setup: if these do not change in time, they can be characterized through calibration and be compensated during the measurement process. The DUT is connected to the network analyzer ports via a test fixture that may consist of coaxial cables and adapters or other coaxial components. But the test fixture is not part of the DUT so its contribution must be removed by the calibration. An elegant way to cope with this topic is to employ signal flow graphs and associate error terms to the test fixture. These error terms are extracted by measuring calibration standards with a known electrical performance, then are used for applying the needed correction that sets the electrical reference plane at the DUT. The calibration routine can be summed up in the following steps:

1. The VNA measures known calibration standards.
2. The results are stored in memory and used to calculate an error model.
3. The error model is employed to remove the effect of systematic error from the measurements.

**VNA error model** A very efficient way for describing the imperfections of the test system is to introduce a fictitious error adapter, which is placed between the two-port DUT and the VNA measurement ports. The error terms are related to the six types of systematic errors. The first is the directivity. This is telling the capability of the reflectometer to discriminate forward and reflected waves. For example, a small portion of forward power could appear in the coupled path, causing an error in reflection measurements. This effect will be studied in section 2.3. The second one is the transmission and reflection tracking errors, they are due to the different frequency response of the VNA receivers. A third error contribution is made by the source and load match errors, as the system characteristic impedance is not matched to the load port and the source port. For example, on the source match side, the incident signal to the DUT is reflected from it, returns to the source port, but due to the mismatch, it is re-reflected back to the DUT, causing an error. The latter contribution is the leakage or crosstalk error which is usually ignored.

For describing the error models, it's possible to model the real VNAs of figures 1.6 and 1.7 as a perfect reflectometer that interfaces an error adapter before the DUT [14]. This is represented in figure 1.8.

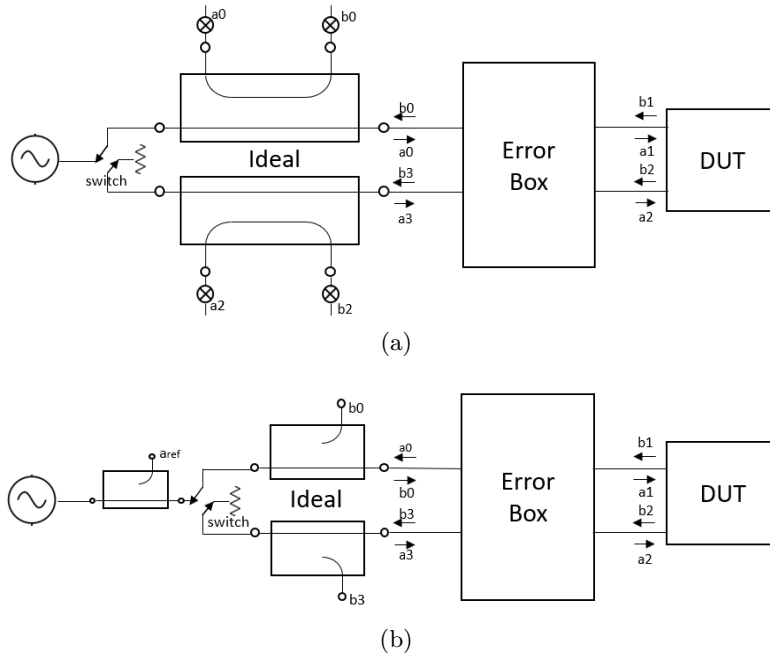


Figure 1.8: VNA architectures with four (a) and three (b) ideal reflectometers cascaded with an error network.

**One-port error model** To have a better insight on the calibration of two-port VNAs, let's consider first the measurement of a one-port DUT (a reflection measurement). The one-port calibration is made by characterizing and removing four systematic error terms: directivity ( $e_{00}$ ), transmission tracking ( $e_{10}$ ), reflection tracking ( $e_{01}$ ) and port-match ( $e_{11}$ ) [14]. The most used one-port calibration is the SOL one (short-open-load). This is made by measuring open, short, load standards and deriving three equations in three unknowns, terminating the unused ports of the VNA on  $50 \Omega$ . The one-port error adapter is used as the interface between the DUT and the VNA port [34]. The goal is to calculate the terms  $e_{00}, e_{11}, e_{10}e_{01}$  that will allow us to transform the incident and the reflected signal  $a_0, b_0$  inside the VNA to the corrected signal  $a_1, b_1$  of the DUT. These terms are called directivity  $e_{00}$ , port match  $e_{11}$ , and tracking  $e_{10}e_{01}$ .

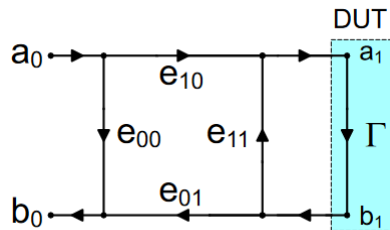


Figure 1.9: Error model for one-port measurements [14].

If we solve the flow graph we obtain:

$$\Gamma_m = \frac{b_0}{a_0} = \frac{e_{00} - \Delta_e \Gamma}{1 - e_{11} \Gamma} \quad (1.29)$$

$$\Gamma = \frac{\Gamma_m - e_{00}}{\Gamma_m e_{11} - \Delta_e} \quad (1.30)$$

$$\Delta_e = e_{00} e_{11} - e_{10} e_{01} \quad (1.31)$$

These are combined in the following generic form:

$$e_{00} + \Gamma \Gamma_m e_{11} - \Gamma \Delta_e = \Gamma_m \quad (1.32)$$

This serves as the basis for calculating the three error terms. In fact, this equation can be inverted to solve for the actual reflection coefficient, given the  $\Gamma_m$  and  $e_{00}, e_{11}, e_{10}e_{01}$ . Measuring the known standards as OPEN, SHORT, LOAD we have a system of 3 equations, to be solved for the 3 error terms:

$$e_{00} + \Gamma_1 \Gamma_{m1} e_{11} - \Gamma_1 \Delta_e = \Gamma_{m1} \quad (1.33)$$

$$e_{00} + \Gamma_2 \Gamma_{m2} e_{11} - \Gamma_2 \Delta_e = \Gamma_{m2} \quad (1.34)$$

$$e_{00} + \Gamma_3 \Gamma_{m3} e_{11} - \Gamma_3 \Delta_e = \Gamma_{m3} \quad (1.35)$$

Solve for the three error terms that represent the independent variables and finally calculate the corrected DUT reflection coefficient. Such measurements and correction routines are implemented in all modern vector network analyzers when performing a one-port calibration. An important point is that even if the one-port model used has four error terms ( $e_{00}, e_{01}, e_{10}, e_{11}$ ) they are not all independent: to obtain the DUT reflection coefficient only  $e_{00}, e_{11}$ , and  $\Delta_e$  are required.

Looking at the signal flow graph of figure 1.9, it's possible to consider the ideal case when there is no systematic error present. The error box would behave like as an ideal "thru" network. In this case,  $e_{00} = 0$  means that no part of the transmitted signal would directly transfer into the reflected one,  $e_{11} = 0$  that there is no impedance mismatch between the components,  $e_{01} = e_{10} = 1$  that the transmission and reflection from the DUT would not be distorted [14].

**Twelve-term error model** The twelve-term error model is used to describe a two-port VNA. As shown in figures 1.6 and 1.7, there are two types of VNAs, one with a complete reflectometer on each port and the other with a reference coupler and a single coupler on each port. The twelve-term error model was derived for the calibration of this second kind of VNAs, for the first time in [13]. For cost reduction, these VNAs are realized with just three receivers. Two of them are getting the reflected waves from the DUT, while another one is switched to measure the incident wave only at the port where the RF power

is applied. When the switch in figure 1.7 is thrown, the error model to be used changes between forward and reverse direction (figure 1.10).

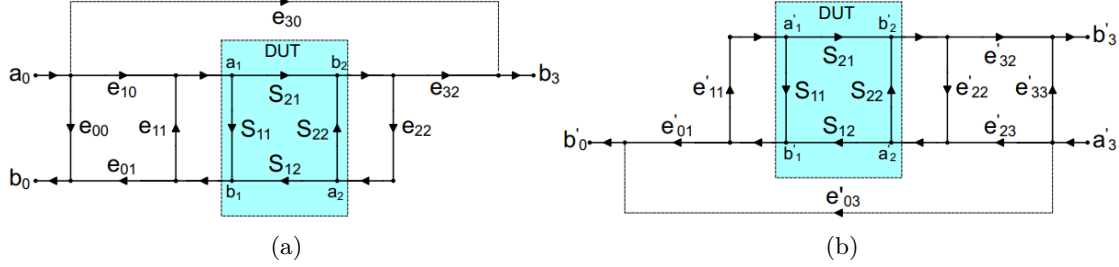


Figure 1.10: VNA error adapter terms for the forward (a) and reverse (b) operation [14].

The error terms can be identified as reported in table 1.1.

$e_{00}$	port-1 directivity	$e'_{33}$	port-2 directivity
$e_{10}$	port-1 transmission tracking	$e'_{23}$	port-2 transmission tracking
$e_{01}$	port-1 reflection tracking	$e'_{32}$	port-2 reflection tracking
$e_{11}$	port-1 match	$e'_{22}$	port-2 match
$e_{22}$	port-2 match	$e'_{11}$	port-1 match
$e_{32}$	port-2 reflection tracking	$e'_{01}$	port-1 reflection tracking
$e_{30}$	port-1-2 leakage	$e'_{03}$	port-2-1 leakage

Table 1.1: Name of the terms of the twelve-term error model [14].

The leakage terms  $e_{30}$  and  $e'_{03}$  are usually neglected and the errors in the models are effectively twelve. This error model can account for the switch imperfections in the reference coupler VNA. In fact, the match error at one port of the VNA changes when that port is acting as a source or as a termination. These error terms are shown in the error model as  $e_{11}$ ,  $e_{22}$ ,  $e'_{22}$  and  $e'_{11}$ . A typical example of a 12-error term calibration is the SOLT (short-open-load-thru) technique that uses the four calibration standards for calculating the error terms. It can be viewed as an extension of the SOL standard for one-port calibration. The three one-port standards are connected to each of the two VNA ports and measured. Equations 1.33 to 1.35 are used to obtain the terms  $e_{00}$ ,  $e_{11}$ , and  $e_{10}e_{01}$ . The same applies to the corresponding terms in the reverse error model. Then it is measured the two-ports directly connected (thru), to obtain  $e_{22}$  and  $e_{10}e_{32}$ . The isolation terms can be obtained by connecting a matched load simultaneously at the two-port and measuring the transmission. In a similar way to the one-port error model, it can be shown that the unknowns to calibrate the system and obtain the DUT S-parameters are just ten. For this reason, the error model is shown in its normalized form (figure 1.11).

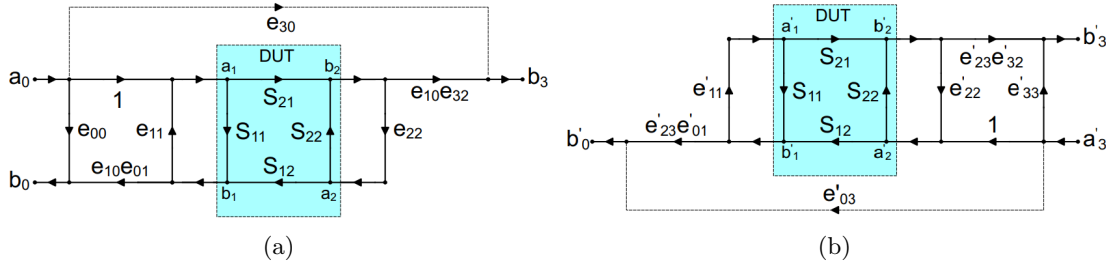


Figure 1.11: Normalized VNA error adapter terms for the forward (a) and reverse (b) operation [14].

**Eight-term error model** The eight-term error model is another model used to describe a two-port VNA (figure 1.12).

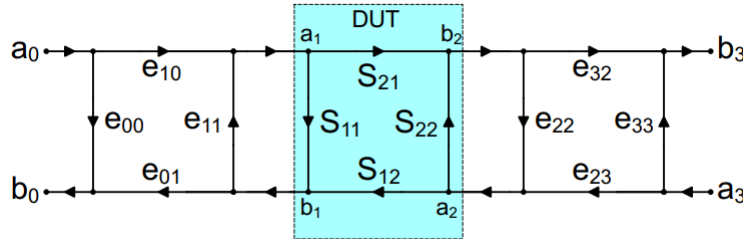


Figure 1.12: Signal flow graph of the eight-term error model [14].

The error terms can be identified as reported in table 1.2. The errors of directivity, tracking and match terms are taken into account in the same way of the twelve-term error model. The terms that are missing are the ones related to the RF switch. These terms are not included in the VNA architecture with two complete reflectometer since the port-1 match, when it is acting as a source, is the same as the port-1 match when the same port behaves as a termination ( $e_{11} = e'_{11}$ ). The same applies for port 2 ( $e_{22} = e'_{22}$ ). This is the same as considering a perfect switch that does not change the port match of the network analyzer as it is switched from forward to reverse measurement. This assumption is valid if the VNA has two complete reflectometers on the DUT side of the switch. In this way, the switch imperfections are ratioed out from the calibration.

$e_{00}$	port-1 directivity
$e_{10}$	port-1 transmission tracking
$e_{01}$	port-1 reflection tracking
$e_{11}$	port-1 match
$e_{22}$	port-2 match
$e_{32}$	port-2 reflection tracking
$e_{23}$	port-2 transmission tracking
$e_{33}$	port-2 directivity

Table 1.2: Name of the terms of the eight-term error model [14].

The eight-term error model directly applies to VNAs with a complete reflectometer on each port (figure 1.6). It is still possible to calibrate a VNA with one reference coupler with the eight-term model, assuming that the switch is perfect ( $e_{11} = e'_{11}$ ,  $e_{22} = e'_{22}$ ). The calibration will be less accurate than a full twelve-term one, as the perfect switch assumptions is just an approximation. The reason for which it could be convenient to apply an eight-term error model for the calibration is that this model has a series of advantages that are described below.

- The eight-term error model represents the system as a cascade of three two-port networks. This representation allows the use of *transmission parameters* to apply the vector error correction. In this way, it is easier to compute the new error terms when additional two-port error boxes (cables, adapters...) are added at the reference plane.
- The eight-term model directly applies to de-embedding problems. In fact, for the de-embedding, the fictitious error boxes correspond to physical two-port fixtures that are connected to the DUT. The eight-term model is useful when the interest is to characterize the S-parameters of the two fixtures rather than their effect on the DUT measurement.
- The most accurate self-calibration techniques (TRL, TRM, LRRM, LRL) can fully characterize a system described with the eight-term model.

**Error model conversion** The twelve-term and the eight-term error models can be related. In fact, they describe a similar system. To obtain the relationship between the two, first, the crosstalk must be neglected in the twelve-term error model. Using signal-flow-graph manipulation, the conversion is made according to the following table 1.3 [6].

normalized twelve-term model	eight-term model
$e_{00}$	$e_{00}$
$e_{01}e_{10}$	$e_{01} \cdot e_{10}$
$e_{11}$	$e_{11}$
$e'_{33}$	$e_{33}$
$e'_{22}$	$e_{22}$
$e'_{23}e'_{32}$	$e_{23} \cdot e_{32}$
$e_{22}$	$e_{22} + \frac{e_{32}e_{23}\Gamma_3}{1-e_{33}\Gamma_3}$
$e_{10}e_{32}$	$e_{10} \frac{e_{32}}{1-e_{33}\Gamma_3}$
$e'_{11}$	$e_{11} + \frac{e_{10}e_{01}\Gamma_0}{1-e_{00}\Gamma_0}$
$e'_{23}e'_{01}$	$\frac{e_{10}e_{32}}{1-e_{00}\Gamma_0}$

Table 1.3: Error terms of the twelve-error model in function of the eight-term one.

In [6] is also reported how the eight-term error model is modified to include the switch terms.

### 1.2.3 Removing fixture contribution

Before starting the measurements, the first tier of calibration is performed, for example by using the SOLT technique to compute the quantities included in the twelve-term error model such to calibrate up to the ends of the coaxial cables attached to the VNA. This operation moves the reference planes at which S-parameters are linked up to the ends of such cables. As explained, usually there is the need of a second step of calibration (second tier), which is referred to as the de-embedding. As reported in [1], the test fixture is the structure used to connect test equipment cables, that have a coaxial interface, to a DUT which is typically non-coaxial. The test fixture is made using a printed circuit board (PCB). The de-embedding is the process that removes mathematically the test fixture effect from the measured data, providing the DUT contribution only. There are different possibilities to remove the fixture contribution [35]. If the test fixture S-matrix is known, the de-embedding consists of the following steps:

- **Transformation of the S-parameters into T - parameters [30]** : The transmission parameters can be obtained from the scattering ones as follows.

$$\begin{bmatrix} T_{11} & T_{12} \\ T_{21} & T_{22} \end{bmatrix} = \begin{bmatrix} \frac{1}{S_{21}} & \frac{-S_{22}}{S_{21}} \\ \frac{S_{11}}{S_{21}} & S_{12} - \frac{S_{11}S_{22}}{S_{21}} \end{bmatrix} \quad (1.36)$$

- **Inverse multiplication of the matrices** : If  $T_1$  and  $T_2$  are the transmission matrices of the left and right fixtures, then the DUT can be de-embedded from the fix-DUT-fix measurement as follows.

$$\mathbf{T}_{\text{fdf}} = \mathbf{T}_1 \mathbf{T}_{\text{DUT}} \mathbf{T}_2 \quad (1.37)$$



$$\mathbf{T}_{\text{DUT}} = \mathbf{T}_1^{-1} \mathbf{T}_{\text{ddf}} \mathbf{T}_2^{-1} \quad (1.38)$$

Considering figure 1.13, the difficult part is then to obtain the fixture scattering parameters, that can't be directly measured by the VNA since they do not have coaxial interfaces. As explained, there are three possibilities to obtain the information on the test fixture scattering matrix: *modeling*, *direct measurement*, and *in-fixture calibration*. The latter technique is also called *two-tier calibration*.

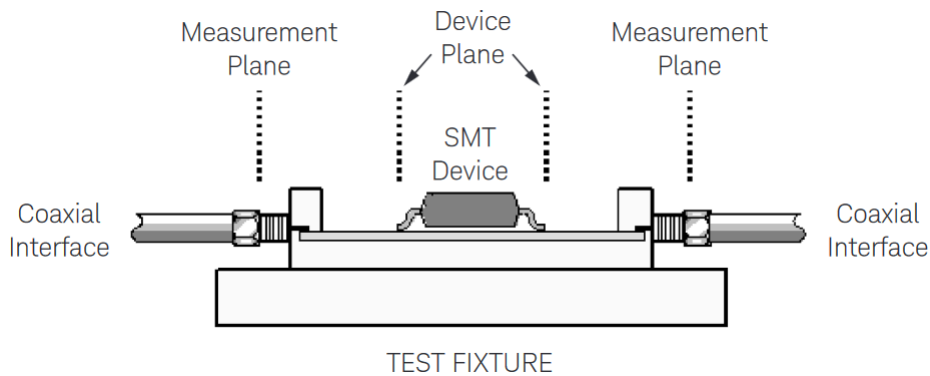


Figure 1.13: Illustration of the de-embedding of a DUT: test fixture effects are removed by moving the reference planes [35].

The *direct measurement* approach is not always practical, as it requires expensive RF probes to measure on-board fixtures (such as PCB traces). The *modeling* approach means to obtain the scattering parameters of the test fixture through a 2D/3D electromagnetic solver. This technique strongly depends on the complexity of the test fixture. A particular case of this approach is the *port-extension*, which is available in every VNA and described below.

#### 1.2.4 Port-extension

If the test fixture can be approximated to a lossless transmission line, with flat magnitude and linear phase response, with constant characteristic impedance, the de-embedding is simply performed by moving the reference planes through the electrical length of the lines. The process is described with reference to figure 1.14.

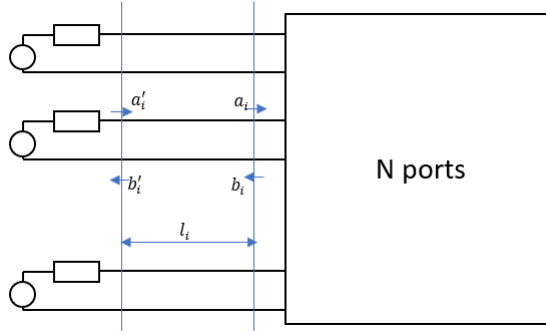


Figure 1.14: Moving the reference planes for eliminating the fixture contribution.

If  $\tau_i$  is the time delay of the  $i$ -th line (that depends on its electrical length and phase velocity)

$$a_i = a_i' e^{-j\omega\tau_i} \quad (1.39)$$

$$b_i' = b_i e^{-j\omega\tau_i} \quad (1.40)$$

$$\Phi = \begin{bmatrix} e^{-j\omega\tau_1} & 0 & \dots & 0 \\ 0 & e^{-j\omega\tau_2} & \dots & 0 \\ \vdots & 0 & \dots & \vdots \\ 0 & 0 & \dots & e^{-j\omega\tau_N} \end{bmatrix} \quad (1.41)$$

From which it's possible to write:

$$\mathbf{b}' = \Phi \mathbf{b}, \mathbf{a} = \Phi \mathbf{a}' \rightarrow \mathbf{a}' = \Phi^{-1} \mathbf{a} \quad (1.42)$$

$$\mathbf{b}' = \mathbf{S} \mathbf{a}' \rightarrow \Phi \mathbf{b} = \mathbf{S} \Phi^{-1} \mathbf{a} \quad (1.43)$$

$$\mathbf{b} = \Phi^{-1} \mathbf{S} \Phi^{-1} \mathbf{a} \quad (1.44)$$

The last equation provides the scattering matrix evaluated at the DUT reference planes.

## 1.3 TRL de-embedding for two-port networks

### 1.3.1 In-fixture calibration

The approach of in-fixture or two-tier calibration is employed in this work. This means characterizing the test-fixture attached to the DUT by using one of the calibration techniques described in the previous section: this requires a special calibration board. The goal of the de-embedding of a multi-port DUT is pursued by first considering the two-port case.

The two-port fixtures connected to the DUT can be modeled as error-boxes, each made up by four terms:  $s_{11}$ ,  $s_{12}$ ,  $s_{21}$  and  $s_{22}$ . The error model which better describes the arrangement of a DUT and its fixtures is the eight-term error model shown in figure 1.12. This allows the use of the self-calibration techniques, such as the TRL. The TRL does not require precise standards as the SOLT and thus allows better results when calibration involves non-coaxial measurements. Moreover, it will make it possible to characterize the test-fixtures as two-port networks rather than just get rid of their effect on the DUT measurement: this will be essential to extend the calibration to the multi-port case.

### 1.3.2 Theoretical derivation

With reference to figure 1.15, the goal is to measure the scattering parameters of the DUT at the reference planes [2]. Typically, the device under test is non-coaxial and mounted on a coaxial test fixture to be measured as in figure 1.13. The system can be calibrated up to the ports of the test fixtures. Reference planes are now on the coaxial cables ends but the measurement will include losses and phase delays caused by the effects of the connectors, cables, transitions of the test fixture that must be used to connect the DUT to the analyzer. At this point the problem is to separate the effect of the test fixtures from the response of the DUT, using de-embedding. As explained in section 1.2.3, if the test fixture is low loss and well-matched, simple port-extension can be performed. In general, the test fixture is not ideal and will introduce discontinuities and attenuation that cannot be modeled easily. These effects can be lumped in a two-port error box placed at each port between the actual measurement reference plane and the desired reference plane for the DUT. These error boxes must be characterized before the DUT measurement can be extracted.

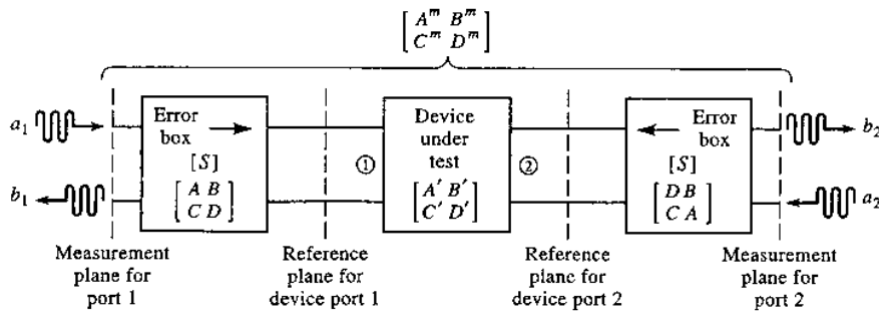


Figure 1.15: Block diagram of a network analyzer measurement of a two-port device [2].

The "thru-reflect-line" (TRL) calibration does not rely on precise impedance standards but on simple transmission line standards [36]. The advantages are that transmission lines are the simplest elements to realize in non-coaxial media and that their characteristic impedance of the transmission line can be accurately determined from measurements of physical dimension and materials or through VNA measurements (section 1.3.3). The "TRL" denomination refers to the three calibration standards required, reported below.

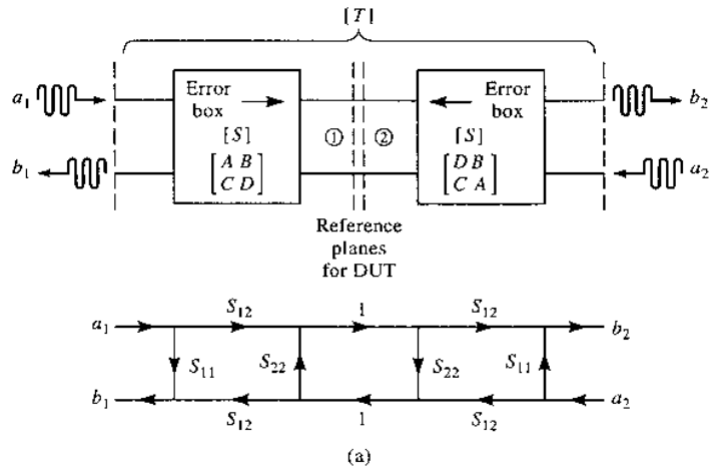


Figure 1.16: Block diagram and signal flow graph for the Thru connection [2].

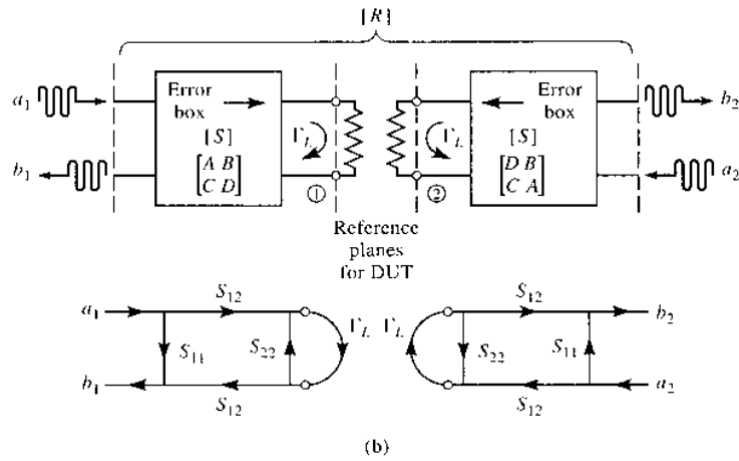


Figure 1.17: Block diagram and signal flow graph for the Reflect connection [2].

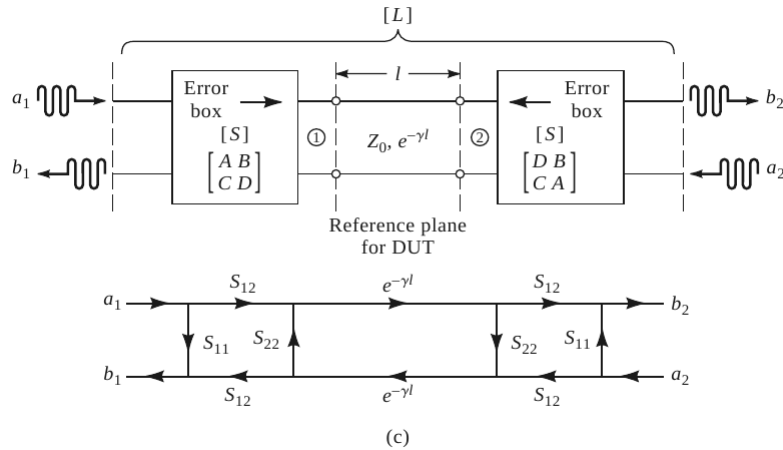


Figure 1.18: Block diagram and signal flow graph for the Line connection [2].

- **Thru:** Connect directly port 1 to port 2 at the desired reference planes, directly. If a short length of a transmission line is used, the de-embedding algorithm is called "line-reflect-line" (LRL) [37].
- **Reflect:** Port 1 and port 2 are terminated on a large  $\Gamma_L$  load like an open: its value will be determined by the TRL calibration process. The advantage of the TRL over other de-embedding techniques is that the reflect standard needs not be accurate, avoiding the difficult requirement of a precise open or short load at high frequency. What it's strictly needed for the algorithm to work it's to know the sign of the real part of  $\Gamma_L$ . For example, if a short circuit is employed as a reflect standard, its reflection coefficient must remain in the left half-plane of the smith chart for the frequency range of the de-embedding.
- **Line:** The two-ports are connected together through a transmission line. The characteristic impedance of the line shall be known and equal to  $50 \Omega$ , as it will determine the reference impedance of the calibration. The line length does not need to be known and a lossy line can be employed.

Figure 1.16 to figure 1.18 show the application of the thru, reflect, line connections at the reference plane for the DUT. As stated previously, the big advantage of the TRL algorithm is that the only precise standard required is the knowledge of the  $Z_0$  of the line standard. The following section explains why is this the case. In fact, at this point, ten measurements have been made that result in ten equations: 2 measurements on the reflect, 4 from the thru, and 4 from the line. The basic TRL error model (described below) has only eight unknowns. Having more measurements than unknowns, the two constants defining the calibration results can be determined: the complex reflection coefficient of the reflect standard and the propagation constant  $\gamma$  of the line are determined [36]. So while in other calibration approaches the accuracy depends on how well the standards are known, in TRL this doesn't happen as the line and reflect are only partially known.

**Relationship with the eight-term error model** Differently from the twelve-term error model, there is no need to consider individual error adapters in the forward and reverse operations [34]. The flow graph (figure 1.12) consists of an error adapter at the input and output of the DUT. It can be seen that the signal flow graph is a cascade of the input error box X, the DUT, and the output error box Y: the cascade can be described with *transmission parameters*. The T-parameter representation permits to relate the measured data  $T_M$  to the actual DUT T-parameters by using the input error adapter  $T_X$  and output error adapter  $T_Y$ .

$$T_M = T_X \times T \times T_Y \quad T = T_X^{-1} \times T_M \times T_Y^{-1} \quad (1.45)$$

$$T_M = \frac{1}{S_{21M}} \begin{bmatrix} -\Delta_M & S_{11M} \\ -S_{22M} & 1 \end{bmatrix} \quad (1.46)$$

$$\Delta_M = S_{11M}S_{22M} - S_{12M}S_{21M} \quad (1.47)$$

$$T_X = \frac{1}{e_{10}} \begin{bmatrix} -\Delta_X & e_{00} \\ -e_{11} & 1 \end{bmatrix}, T_X^{-1} = \frac{1}{e_{10} \cdot e_{10}e_{01}} \begin{bmatrix} 1 & -e_{00} \\ e_{11} & -\Delta_X \end{bmatrix} \quad (1.48)$$

$$T_Y = \frac{1}{e_{32}} \begin{bmatrix} -\Delta_Y & e_{22} \\ -e_{33} & 1 \end{bmatrix}, T_Y^{-1} = \frac{1}{e_{32} \cdot e_{32}e_{23}} \begin{bmatrix} 1 & -e_{22} \\ e_{33} & -\Delta_Y \end{bmatrix} \quad (1.49)$$

$$\Delta_X = e_{00}e_{11} - e_{10}e_{01} \quad (1.50)$$

$$\Delta_Y = e_{22}e_{33} - e_{32}e_{23} \quad (1.51)$$

$$T = \frac{1}{e_{10}e_{32}} \frac{1}{e_{10}e_{01}} \frac{1}{e_{32}e_{23}} \begin{bmatrix} 1 & -e_{00} \\ e_{11} & -\Delta_X \end{bmatrix} \times T_M \times \begin{bmatrix} 1 & -e_{22} \\ e_{33} & -\Delta_Y \end{bmatrix} \quad (1.52)$$

Where  $e_{00}, e_{11}, \Delta_X$  are three error terms at port 1,  $e_{22}, e_{33}, \Delta_Y$  are at port 2, one transmission term  $e_{10}e_{32}$ . Although there are eight terms in the error boxes, only seven error terms are needed to obtain the S-parameters of the DUT. This means that to calibrate out the error boxes, their partial knowledge is sufficient. From the ten independent equations of the thru, reflect, line standards three are used to determine the line length, the propagation constant, and the impedance of the reflect standard, while the other seven give the DUT S-parameters. The mathematical derivation of this result is in appendix A.2. When the error networks are asymmetric, then only the DUT scattering parameters can be obtained, and the test fixtures are not completely characterized.

The case of reciprocal and identical error boxes results in  $s_{12} = s_{21}$  and  $s_{11} = s_{22}$  for both the error boxes. This provides additional equations that allow obtaining both the scattering parameters of the DUT and of the test-fixtures. Before explaining how this can be used for multi-port de-embedding, the main limitations of two-port TRL are considered.

### 1.3.3 Limitations of the TRL de-embedding

The TRL algorithm is capable of providing accurate de-embedding of the test fixtures. However, it has some limitations that have to be taken into account for minimizing the error affecting the computed DUT and fixture scattering matrices.

#### TRL bandwidth

The most important limitation consists in the restricted bandwidth in which the TRL is applicable. As stated earlier, the electrical length difference between the line and thru standard must be different from  $0^\circ$  or  $180^\circ$  at every frequency in the desired bandwidth to avoid the presence of singular matrices that make the math of the algorithm fail. In practice, accounting for non-ideal behavior of the PCB lands or coaxial lines, (frequency dependence of the primary per unit length parameters and the non-homogeneous medium) the line standard shall provide a phase shift between  $20^\circ$  and  $160^\circ$ . This consideration limits the bandwidth in which the TRL can be used. If the electrical length of a transmission line is expressed (in degrees) as:

$$\beta l^\circ = \frac{180}{\pi} \frac{2\pi}{\lambda} l = \frac{180}{\pi} \frac{2\pi}{\lambda} \frac{f_0}{f_0} l = \frac{180}{\pi} \frac{2\pi}{\lambda_0} l \frac{f}{f_0} \frac{\lambda_0 f_0}{c_0} = \beta l_{f_0} \cdot \frac{f}{f_0} \frac{180}{\pi} = \beta l_{f_0}^\circ \cdot \frac{f}{f_0} \quad (1.53)$$

If the line physical length  $l$  is chosen such that at  $f_0$  the electrical length of the line is equal to  $20^\circ$ , then the same line will have a delay of  $160^\circ$  at:

$$f = \frac{160}{20} \cdot f_0 = 8f_0 \quad (1.54)$$

The equation above provides the result that a single line standard can be used in a bandwidth in which lower and upper frequencies are in the ratio of 1:8. In other words, if a line is  $20^\circ$  long at 1 GHz, this standard can be employed in the TRL algorithm up to 8 GHz. When the bandwidth of the de-embedding increases, there are two consequences.

- **The increasing number of line standards** : If the DUT has to be de-embedded in a broader bandwidth, the number of line standards will increase. If, as an example, the ratio between the upper and lower frequencies is 1:64, then two line standards are needed: the first for the bandwidth covering 64:8 frequencies, and the other in the 8:1 one. This result can be schematized according to the following table 1.4:

De-embedding bandwidth	Number of line standards required
1:8	1
1:64	2
1:512	3
1:4096	4

Table 1.4: Required number of line standard for the TRL de-embedding as the bandwidth increases.

The table above provides the minimum number of lines to be used. For improving the accuracy of the de-embedding, one line more than strictly needed can be employed. In fact, the coverage of the same frequency range with one more line standard will result in an electrical length farther from the interval 20°-160°.

- **Low-frequency issues** : The physical length of the line standard needed for the lowest frequency octave causes the TRL de-embedding to be unpractical at frequencies lower than 10 MHz. The physical length of a transmission line is related to its electrical delay as:

$$\beta l^\circ = \frac{180}{\pi} \frac{2\pi}{\lambda} l \quad (1.55)$$

$$l = \frac{\lambda}{2 \cdot 180^\circ} \beta l^\circ = \frac{c}{f} \frac{\beta l^\circ}{360^\circ} = \frac{c_0}{f \sqrt{\epsilon_r}} \frac{\beta l^\circ}{360^\circ} \quad (1.56)$$

Considering an fr4 dielectric layer ( $\epsilon_r = 4$ ) and  $f=10$  MHz, the required length for a line with a 20° delay at this frequency is around 80 cm. Due to this consideration, the low-frequency de-embedding is performed using the thru-reflect-match (TRM) algorithm as explained in the next section. Other numerical examples on line standard requirements are shown in appendix A.1.

### Line standard characteristic impedance

The characteristic impedance  $Z_0$  of the line standard is setting the reference impedance of the computed s-parameter of the DUT and fixture. For achieving accurate de-embedding, the  $Z_0$  impedance for each line employed has to be known and typically equal to 50  $\Omega$ . In this way, even if  $Z_0 \neq 50 \Omega$ , a re-normalization of S-parameters can be done in order to refer them to the usual 50  $\Omega$  reference value.

In more detail, re-normalization is performed as described, assuming that all the measurements are made with a reference impedance of  $Z_0 = 50 \Omega$ . First, the "line" standard characteristic impedance has to be known, for example using the algorithm described in the next paragraph. This impedance is indicated as  $Z_{ren}$ . The measured S-parameters of the "line" standard are re-normalized from  $Z_0$  to  $Z_{ren}$ . The same operation is applied also for "thru" and "reflect". The de-embedding procedure is then applied, and the obtained DUT and fixture scattering matrix are referred to the impedance  $Z_{ren}$ . The resulting S-parameters are then re-normalized from  $Z_{ren}$  to  $Z_0$ .

#### 1.3.4 Line standard impedance correction

If the actual characteristic impedance of the line standard can be determined, the de-embedding accuracy can be improved by performing a re-normalization of the S-parameters. In [38] is reported a method to measure the characteristic impedance of PCB tracks using a VNA. This strategy requires the fabrication of additional standards on the calibration PCB, other than the ones employed to perform the de-embedding. As reported in [39],



"A common problem is the determination of the characteristic impedance and propagation constant of a given transmission line which is physically available for measurement and test. These quantities can be found by the measurement of the input impedance of the line under two conditions: with the far end short-circuited, and with the far end open-circuited". This results in the following formula:

$$Z_0 = \sqrt{Z_{in,s}Z_{in,o}} \quad (1.57)$$

The above result is coming from the input impedance formula for transmission lines in trigonometric form:

$$Z_{in,s} = Z_0 \frac{Z_L + Z_0 \tanh(\gamma l)}{Z_0 + Z_L \tanh(\gamma l)} \Big|_{Z_L=0} = Z_0 \tanh(\gamma l) \quad (1.58)$$

In a similar way, for ( $Z_L \rightarrow \infty$ ):

$$Z_{in,o} = Z_0 \frac{1}{\tanh(\gamma l)} \quad (1.59)$$

The 1.57 follows from the 1.58 and 1.59. As the characteristic impedance depends on per unit length parameters, the length of the line makes, in principle, no theoretical difference in the computation of  $Z_0$ . However, to practically determine the characteristic impedance with sufficient accuracy, an important point has to be made regarding the electrical length (and thus the measurement frequency) at which the two impedances are evaluated. This indication is provided in [39]. In particular, assuming negligible attenuation ( $\alpha \simeq 0$ ), the 1.58 and 1.59 result in:

$$Z_{in,s} = jZ_0 \tan(\beta l) \quad (1.60)$$

$$Z_{in,o} = -jZ_0 \frac{1}{\tan(\beta l)} \quad (1.61)$$

If we consider if the length of the line is close to an odd multiple of a quarter wavelength, the angle  $\beta l$  is an odd integer times  $90^\circ$ , with the input impedance of the line closed on a short approaching the open circuit on the smith chart and the opposite happening for the line closed on an open. When the length of the line is close to an even number of a quarter wavelength, the opposite happens:  $Z_{in,s}$  will be close to the short circuit point, being very small, while  $Z_{in,o}$  is close to open circuit one. In these cases, it's difficult to obtain accurate results. It becomes an advantage to have both impedances of the same order of magnitude: this is made by selecting the line length such to have  $\tan(\beta l) \simeq \frac{1}{\tan(\beta l)}$  or  $\tan^2(\beta l) \simeq 1$ , which happens when the line length is an odd number of an eighth of wavelength ( $\beta l = (2k + 1)\frac{\pi}{4}$ ) or when the phase shift of the input reflection coefficient measured by the VNA is crossing  $\pm 90^\circ$ .

Summing up, to measure the characteristic impedance of a microstrip line fabricated on a PCB, it is sufficient to make two input reflection coefficient measurements at the frequencies where the line is long an odd multiple of  $\frac{\lambda}{8}$ , and take the square root of the real part (as the imaginary will be negligible) of the product  $Z_{in,o}Z_{in,s}$ .

However, there is another problem to be considered. As discussed in [38], the parasitics of the SMA connector and the non-ideal terminations are causing a large error in the measured reflection coefficient. To avoid this issue, a track of the same nominal  $Z_0$  but shorter (for example a tenth long) of the one under test can be fabricated, its input reflection coefficient measured, and a port-extension calibration [40] can be performed through the VNA. This will move the reference plane along the track of a length equal to the shorter line, in this way the measurement made by the VNA is ignoring the first part of the line and the connector. Another trick is to use two separate tracks for the open and short measurements, to improve their quality.

### 1.3.5 Calculation of the TRL line standard lengths

As explained in 1.3.3, the length of the line standard is of importance when realizing the calibration structures needed for the TRL. According to [36], the optimal line is of  $\frac{\lambda}{4}$  in length. This condition can't be met for all data points. In section 1.3.3, was reported that the math of the de-embedding falls apart when the electrical length difference between the thru or line standard is  $0^\circ$  or  $180^\circ$ . As a rule of thumb [36], the difference between the two lengths must be between  $20^\circ$  and  $160^\circ$ , a condition that can be met with a line standard in a  $\frac{f_h}{f_l} = \frac{8}{1}$  frequency span. Considering the linear phase shift introduced by the line, at the middle frequency  $f_c = \frac{f_h + f_l}{2}$  the line length is  $l = \frac{\lambda}{4}$ . However, if the bandwidth is greater than 1:8 and less or equal to 1:64 two lines shall be employed. This will arise the problem to decide the line lengths and frequency crossover point (i.e. the frequency at which the measurement on the shorter line standard is employed). In the case of two lines, the optimal crossover frequency is the geometric mean  $f_t = \sqrt{f_l f_h}$  [36]. In this way each line is long  $\frac{\lambda}{4}$  at the two center frequencies  $f_{c1} = \frac{f_l + f_t}{2}$  and  $f_{c2} = \frac{f_t + f_h}{2}$ . A detailed computation of the different crossover and center frequencies along with the line length calculation is reported in appendix A.1. The relative Matlab code is shown in appendix B.

### 1.3.6 Thru reflect match (TRM) de-embedding for two-port networks

If the DUT data at lower frequencies is required, then the length of the transmission line standard is too long to be realized. In this case, the "thru-reflect-match" (or TRM) de-embedding is employed, with the mathematical derivation reported in appendix A.3. The TRM de-embedding allows to extract the DUT scattering matrix by employing three standards:

- **Thru:** As for the TRL de-embedding, this standard consists in a back-to-back connection of the test fixtures (figure 1.16).
- **Reflect:** Also this standard is the same employed for the TRL (figure 1.17), and likewise to it there is no need to have a precise load as a reflect since what it's

needed for the de-embedding is the knowledge of the real part sign of the load reflection coefficient (load phase shall thus be known within a  $180^\circ$  interval).

- **Match:** The line standard is replaced by a  $50\ \Omega$  load, as reported in figure 1.19.

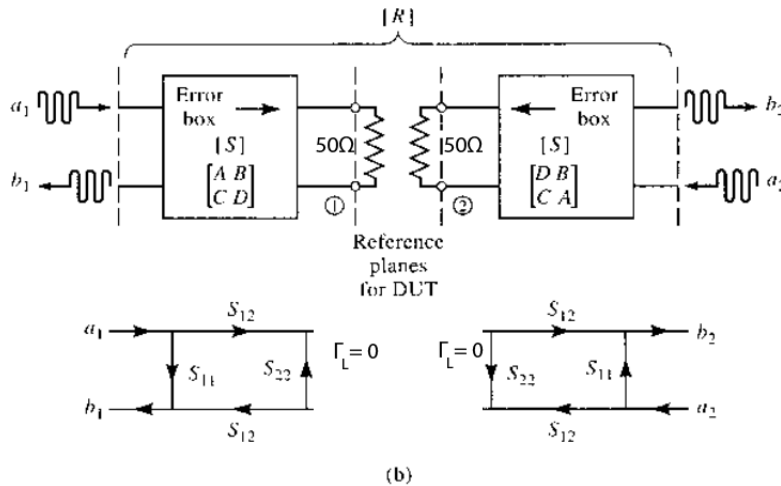


Figure 1.19: Block diagram and signal flow graph for the Match connection.

The TRM technique has an accuracy comparable to the TRL, and it is used in a complementary way to the latter in order to de-embed the DUT at lower frequency. It is easy to realize a sufficiently precise match standard to be used at lower frequencies where the parasitic inductances and capacitances are negligible. This standard can replace the line one, which would be unpractical at low frequencies as stated in section 1.3.2. The mathematical procedure for performing TRM de-embedding is reported in the appendix.

As for the TRL "line" standard, the "match" impedance  $Z_{ren}$  is determining the reference impedance of the computed s-parameter of the DUT and fixture. To obtain these referenced to  $Z_0 = 50\ \Omega$ , the same procedure of the TRL is applied: "match", "thru" and "reflect" S-parameters are re-normalized from  $Z_0$  to  $Z_{ren}$ , the algorithm is performed, and then the DUT and fixture **S** matrices are re-normalized from  $Z_{ren}$  back to  $Z_0$ .

### 1.3.7 Validation of the method

In this section, different circuits are simulated in a SPICE environment. By performing a ".AC" simulation is possible to use SPICE directives to extract the scattering parameters of the networks. The MATLAB<sup>®</sup> scripts of appendix B are used to apply the described de-embedding strategies to this data. The purpose is to assess the functioning of the de-embedding before making measurements on real devices in chapter 2.

**Example 1: De embedding of a low pass filter**

In this example, a low pass filter realized using lumped elements is considered as a DUT, and will be de-embedded from the fix-DUT-fix measurement made with the VNA. The test fixtures are considered to be symmetrical. The overall structure is reported in (figure 1.20).

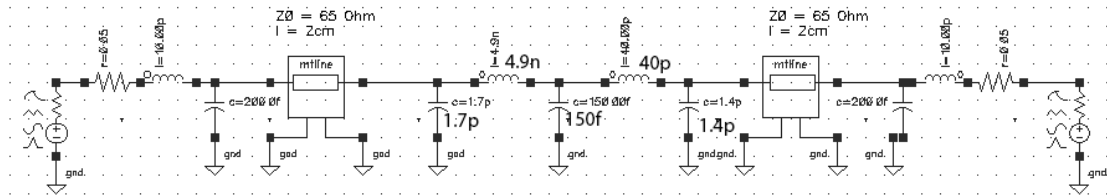
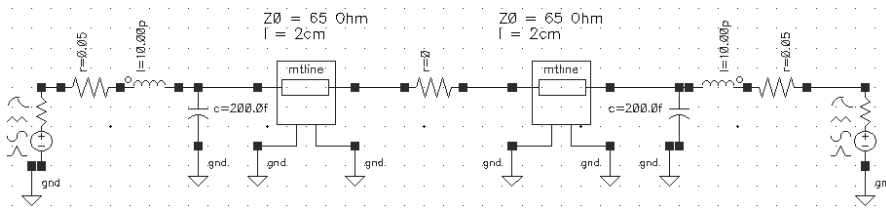
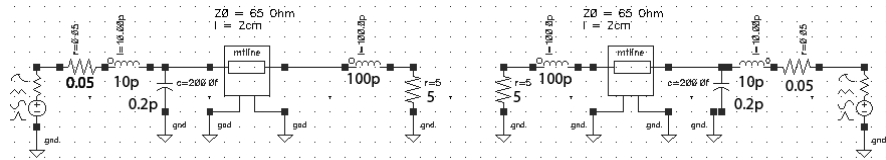


Figure 1.20: Total, or fix-DUT-fix, simulated structure (symmetric error networks case).

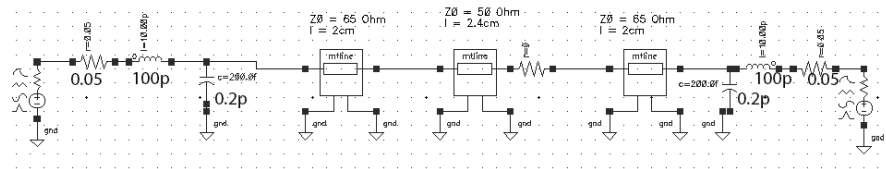
The test fixture consists of the combination of a lumped model of an SMA connector [41] and of a PCB trace with a characteristic impedance of  $65 \Omega$  and 2 cm long. The DUT is a low pass filter, designed to provide an  $S_{11} < -10 \text{ dB}$  in the passband up to 2 GHz, frequency from which the  $S_{21}$  is decreasing at a slope of -40 dB per decade. In order to characterize the two error networks, the TRL algorithm requires the measurements of the scattering parameters of the standards in figure 1.21. Two line standards are realized and the chosen reflect standard is a short circuit termination. The de-embedded DUT and test fixture scattering parameters are consistent with the actual ones obtained by direct simulation and are shown in figure 1.22. The extracted model for the test fixture is reported in figure 1.23.



(a) Thru connection.

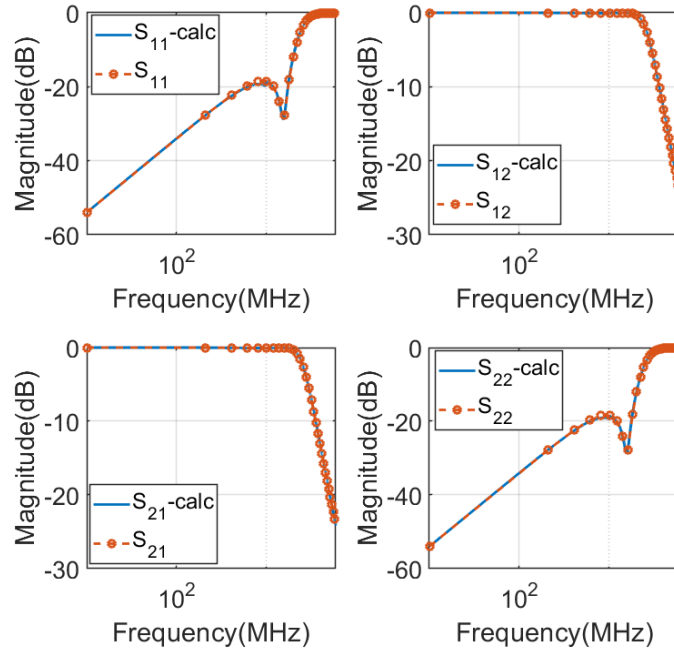


(b) Reflect connection.

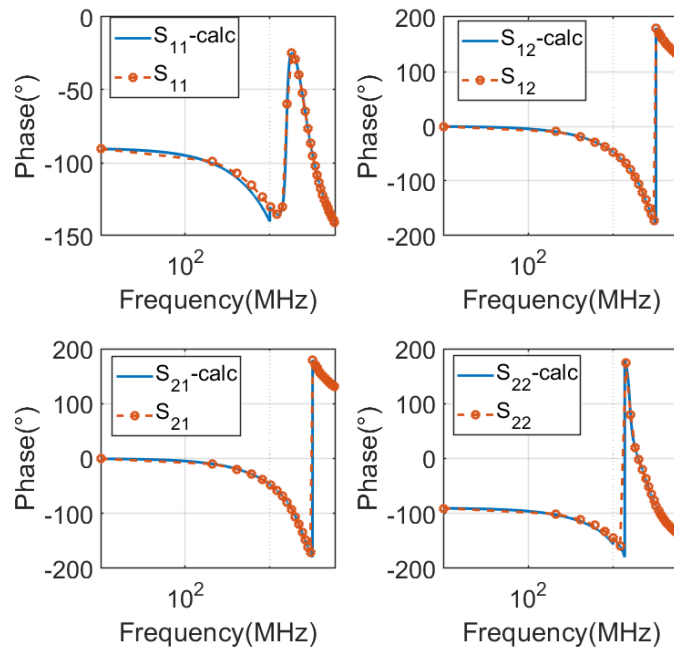


(c) Line 1 connection

Figure 1.21: Connection required by TRL algorithm.

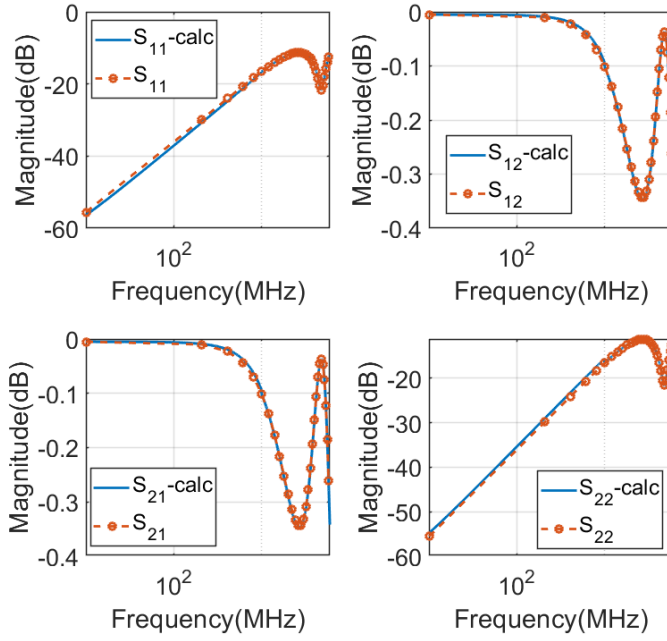


(a)

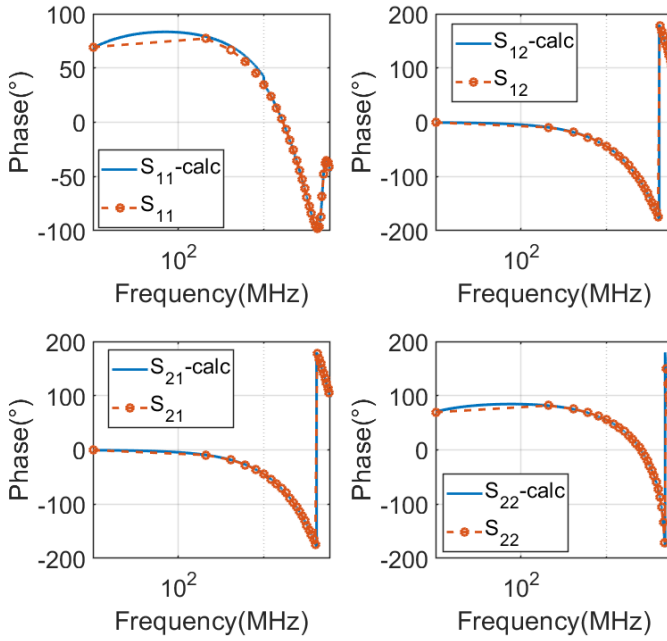


(b)

Figure 1.22: Comparison of the DUT de-embedded scattering matrix and the actual one.



(a)



(b)

Figure 1.23: Comparison of the test fixture de-embedded scattering matrix and the actual one.

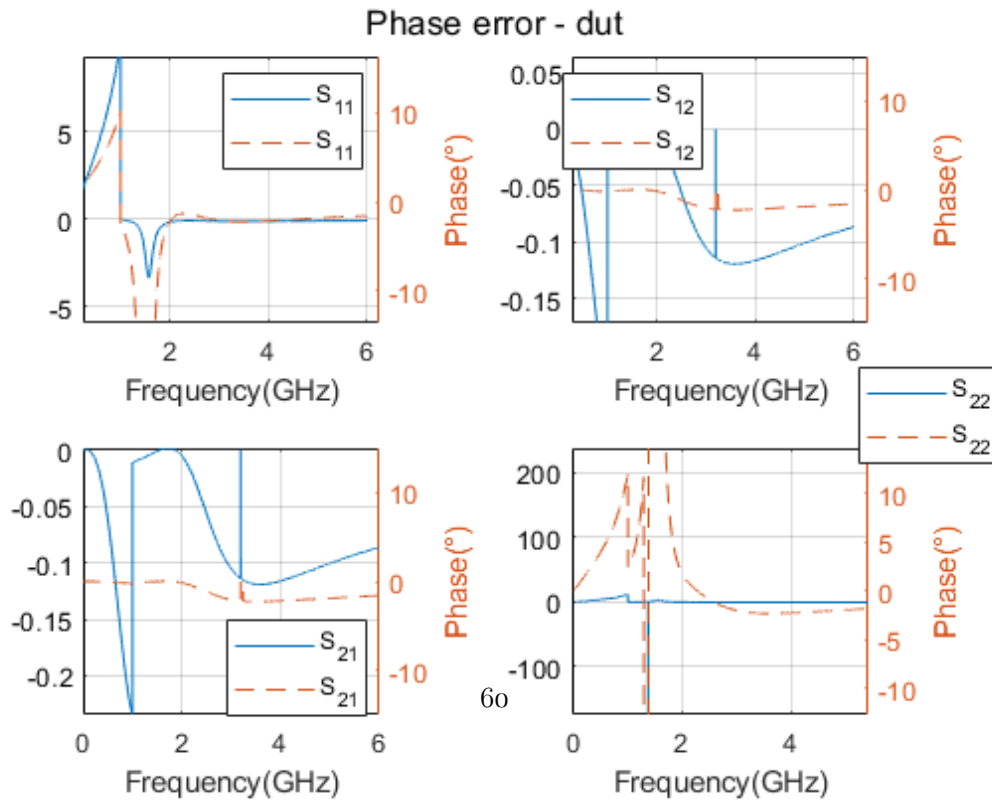
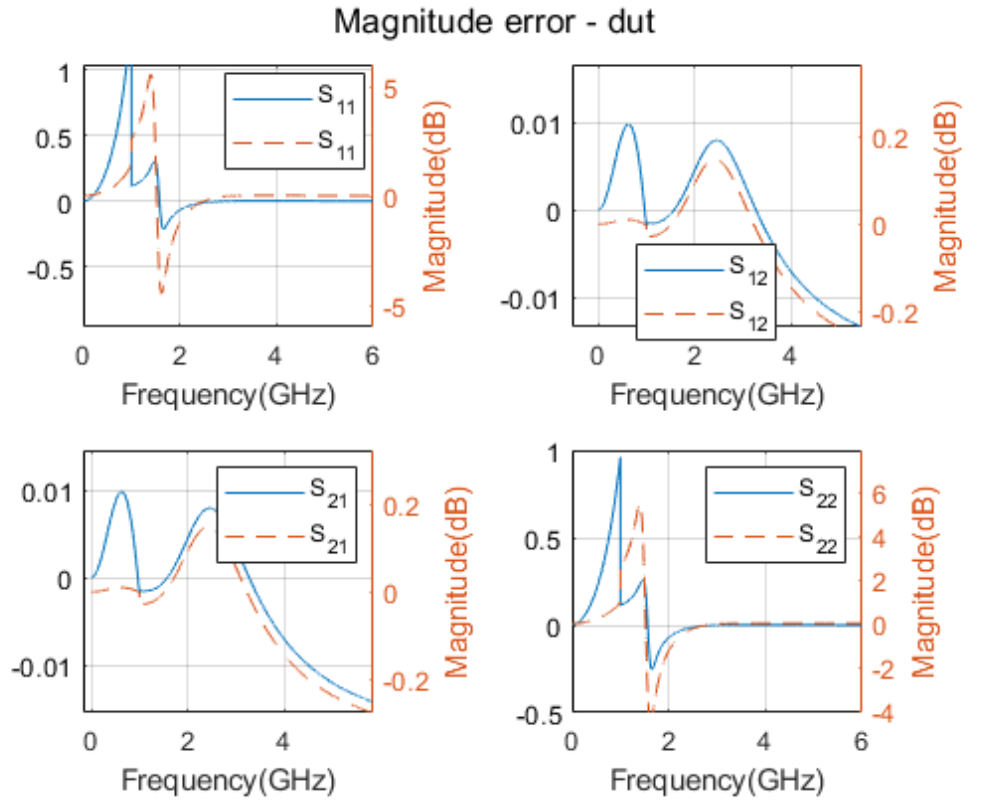


Figure 1.24: Error on the DUT (dashed traces are for no re-normalization).



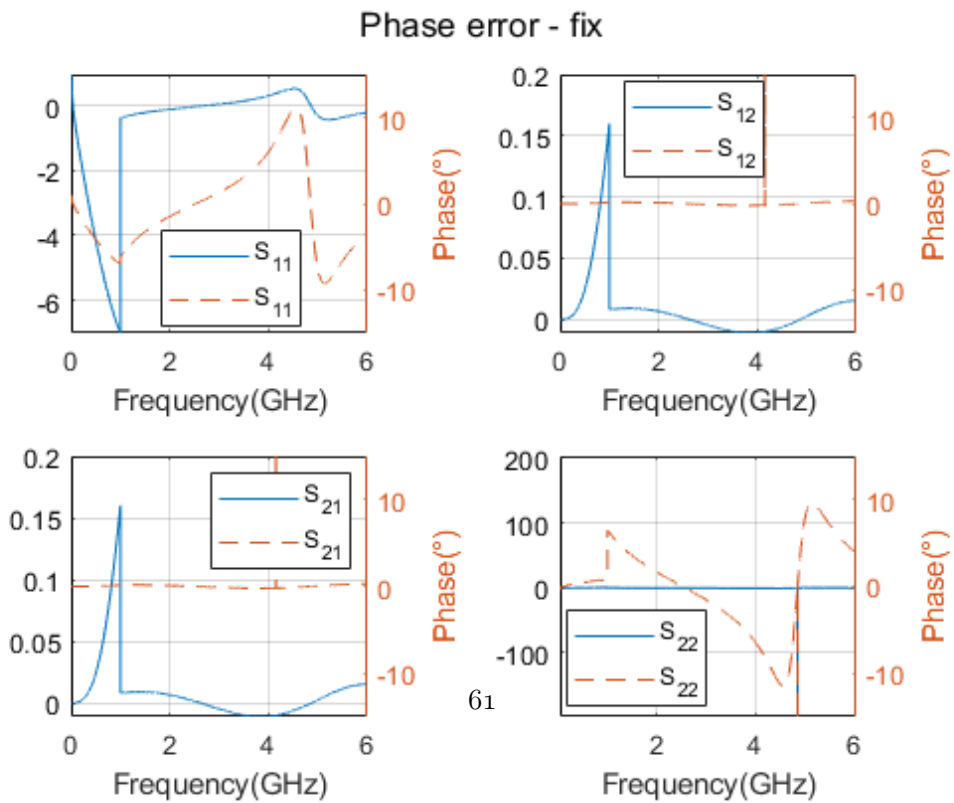
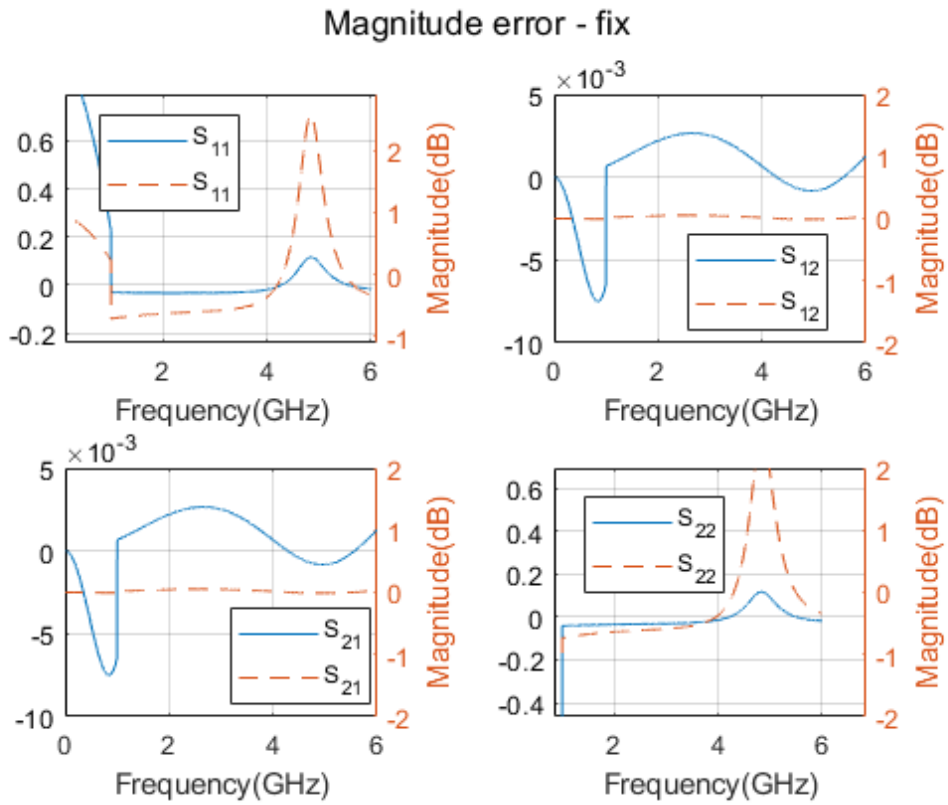


Figure 1.25: Error on the fixture (dashed traces are for no re-normalization).

In the above example, the DUT data are computed on the 0 Hz-6 GHz bandwidth, by employing the TRM for de-embedding up to 1 GHz and using the TRL standard in the upper bandwidth.

**Match standard** The match standard is reported in figure 1.26. It consists on 50  $\Omega$  load with a series inductance of 1 nH and a parasitic capacitance of 0.5 pF. This limits the accuracy of the de-embedding, as at 1 GHz frequency they result in  $2\pi fL \approx 6.28 \Omega$  and  $\frac{1}{2\pi fC} \approx 320 \Omega$ .

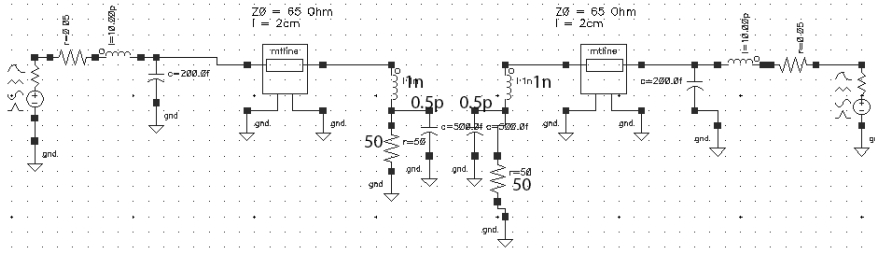


Figure 1.26: Match connection

In any case, the TRM could be extended up to higher frequencies, with a degradation of the results.

**Choice of the line standards** Table 1.5 reports the required line standard for the case of a single line or two.

	Line 1A	Line 1B	Line 2B
<b>f<sub>l</sub> (GHz)</b>	1	1	2.44
<b>f<sub>h</sub> (GHz)</b>	6	2.44	6
<b>f<sub>c</sub> (GHz)</b>	3.5	1.72	4.22
<b>l<sub>fc</sub> (mm)</b>	11.8	23.93	9.77
<b>θ<sub>l</sub> °</b>	25.7	52.2	52.2
<b>θ<sub>h</sub> °</b>	154.3	127.8	127.8
<b>f<sub>t</sub> (GHz)</b>	n/d	2.44	n/d

Table 1.5: Required line standards, computed with equations of appendix A.1.

In the first solution (**1A**) the single line is chosen to be long  $\frac{\lambda}{4}$  at the mean frequency between  $f_l$  and  $f_h$ . In this way, the two phases at lower and upper frequencies are between 20° and 160°, but as the 1:6 ratio is approaching an octave, the phase delays are close to these values. This suggests the possibility of employing two lines, as solution **B**. The transition frequency between line 1B and 2B is chosen as the geometric mean  $\sqrt{f_l f_h}$ , and the line lengths are selected as in the previous case. For this example, the chosen solution

is the two lines one, as more accurate results are expected since the higher margin obtained on  $\theta_l$  and  $\theta_h$ .

The de-embedding effect on data is reported in figure 1.27.

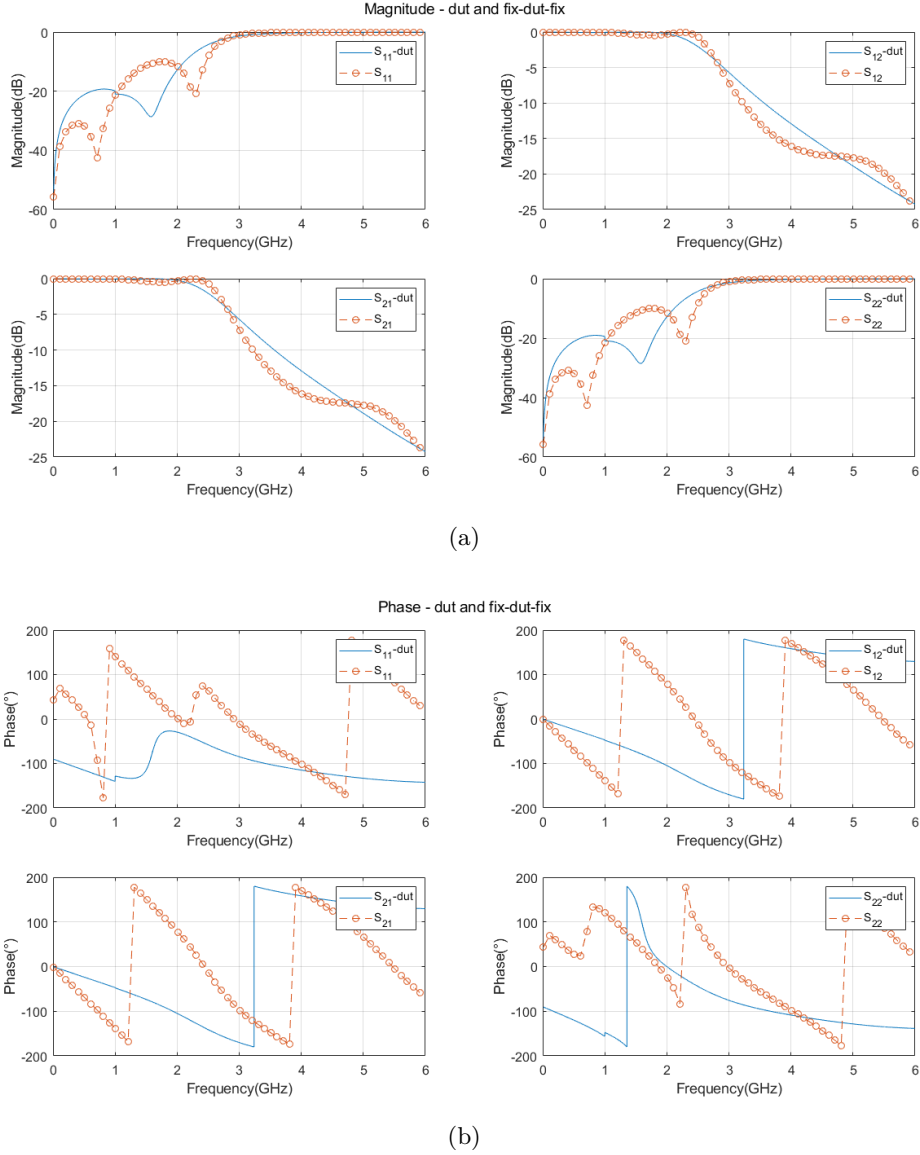


Figure 1.27: De-embedding effect on measured data.

**Impedance re-normalization of the scattering parameters** As stated previously, the most critical connection in the TRL procedure is the line standard. In particular, the characteristic impedance of the line connection will fix the reference impedance of the scattering parameters of the de-embedded DUT and the extracted fixture [42]. For this

reason, the characteristic impedance of the line shall be  $50 \Omega$ . Otherwise, in the case it differs from this value, the computed S parameters can be referred back to  $50 \Omega$  by performing a re-normalization with the known characteristic impedance of the line. The line standard of the example above has a cross-section as reported in figure 1.28.

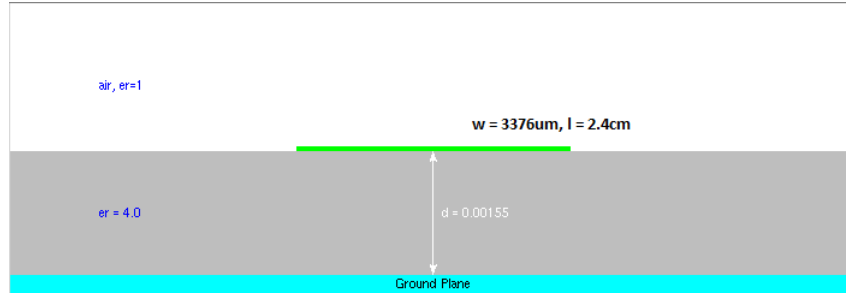


Figure 1.28: Cross-section of the line standard.

The computation of the characteristic impedance according to [43] provides the result of  $48 \Omega$ , and the scattering parameters are re-normalized according to this value. If no renormalization is performed, it's possible to show that the error is larger, corresponding to the dashed traces.

**"Thru" standard of finite length** In the ideal scenario, the calibration standard required is a zero-length "thru". This is normally very simple to implement, but the de-embedding accuracy at the simulation level can be investigated when the "thru" standard is a short transmission line of  $50 \Omega$  characteristic impedance. In particular, a finite length "thru" 1 mm long is considered, as reported in figure 1.29. The de-embedding is performed as before, and the error made on the fixture and DUT S-parameters are shown below. It is observed that the error on the magnitude is very little affected by the finite length "thru" with respect to the previous case, while the error on the phase, reported in the last picture, is more evident. The phase error on the transmission parameters of the fixture (figure 1.31 (b)) is related to the length of the "THRU" standard. In particular, it is linearly dependent on frequency as the phase shift is introduced by a transmission line. The error profile matches the phase shift introduced by the 1 mm length "THRU". This is confirmed from the fact that at 6 GHz the phase shift of the line is computed as:

$$\beta l^\circ = \frac{2\pi}{\lambda|_6 \text{ GHz}} l \simeq 8^\circ \quad (1.62)$$

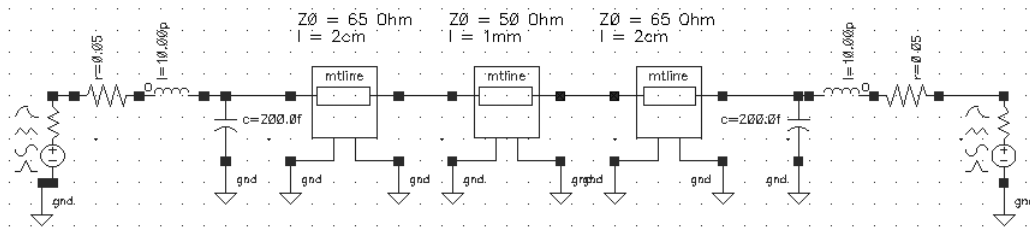
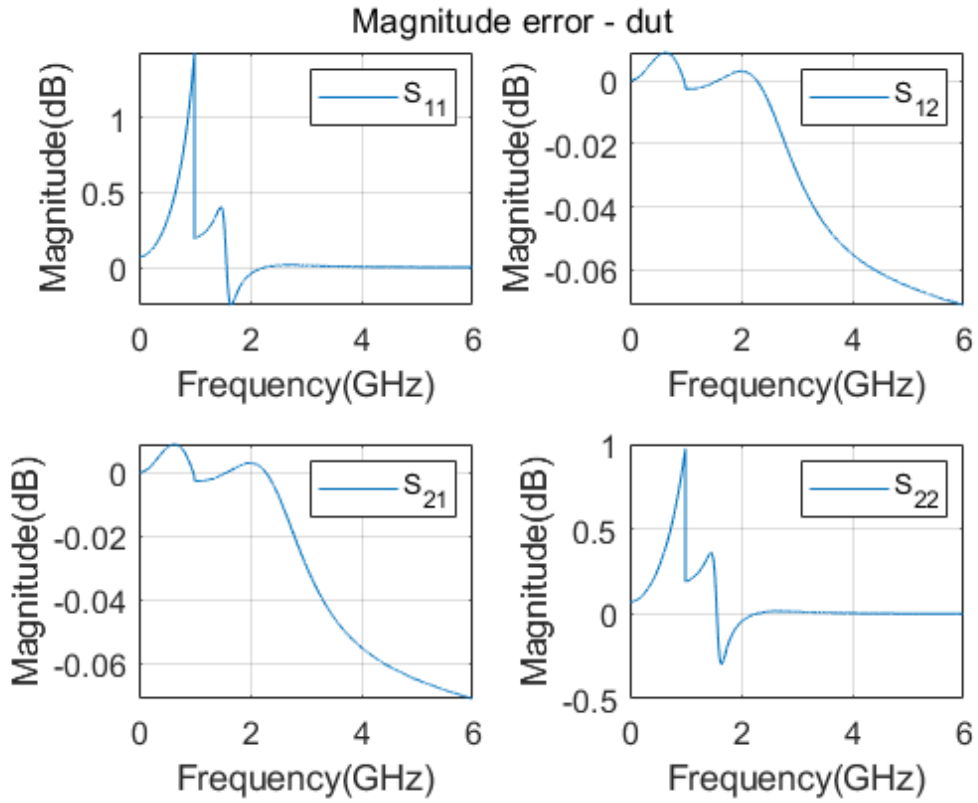
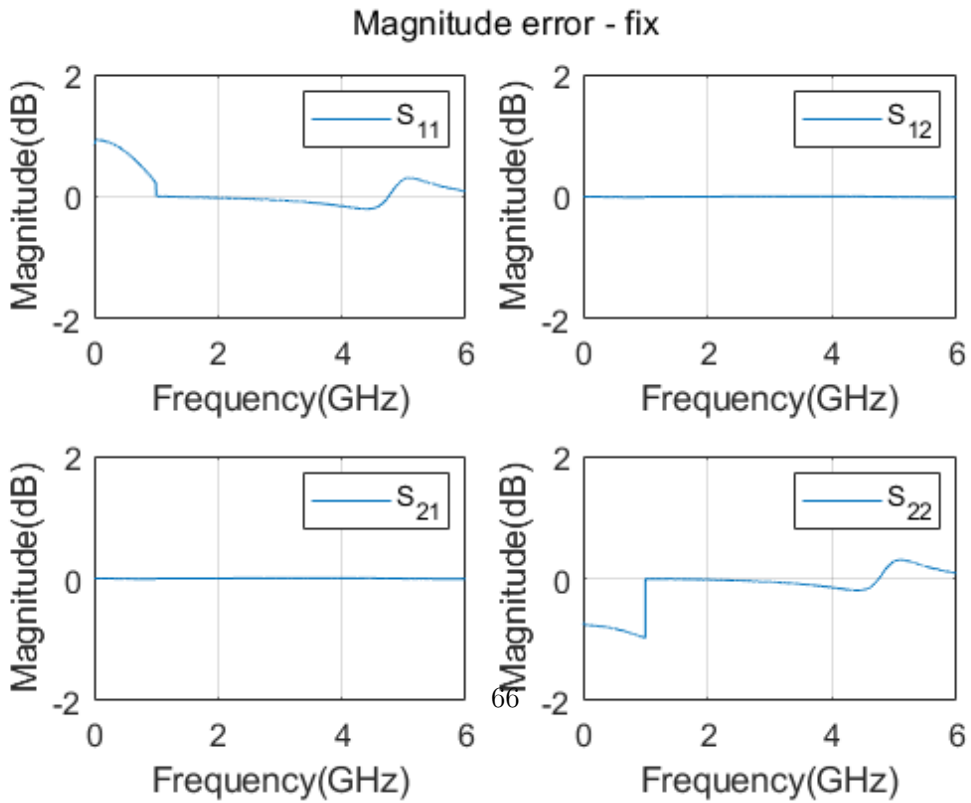


Figure 1.29: "Thru" standard realized with a physical line.

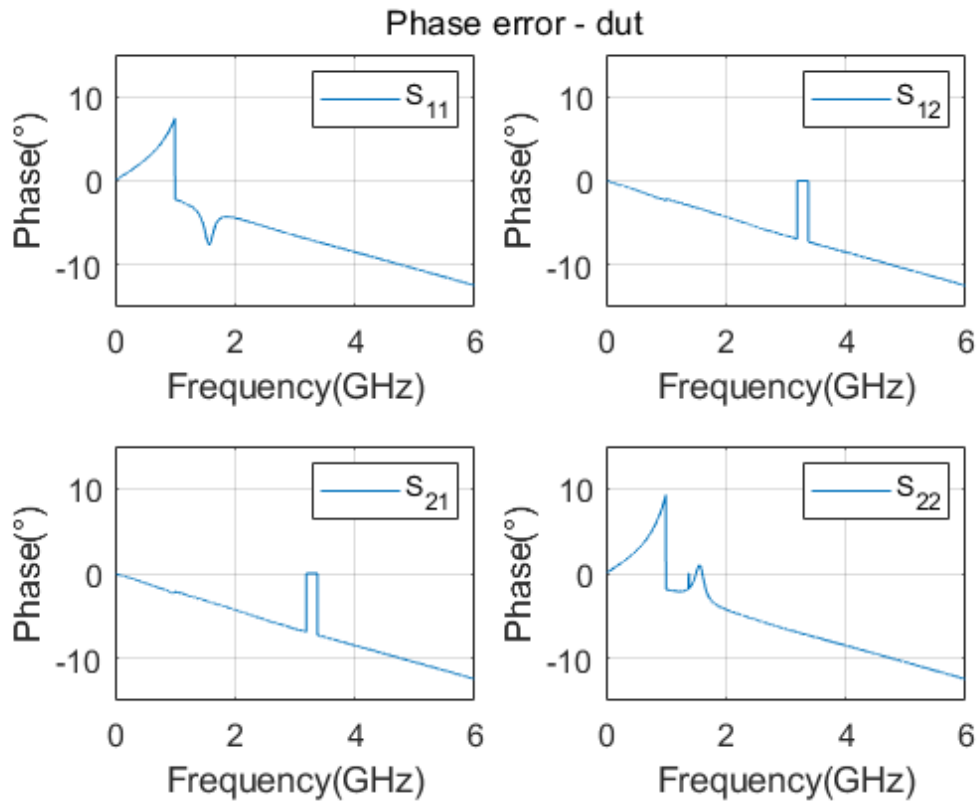


(a)

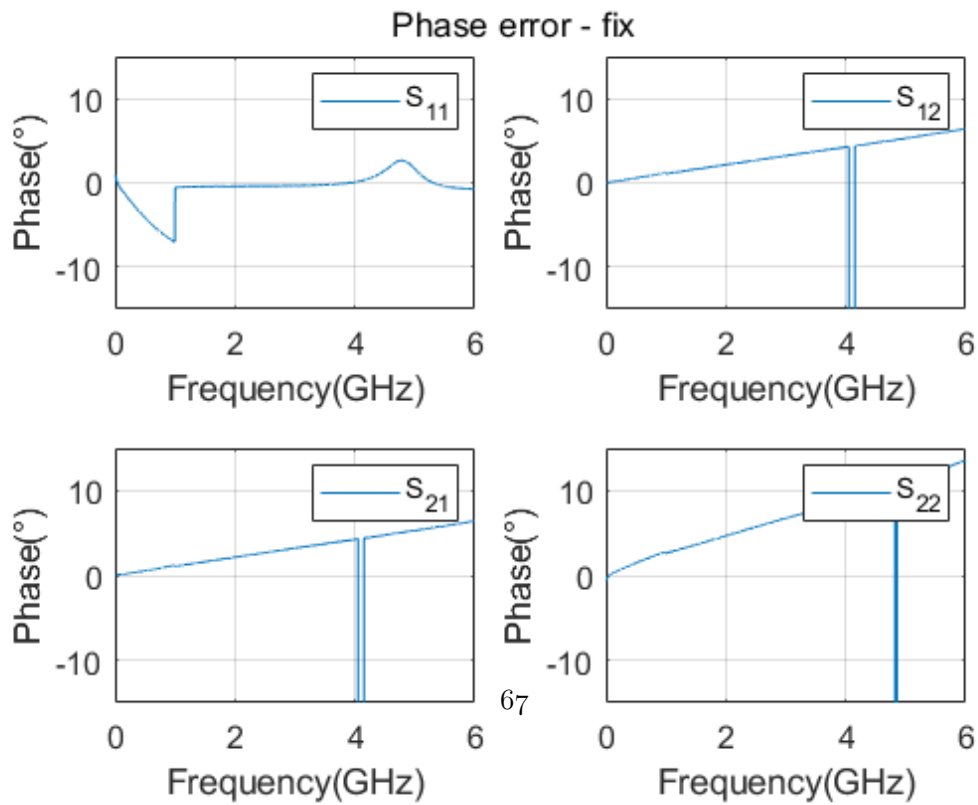


(b)

Figure 1.30: Error on the magnitude for DUT and error network.



(a)



(b)

Figure 1.31: Error on the phase for DUT and error network.

**Example 2: Asymmetric test fixtures**

If the test fixtures are asymmetric the de-embedding of the DUT with TRL/TRM strategy can still be performed, but the scattering parameters of the individual error boxes cannot be obtained. The mathematical evidence of this is in equation A.68. When the number of ports is greater than two, the knowledge of the S-parameters of each fixture has to be known. A solution to this problem will be proposed in section 1.4.

With reference to the first example, the test fixtures are modified as in figure 1.32.

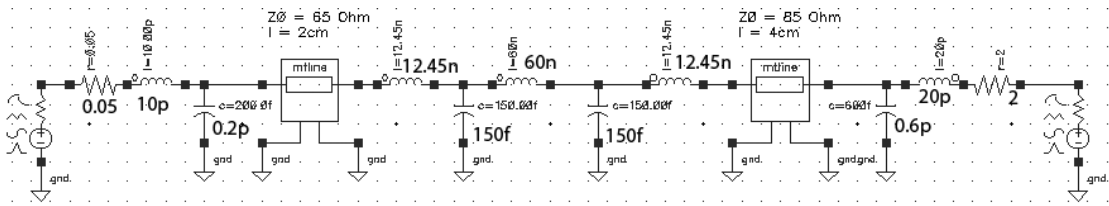


Figure 1.32: Fix-dut-fix simulated structure (asymmetric error networks).

The TRL (and TRM) de-embedding is based on building the same standards as the previous example, considering that as can be seen above the two test fixtures are different. The measurement of the total structure (fixtures and DUT) is shown in figure 1.35. The TRL technique allows accurate de-embedding: simulations show perfect accuracy in extracting the DUT scattering parameters in both cases of symmetric and unsymmetric test fixtures. The individual error boxes can't be obtained in the asymmetric case. The extracted S-parameters of the DUT and the actual ones are compared in figure 1.33.



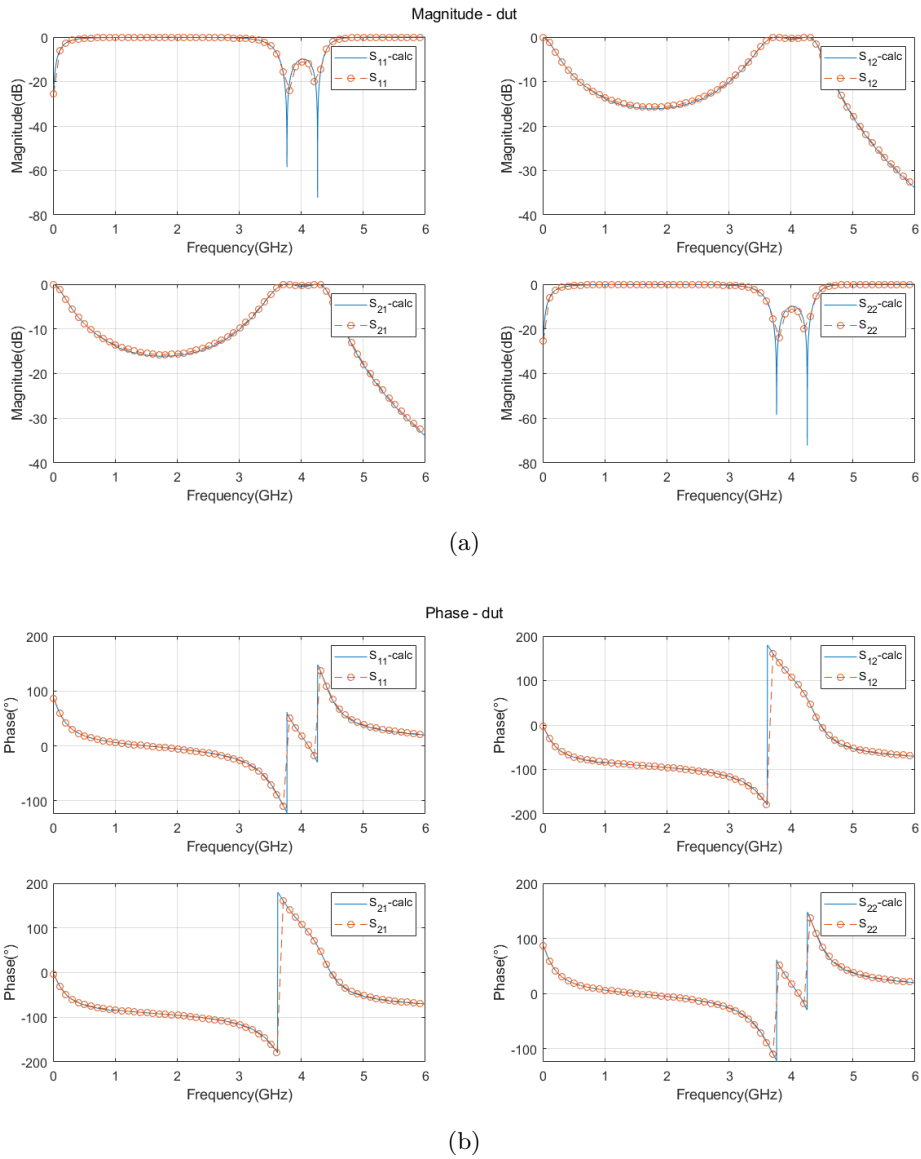
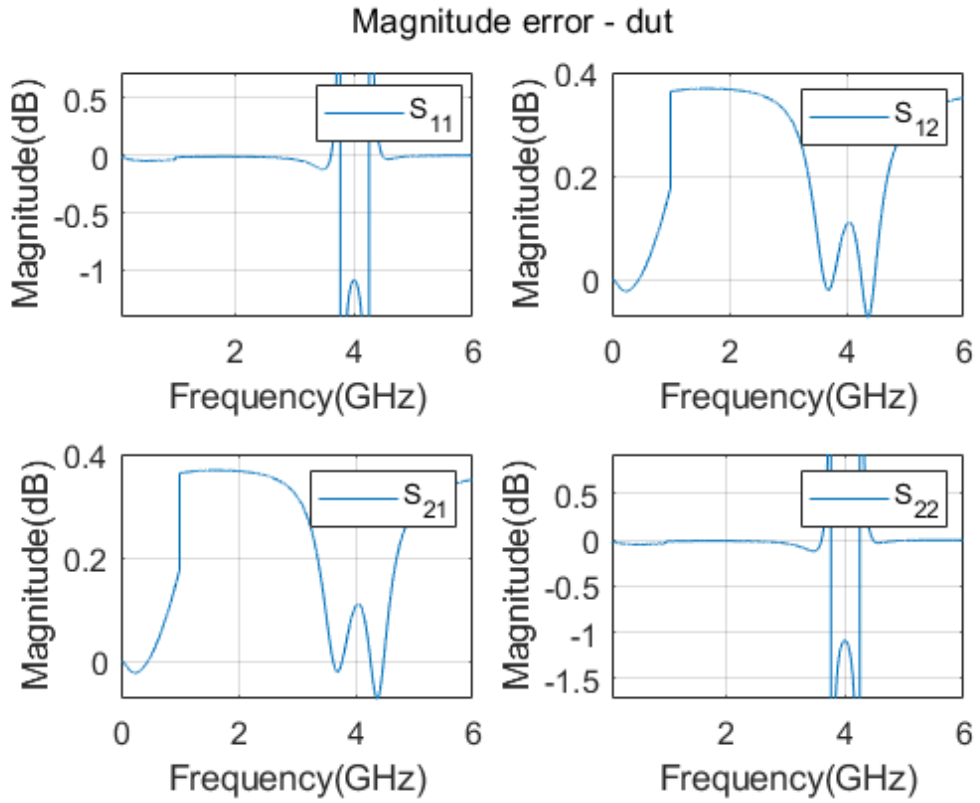
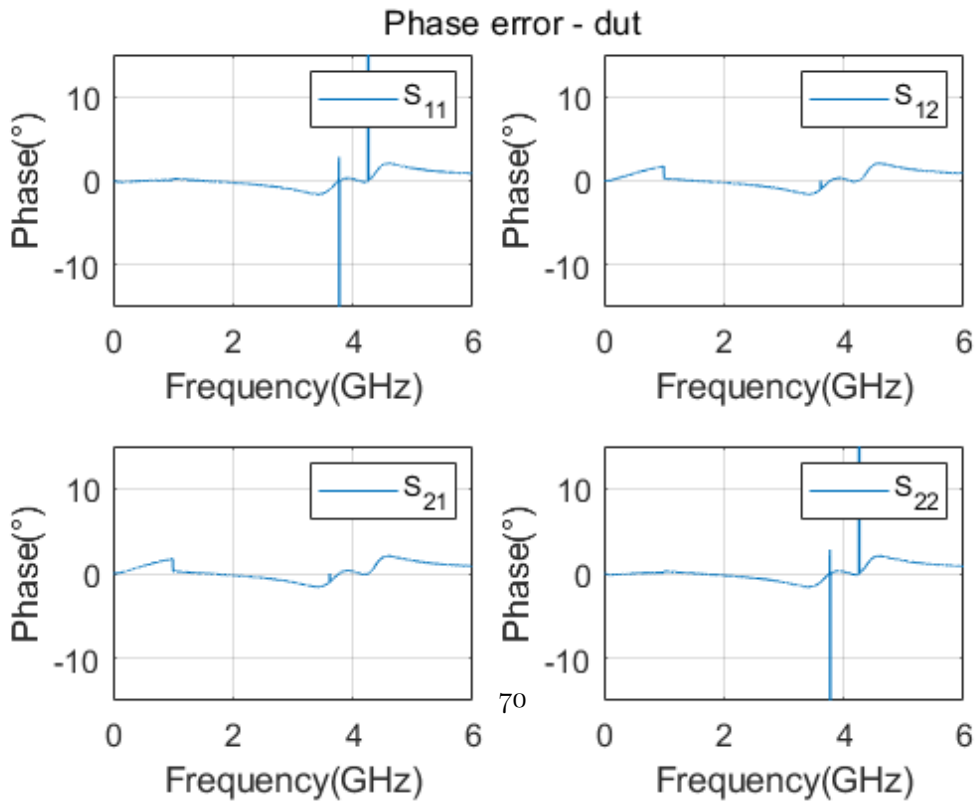


Figure 1.33: Comparison of the DUT de-embedded scattering matrix and the simulated one.



(a)



(b)

Figure 1.34: Error on the DUT.

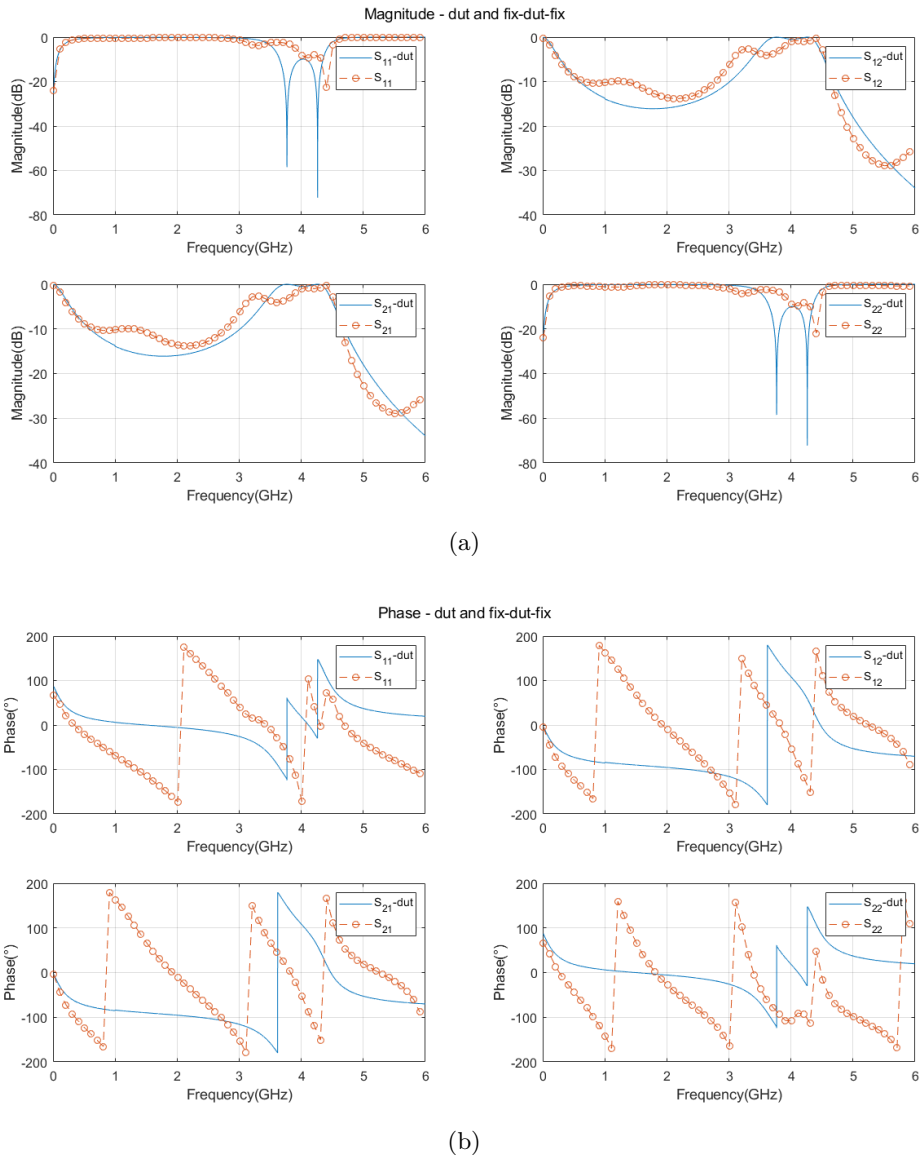


Figure 1.35: De-embedding effect on measured data.

## 1.4 Multi-port de-embedding

In the previous sections, the de-embedding of two-port networks was addressed. In the following chapter, the de-embedding is extended to the case of multi-port DUT. The steps consist in characterizing the test fixtures that are connected to the DUT by using TRL or TRM and then employing de-embedding equations that are suitable for the multi-port case. There are two cases that need to be considered:

- **2N-ports** (4-6-8-...) : In this case the extended de-embedding equations can be applied directly.
- **2N+1-ports** (3-5-7-...) : To apply the algorithm, there is the need to add a virtual DUT port and a virtual fixture, that is represented as an ideal THRU ( $S_{11} = S_{22} = 0$ ,  $S_{12} = S_{21} = 1$ ).

#### 1.4.1 Theoretical derivation

The starting point for extending the de-embedding to the case of 2N ports are the equations of the cascade of two 2N ports scattering matrices  $\mathbf{S}^{(1)}$  and  $\mathbf{S}^{(2)}$ , as in figure 1.36.

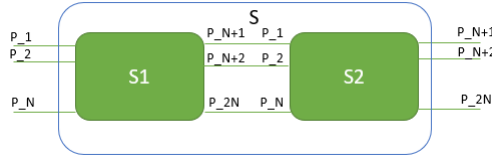


Figure 1.36: Cascade of 2N scattering matrices.

The scattering parameters of the cascade can be computed as follows [29]:

$$\mathbf{S}_{11} = \mathbf{S}_{11}^{(1)} + \mathbf{S}_{12}^{(1)}\mathbf{S}_{11}^{(2)}(\mathbf{I} - \mathbf{S}_{22}^{(1)}\mathbf{S}_{11}^{(2)})^{-1}\mathbf{S}_{21}^{(1)} \quad (1.63)$$

$$\mathbf{S}_{12} = \mathbf{S}_{12}^{(1)}(\mathbf{I} - \mathbf{S}_{11}^{(2)}\mathbf{S}_{22}^{(1)})^{-1}\mathbf{S}_{12}^{(2)} \quad (1.64)$$

$$\mathbf{S}_{21} = \mathbf{S}_{21}^{(2)}(\mathbf{I} - \mathbf{S}_{22}^{(1)}\mathbf{S}_{11}^{(2)})^{-1}\mathbf{S}_{21}^{(1)} \quad (1.65)$$

$$\mathbf{S}_{22} = \mathbf{S}_{22}^{(2)} + \mathbf{S}_{21}^{(2)}(\mathbf{I} - \mathbf{S}_{22}^{(1)}\mathbf{S}_{11}^{(2)})^{-1}\mathbf{S}_{22}^{(1)}\mathbf{S}_{12}^{(2)} \quad (1.66)$$

While  $\mathbf{S}$  terms are complex number in the case of two-port networks, when dealing with 2N port network they are submatrices (NxN) of the overall corresponding 2Nx2N scattering matrix:

$$\mathbf{S}_{11} = \begin{pmatrix} S_{11} & \cdots & S_{1N} \\ \cdots & \cdots & \cdots \\ S_{N1} & \cdots & S_{NN} \end{pmatrix} \quad (1.67)$$

$$\mathbf{S}_{12} = \begin{pmatrix} S_{1,(N+1)} & \cdots & S_{1,2N} \\ \cdots & \cdots & \cdots \\ S_{N,(N+1)} & \cdots & S_{N,2N} \end{pmatrix} \quad (1.68)$$

$$\mathbf{S}_{21} = \begin{pmatrix} S_{(N+1),1} & \cdots & S_{(N+1),N} \\ \cdots & \cdots & \cdots \\ S_{2N,1} & \cdots & S_{2N,N} \end{pmatrix} \quad (1.69)$$

$$\mathbf{S}_{22} = \begin{pmatrix} S_{(N+1),(N+1)} & \cdots & S_{(N+1),2N} \\ \cdots & \cdots & \cdots \\ S_{2N,(N+1)} & \cdots & S_{2N,2N} \end{pmatrix} \quad (1.70)$$

**Right de-embedding** This process consists of de-embed the known  $\mathbf{S}^{(2)}$  from the knowledge of  $\mathbf{S}$  and solving for  $\mathbf{S}^{(1)}$ . This is made by solving the previous equations as reported in appendix A.4.

$$\mathbf{S}_{22}^{(1)} = (\mathbf{S}_{21}^{(2)})^{-1}\mathbf{S}_{22} - (\mathbf{S}_{21}^{(2)})^{-1}\mathbf{S}_{22}^{(2)}(\mathbf{S}_{11}^{(2)}(\mathbf{S}_{21}^{(2)})^{-1}\mathbf{S}_{22} - \mathbf{S}_{11}^{(2)}) \quad (1.71)$$

$$\mathbf{S}_{21}^{(1)} = (\mathbf{I} - \mathbf{S}_{22}^{(1)}\mathbf{S}_{11}^{(2)})\mathbf{S}_{21}^{(2)} \quad (1.72)$$

$$\mathbf{S}_{12}^{(1)} = \mathbf{S}_{12}(\mathbf{S}_{12}^{(2)})^{-1}(\mathbf{I} - \mathbf{S}_{11}^{(2)}\mathbf{S}_{22}^{(1)}) \quad (1.73)$$

$$\mathbf{S}_{11}^{(1)} = \mathbf{S}_{11} - \mathbf{S}_{12}^{(1)}\mathbf{S}_{11}^{(2)}(\mathbf{I} - \mathbf{S}_{22}^{(1)}\mathbf{S}_{11}^{(2)})^{-1}\mathbf{S}_{21}^{(1)} \quad (1.74)$$

**Left de-embedding** This process consists of de-embed the known  $\mathbf{S}^{(1)}$  from the knowledge of  $\mathbf{S}$  and solving for  $\mathbf{S}^{(2)}$ . This is made by solving the previous equations as reported in appendix A.4.

$$\mathbf{S}_{11}^{(2)} = (((\mathbf{S}_{12}^{(1)})^{-1}(\mathbf{S}_{11} - \mathbf{S}_{11}^{(1)})(\mathbf{S}_{21}^{(1)})^{-1})\mathbf{S}_{22}^{(1)} + \mathbf{I})^{-1}(\mathbf{S}_{12}^{(1)})^{-1}(\mathbf{S}_{11} - \mathbf{S}_{11}^{(1)})(\mathbf{S}_{21}^{(1)})^{-1} \quad (1.75)$$

$$\mathbf{S}_{21}^{(2)} = \mathbf{S}_{21}(\mathbf{S}_{21}^{(1)})^{-1}(\mathbf{I} - \mathbf{S}_{22}^{(1)}\mathbf{S}_{11}^{(2)}) \quad (1.76)$$

$$\mathbf{S}_{12}^{(2)} = (\mathbf{I} - \mathbf{S}_{11}^{(2)}\mathbf{S}_{22}^{(1)})(\mathbf{S}_{12}^{(1)})^{-1}\mathbf{S}_{12} \quad (1.77)$$

$$\mathbf{S}_{22}^{(2)} = \mathbf{S}_{22} - \mathbf{S}_{21}^{(2)}(\mathbf{I} - \mathbf{S}_{22}^{(1)}\mathbf{S}_{11}^{(2)})^{-1}\mathbf{S}_{22}^{(1)}\mathbf{S}_{12}^{(2)} \quad (1.78)$$

**DUT de-embedding** The left and right de-embedding equations are used in sequence to de-embed a DUT from the test fixtures. The necessary requirement is the knowledge of the scattering matrices of the two fixtures, represented by  $\mathbf{S}_1$  and  $\mathbf{S}_2$ . For this moment they are assumed to be known, leaving the description of how this is possible to section 1.4.2.

First (figure 1.37) left de-embedding is performed, and  $\mathbf{S}_2$  is obtained, consisting in the cascade of the DUT and the right fixture. In this step,  $\mathbf{S}$  is the total fix-DUT-fix scattering matrix and  $\mathbf{S}_1$  is the left-fixture one, the output is  $\mathbf{S}_2$ . Secondly (figure 1.38), right de-embedding is performed: the DUT is extracted by knowing the right-fixture scattering matrix and the DUT-fix ( $\mathbf{S}_2$  of the previous step).

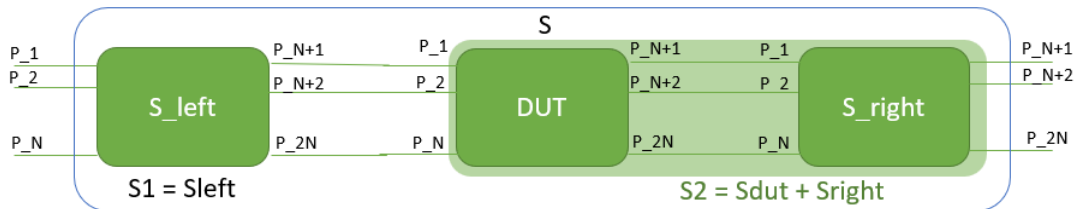


Figure 1.37: First step of the multi-port de-embedding.

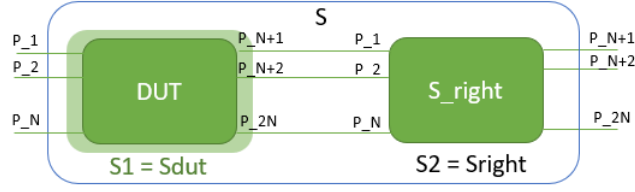


Figure 1.38: Second step of the multi-port de-embedding.

### Extension to odd number of port case

**3 port network** In the case when the number of ports is not even, the left and right de-embedding equations cannot be directly applied. For example, if the DUT has 3 ports, a fictitious fourth port and fourth fixture have to be added. More specifically:

- **Virtual fixture** : This is represented as a THRU connection.

$$\mathbf{F}^{\text{virtual}} = \begin{pmatrix} 0 & 1 \\ 1 & 0 \end{pmatrix} \quad (1.79)$$

- **Total measurement** : The scattering matrix of the FDF is extended with a fourth row and column such that  $s_{41} = s_{42} = s_{43} = 0$  and  $s_{14} = s_{24} = s_{34} = 0$  (no transmission through the fictitious port) but  $s_{44} = 1$  (reflection equal to 1).

$$\mathbf{S}_{\text{total}} = \begin{pmatrix} S_{11}^{FDF} & S_{12}^{FDF} & S_{13}^{FDF} & 0 \\ S_{21}^{FDF} & S_{22}^{FDF} & S_{23}^{FDF} & 0 \\ S_{31}^{FDF} & S_{32}^{FDF} & S_{33}^{FDF} & 0 \\ 0 & 0 & 0 & 1 \end{pmatrix} \quad (1.80)$$

Now the algorithm can be applied. The embedded DUT will have the form:

$$\mathbf{S}_{\text{DUT}} = \begin{pmatrix} S_{11}^{DUT} & S_{12}^{DUT} & S_{13}^{DUT} & 0 \\ S_{21}^{DUT} & S_{22}^{DUT} & S_{23}^{DUT} & 0 \\ S_{31}^{DUT} & S_{32}^{DUT} & S_{33}^{DUT} & 0 \\ 0 & 0 & 0 & 1 \end{pmatrix} \quad (1.81)$$

The last column and row can be eliminated in order to get the S-parameters of the DUT.

**2N + 1 odd-port** In this general case, the FIX-DUT-FIX scattering matrix is equal to the following  $(2N+2) \times (2N+2)$  matrix.

$$\mathbf{S}_{\text{total}} = \begin{pmatrix} S_{11}^{FDF} & \cdots & S_{1,(2N+1)}^{FDF} & 0 \\ \cdots & \cdots & \cdots & 0 \\ S_{(2N+1),1}^{FDF} & \cdots & S_{(2N+1),(2N+1)}^{FDF} & 0 \\ 0 & \cdots & 0 & 1 \end{pmatrix} \quad (1.82)$$

## 1.4.2 Multi-port TRL

As explained in section 1.4.1, to de-embed the DUT S-parameters the knowledge of the scattering matrices of the test fixtures attached to the DUT is required. So the multi-port de-embedding consists of the following two steps:

1. Obtain the S-parameters of the test fixtures.
2. Apply the de-embedding equations of section 1.4.1 according to the even or odd number of ports.

While the second step is a matter of applying a well-defined mathematical procedure, the same can't be said for the first one. In fact, as explained in section 1.2.3 the fixture S-parameters can't be measured directly using a VNA. To solve this problem, the idea is to apply the concept of TRL calibration along with the concept of left/right de-embedding as follows.

If a DUT consists of N-ports, the test fixtures connected to it are represented as N 2-ports networks. The first step is to fabricate the calibration standards of "thru", "reflect", "line(s)", "match" for a selected 2-port fixture. This structure is realized on the same PCB of the DUT or another one, by building replicas of the selected fixture along with the standards above. In this way the S-parameters of the fixture are obtained, after the TRL (TRM) procedure is applied. Secondly, N-1 "thru" are fabricated by connecting back-to-back a replica of the fixture characterized by the TRL in the previous step and the other ones. The S-parameters of the "thru" structures are measured by the VNA. The equations for one-side (left or right) de-embedding are applied and the scattering matrices of the remaining N-1 fixtures can be derived. The proposed algorithm is better clarified with an example.

**4-port de-embedding** Let's consider an IC, mounted on a PCB, that is representing a 4-port DUT. This is depicted in figure 1.39.



Figure 1.39: DUT with four ports.

After a SOLT calibration to move the reference planes up to the tips of the coaxial cables of the measurement system, the VNA is connected to the ports numbered from one to four to measure the fix-DUT-fix S-parameters. The calibration structure required is shown in figure 1.40.

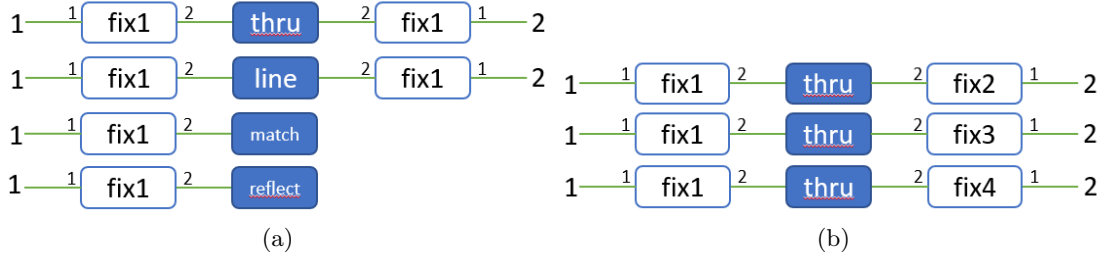


Figure 1.40: Schematic representation of multi-port TRL calibration kit.

The fixture "1" is fully characterized by TRL. Later, it is employed as a pivot point for realizing the "thru" structures with the fixture "2", "3" and "4". The left d-embedding is applied to derive the scattering parameters of the remaining fixtures. Finally, the multi-port de-embedding equations are used to obtain the DUT scattering matrix.

### 1.4.3 Validation of the method: de-embedding of an op-amp S-parameters

The goal of this section is to validate the discussed method with experimental measurements after the setup is described in a SPICE simulation. The scattering parameters of a general-purpose op-amp (TS912) in voltage follower configuration have to be obtained by de-embedding the effect of the test fixtures that are required for the dc-bias of the IC and the VNA connection.

#### Test setup description

The system is shown in figure 1.41.

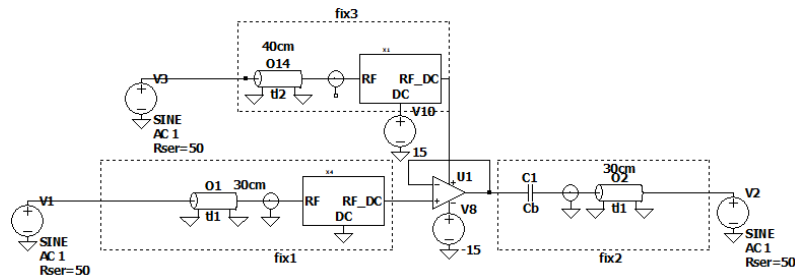


Figure 1.41: Complete system made up of the DUT and three asymmetric fixtures.

It is shown the DUT, fed by a dual supply voltage, and three different and asymmetric test fixtures required to connect the VNA. The VNA ports are represented by the voltage sources  $V_1$ ,  $V_2$ ,  $V_3$ , and a SOLT calibration is performed up to that point: in this way, the reference plane of the measurements is moved up to this level. The error networks are represented by an rg-58 cable, a female SMA connector mounted on the PCB where the DUT is placed, and on board bias-T and dc-block networks. These two are employed to



supply the DUT and to bias the input port properly while avoiding any DC voltage component reaching the VNA ports. The second tier of calibration requires the de-embedding of these test fixtures. Before entering in the details, some words have to be spent on the design of a bias-T with lumped elements, that can be soldered on the PCB.

### Lumped element bias tee

**Bias tee basics** A bias tee is an electric circuit used for different applications, the most common to add DC supply signal to RF paths, providing power or bias voltages to transistors, diodes or low noise and power amplifiers. From an ideal perspective, a bias-T can be schematized as in figure 1.42. From a network analysis point of view, it consists of a three port device, usually labeled as shown in the picture. Port 1 to 3 is the RF path, port 2 to 3 is the DC path. The capacitor  $C_1$  between the **RF** and **RF+DC** port is coupling a radiofrequency signal from the RF input to the output, blocking the DC, while the inductor  $L_1$  is an RF block but it's acting with low impedance at DC, allowing DC to be coupled to the output. While  $C_1$  and  $L_1$  are absolutely critical for the RF path response,  $C_2$  is optional and its purpose is supply decoupling.

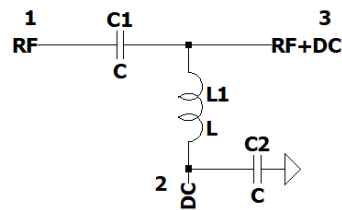


Figure 1.42: Schematic of a bias tee with idealized elements.

Ideally, the RF path will block any DC component in the RF path, passing only signals that are not at 0 Hz frequency; while the DC path will pass DC only and block any signal which is not DC. For a real device, this behavior can't be realized. The first reason is that the impedance to RF signals of an inductor and capacitor is  $X_L = \omega L$  and  $X_C = \frac{1}{\omega C}$ , so they can't act as perfect open and short circuits at radiofrequency. The second, and most important, reason is that real components have parasitics: this will limit the frequency bandwidth in which the device behaves as wanted. S-parameters are usually employed to design and characterize a bias tee, as they can be used to ensure that the RF path is passing the radiofrequency signal while the DC does not at RF frequencies in the design bandwidth. The main specifications for a bias tee are described below [44]:

- **Insertion loss of the RF path:** Ideally,  $|S_{31}|$  is equal to 0 dB. In the real case,  $S_{31}$  depends on  $C_1$  response, and it is representing the insertion loss of the RF path which shall be kept low to avoid attenuation of the RF signal. The low frequency limit is determined by the value of  $C_1$ , while the upper is depending on the parasitics of the components. The upper limit is identified by the crossover frequency, when  $|S_{31}|$  drops by 3 dB.

- **Power limitation:** Another impairment is the amount of DC voltage and current that can be applied to the DC path: this is determined by the rated voltage of the capacitors  $C_1$  and  $C_2$  and on the maximum peak and RMS current of the inductor  $L_1$ .
- **Return loss:** Another quantity that should be controlled is the return loss at the RF port, defined as  $-20\log_{10}|S_{11}|$ , which shall guarantee matching in the design bandwidth.
- **Isolation:** The isolation, defined as  $-20\log_{10}|S_{21}|$ , is representing the attenuation of the RF signal at the DC port which shall be kept as high as possible.

The most critical aspect when designing a bias-T from lumped elements is represented by the parasitics of the passive elements that cause self-resonance. These make it difficult to achieve high bandwidth with a simple design as figure 1.42.

**Self-resonant frequency** Lumped elements such as inductors and capacitors are characterized by a self-resonant frequency. "Resonance" is not implying that capacitors and inductors can oscillate by themselves, but is rather referring to a characteristic in the frequency response of the component. For an inductor, the self-resonant frequency is that at which the inductance provided by the coil of insulated wire is resonating with the parasitic capacitance of the inductor. At this frequency the device will show a large impedance, looking like an open circuit. The equivalent circuit of a real inductor can be represented as in figure 1.43.

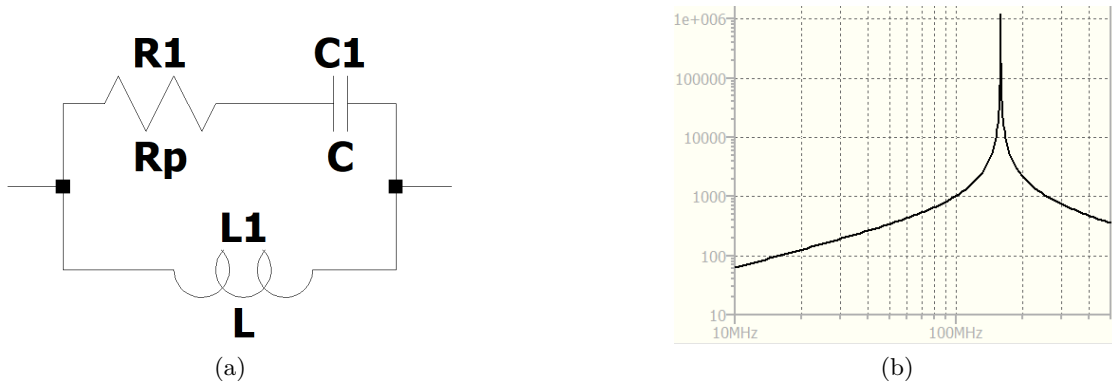


Figure 1.43: Schematic of a real inductor. Impedance ( $\Omega$ ) for  $L = 1 \mu H$ ,  $C = 1 pF$ ,  $R = 100 m\Omega$ . The SRF results around 157 MHz.

This representation accounts for the fact that any real can be thought as an ideal one with in series a resistor (finite wire resistance) and a capacitor in parallel with it (parasitic capacitance). The capacitive contribution is coming from the tiny parasitic capacitances between the windings that made up the coil. At high frequency, the impedance of the capacitor is much lower than the impedance of the inductor, so the behavior of the impedance

resembles like a capacitor. Thus the inductor does not function as an inductor beyond this frequency. When selecting an inductor to be used in RF system, the self-resonant (SRF) frequency must be higher than the usage frequency. The SRF corresponds to the condition  $X_L = X_C$ , or:

$$2\pi(SRF)L = \frac{1}{2\pi SRF C}, SRF = \frac{1}{2\pi\sqrt{LC}} \quad (1.83)$$

Similarly to inductors, also capacitors have a SRF after which their behavior becomes inductive. The equivalent circuit of a real capacitor can be represented as in figure 1.44. The parasitic inductance is due to the terminals, while the resistance is representing the one of the plates.

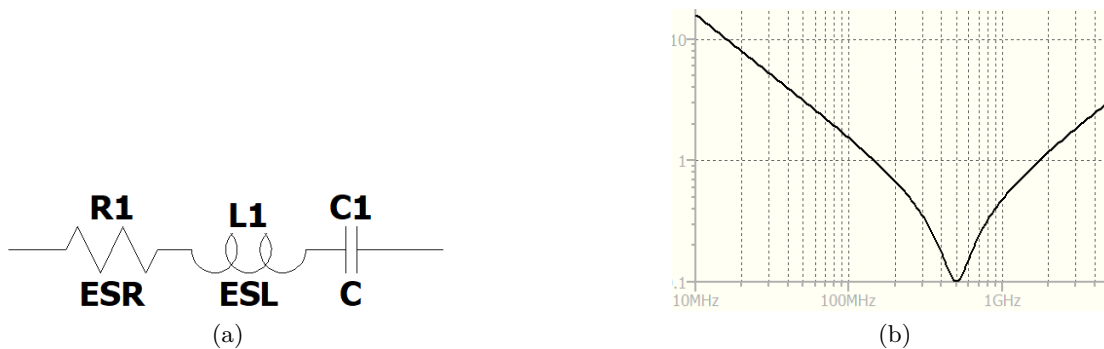


Figure 1.44: Schematic of a real capacitor. Impedance ( $\Omega$ ) for  $L = 100 \text{ pH}$ ,  $C = 1 \text{ nF}$ ,  $R = 100 \text{ m}\Omega$ . The SRF results around 500 MHz.

Generally, the inductor parasitics are of more importance than the capacitor ones, which are closer to the ideal behavior. This means that to realize an RF choke or an RF decoupling network over a broadband a given number of inductors, with increasing SRF, are placed in series [44]. In fact, a single inductor can't cover the entire frequency bandwidth. For an RF decoupling network, the smallest value inductor is connected closer to the RF  $50 \Omega$  path, and progressively larger values are connected to the DC port [45]: this will guarantee a smooth frequency crossover from one inductor to the next. Typically, one inductor of the series can cover one octave/decade in frequency [45].

**Design procedure** The goal is to design a bias tee made with lumped elements, working in the bandwidth 150 kHz - 1 GHz. The first step is to design the circuit using ideal elements, according to the topology of figure 1.42. The design is made by considering a system with a reference impedance of  $Z_0 = 50 \Omega$ , even if in the operating conditions it is unlikely that the DC and DC+RF port will be loaded with  $50 \Omega$ . In fact, the DC port will be terminated in a low impedance of the DC source connected to it, while the DC+RF port is at the input of an active device, which impedance shows a large real part with a capacitive behavior. The values of  $L_1$  and  $C_1$  are computed according to the cut-off frequency of the design. The upper cut-off frequency for the low pass DC path has to be

lower than the lower cut-off frequency of the high pass RF path. Thus, in the RF band, the inductor is regarded as an open circuit and the cut-off frequency for the RF path is given by  $f_c = \frac{1}{2\pi Z_0 C}$ . To have a lower frequency of  $f_l = 150 \text{ kHz}$ , then:

$$\frac{1}{2\pi f_l C} \ll Z_0, C \gg \frac{1}{2\pi f_l Z_0} = 21 \text{ nF} \quad (1.84)$$

So it is chosen  $C_1 = 220 \text{ nF}$ . Regarding the inductor in the DC path, assuming that  $C_1$  still behaves as an open circuit, the cut-off frequency can be computed as  $f_l = \frac{1}{2\pi \frac{Z_0}{L}}$ . For

an upper frequency of  $f_h = 1 \text{ GHz}$ , and to account for the available inductor values, then the inductor value is chosen as  $L_1 = 330 \mu\text{H}$ . From this first choice of the elements the transmission and reflection scattering parameters at the RF port are represented on the left of figure 1.45. It is possible to notice a flat response and good matching in the design bandwidth. According to the datasheet, the minimum SRF for the inductor is 2.6 MHz, leading to a parasitic capacitance of value  $C = \frac{1}{(2\pi \text{SRF})^2 L} = 11.3 \text{ pF}$ . When taking into account this parasitic, the response becomes the one at the right. The -3 dB cut-off frequency for the RF path results close to 500 MHz and the  $S_{11}$  is having resonance: this behavior is unwanted as it will cause a poor time-domain response, which is particularly important when transmitting fast pulses through the bias-T.

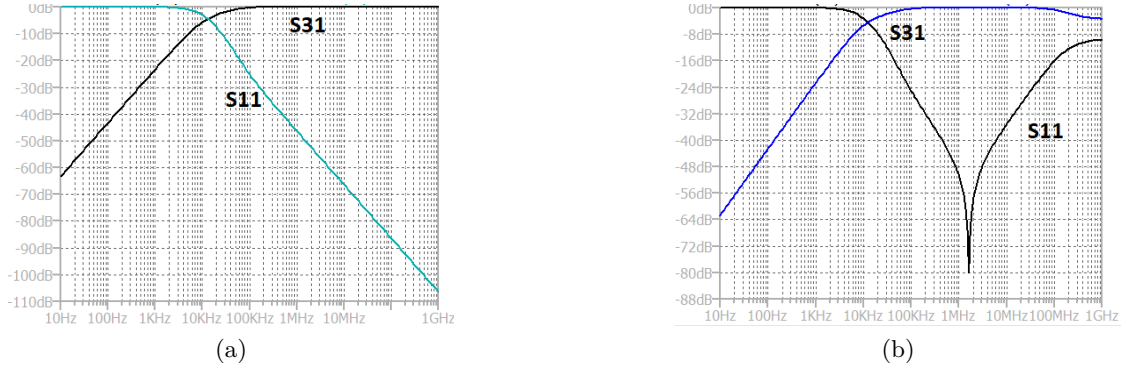


Figure 1.45: S-parameters for the initial design of the bias-T. The right one accounts for the inductor parasitics.

From this initial analysis, the required  $L_1$  and  $C_1$  values are identified, but when parasitics are included the non-ideal behavior of the bias-T shows up. The next step for the design is then to cope with the impairments caused by the parasitics. As a starting point, the topology of the bias-T has to be picked. The chosen strategy consists of the use of three different sections, where each one covers a little more than one decade in frequency. The single section is made up of a series inductor and a shunt capacitor, resembling a low-pass filter [45]. However, this will set up other resonances caused by the interaction between the different reactive elements. Each L-C cell is including resistors as

damping elements: these are called "de-Q" resistors and are used to eliminate resonances, their value is experimentally determined. The final design is shown in figure 1.46.

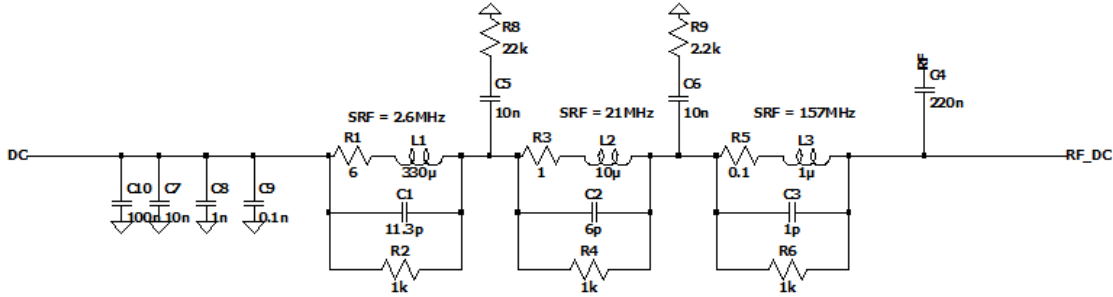


Figure 1.46: Final design of the bias-T.

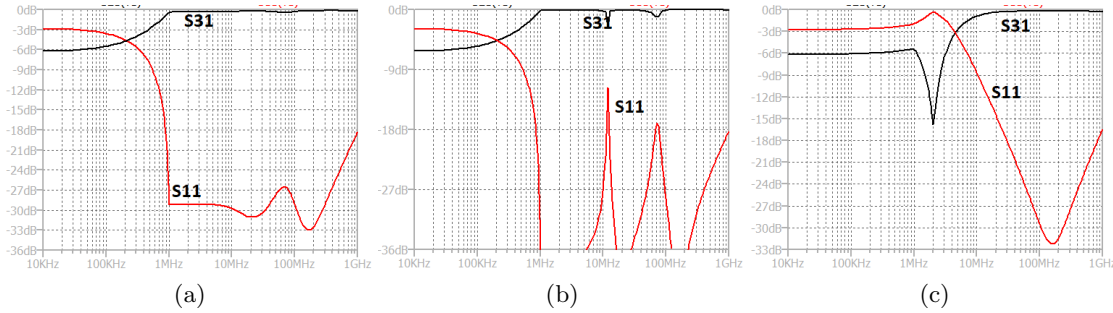


Figure 1.47: S-parameters when tuning the values of the elements in the bias-T design.

The inductor  $L_1$ , being the one with the lowest SRF, is critical for the low-frequency response.  $L_2$ ,  $L_3$ , and  $C_1$  are affecting the high-frequency range.  $C_5$ ,  $C_6$  are decoupling capacitors, while  $R_2$ ,  $R_4$ ,  $R_6$ ,  $R_8$  and  $R_9$  are the de-Q resistors. The capacitors  $C_7$  to  $C_9$  are shorting to ground any RF component at the DC port. Their presence is needed as shown in figure 1.47: the left of the response achieved with the final design. The center figure is corresponding to the case when  $R_2$ ,  $R_4$ , and  $R_6$  are not present, while the rightmost one is corresponding to  $R_8 = R_9 = 0 \Omega$ .

### De embedding results

To provide a comparison result between the de-embedded S-parameters and the DUT one, the opamp is simulated first. It consists of a TS912 from STMicroelectronics of which the model is available. The DUT circuit is shown on the left of figure 1.48. It consists of the opamp in voltage follower configuration, biased on the non-inverting pin with 1 V DC supply voltage, provided with a 3 V power supply. The simulated opamp includes the baseband model available from the manufacturer along with an high-frequency network used to describe its out of band behavior [46], useful for the computation of the

S-parameters. The bias tee and the DC block used in the DUT simulation are ideal, having a behavior as described in the previous section.

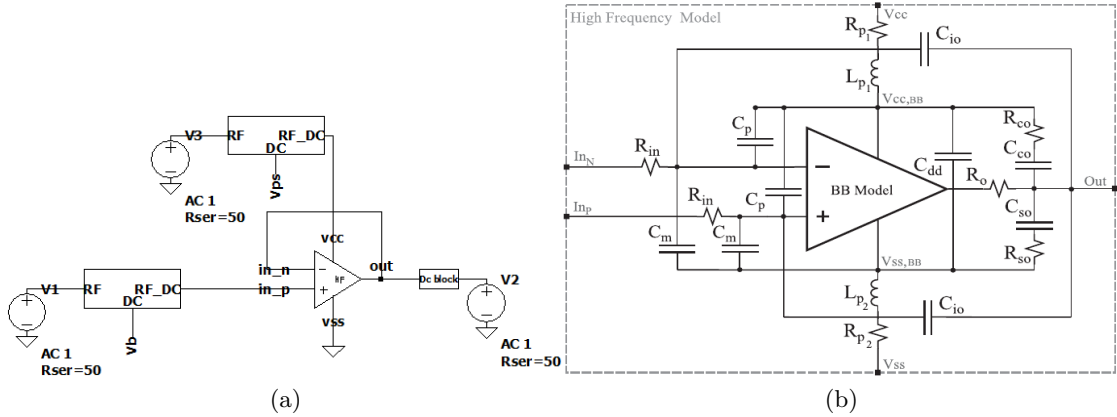


Figure 1.48: Schematic for the DUT measurements. On the right, the high frequency network used to model the parasitic elements between the terminals [46].

First, the scattering parameters of the fixture connected to the port 2 of the DUT are derived. The strategy chosen is the TRM up to 200 MHz, and TRL from this frequency up to 1 GHz. According to what is described in section 1.3.3, the single line standard required is chosen for an FR4 board ( $\epsilon_{eff} \simeq 3.3$ ) of 68.81 mm long, such to provide a phase shift of  $30^\circ$  at 200 MHz and  $150^\circ$  at 1 GHz. The match standard is non-ideal, and it is represented by a  $50 \Omega$  resistor with a series inductance of 1 nH and a shunt capacitance of 0.2 pF. This will limit the application of the TRM up to 1 GHz, as the match standard is no more presenting a  $50 \Omega$  impedance. Also, the line standard is presenting a non-ideality, that is a 2 % variation of its characteristic impedance ( $51 \Omega$  instead of  $50 \Omega$ ). Re-normalization on the S-parameters is made to take into account the mismatch. To apply the proposed multi-port strategy, the combination of TRM and TRL is applied to the error network "2". The standards required for the de-embedding are shown in figure 1.49, instead the results are in figure 1.51 and 1.56. The next step is to consider two other de-embedding calibration structure that allow to get the S-matrices of the fixture "1" and "3". As explained in the previous section, these consists of two "thru" of fixture "2" with fixture "1" and "3" (figure 1.50). Fixture "1" and fixture "3" S-parameters are obtained by left de-embedding the obtained fixture "2" scattering matrix from the "thru". The S-parameters of the fixture "3" are shown in figure 1.52. Now, all the matrices are known, so the opamp scattering parameters can be obtained from the total measurement.

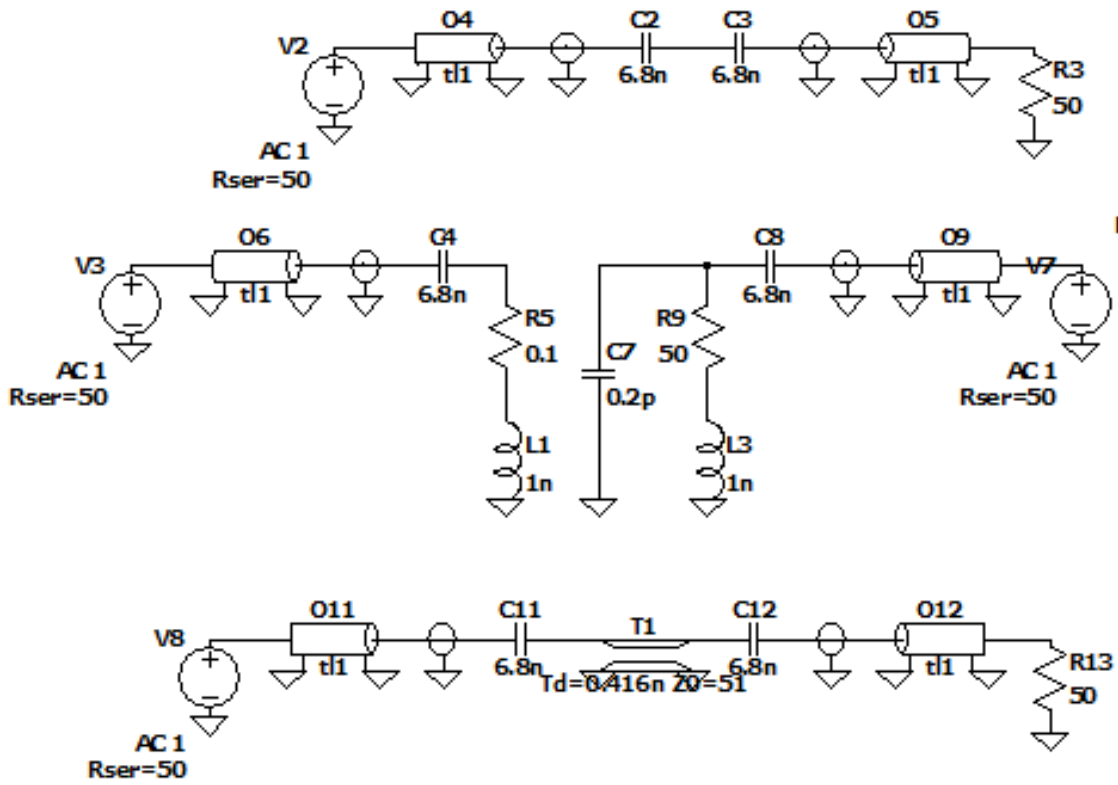


Figure 1.49: Standards required to obtain the S-matrix of the fixture "2". In the characterization of this fixture, the "reflect" and "match" are one-port measurements.

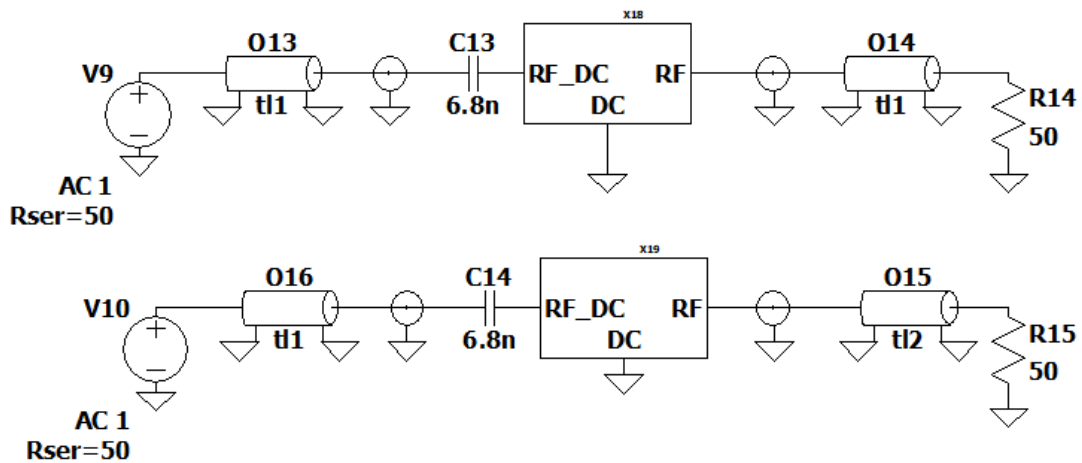
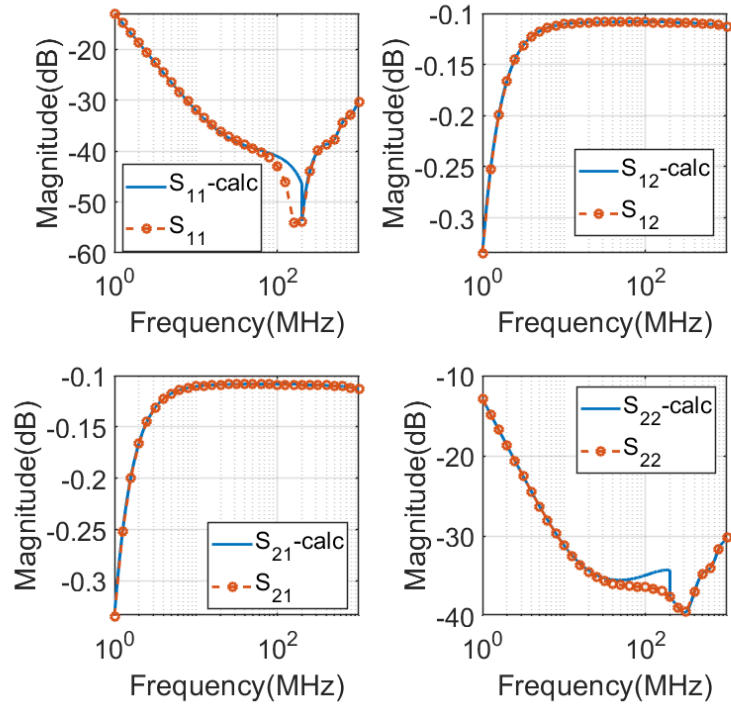
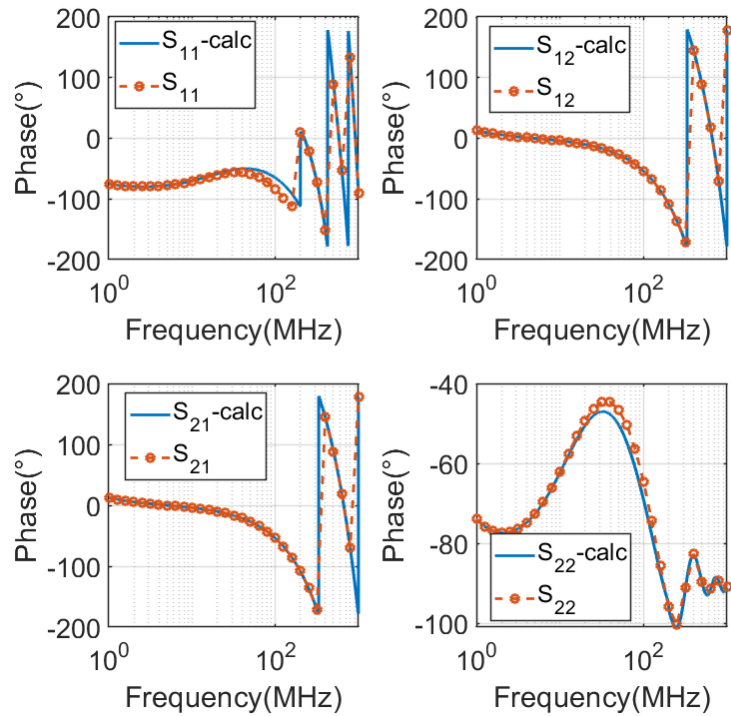


Figure 1.50: "Thru" standards required to obtain the S-matrix of the fixture "1" and "3".



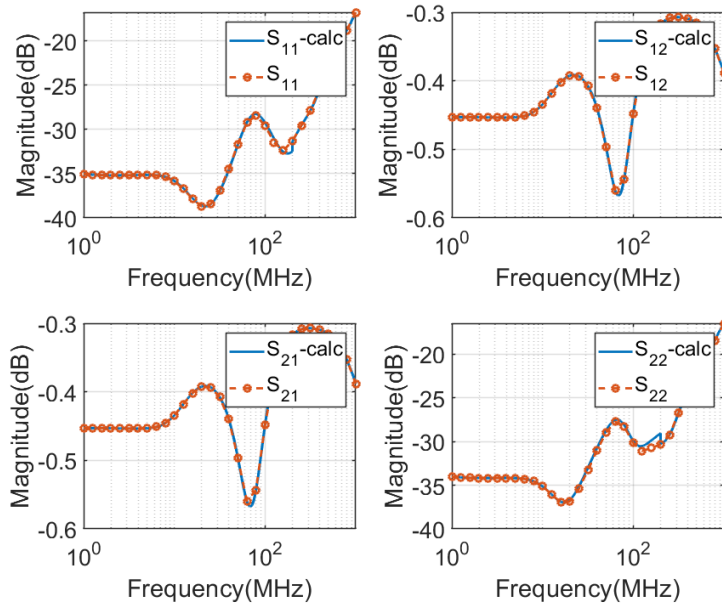
(a)



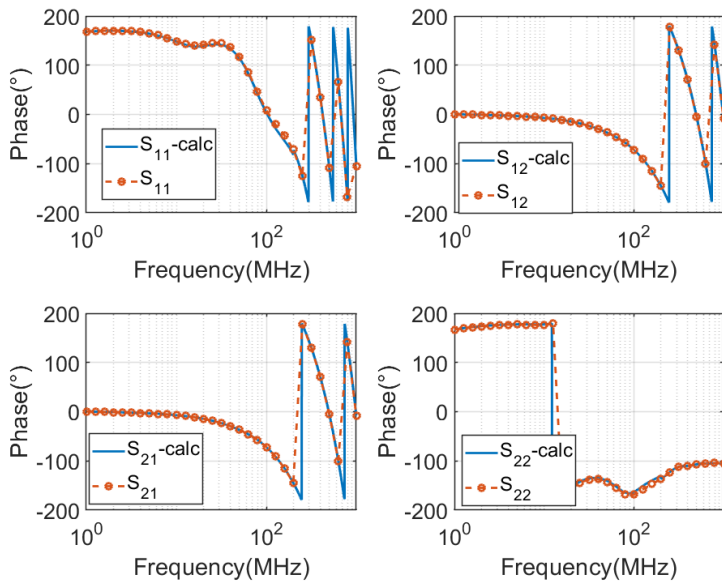
(b)

Figure 1.51: S-parameters of the fixture "2" compared with directly simulated.



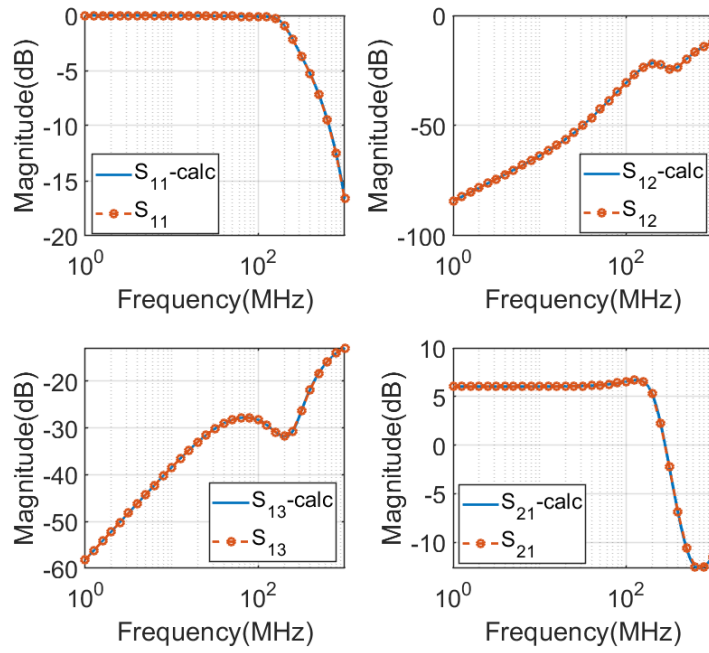


(a)

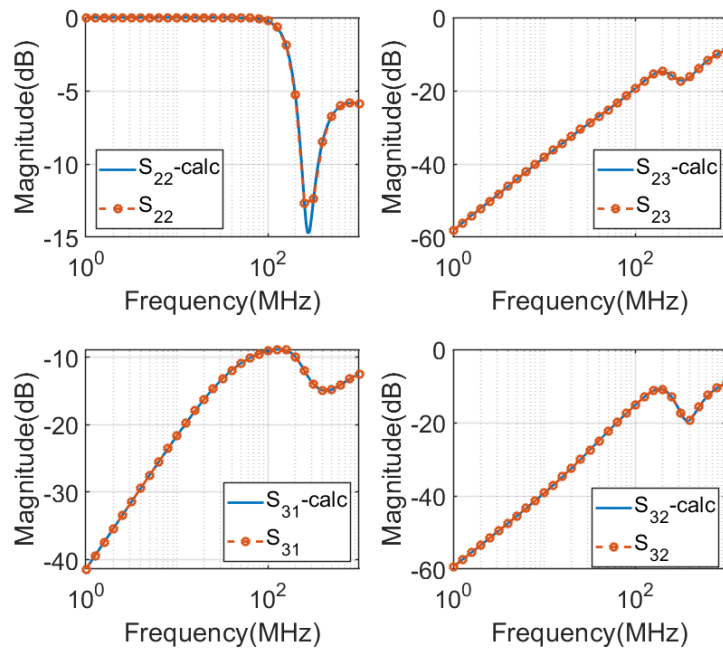


(b)

Figure 1.52: S-parameters of the fixture "3", obtained by left de-embedding the fixture "2" from the "thru" of them, compared with directly simulated.



(a)



(b)

Figure 1.53: S-parameters of the DUT(1).

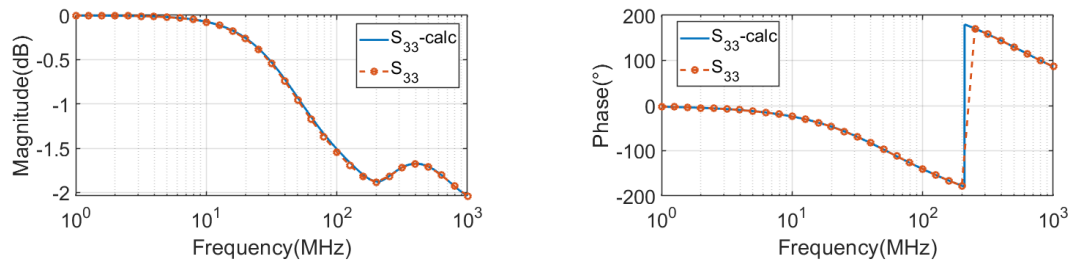
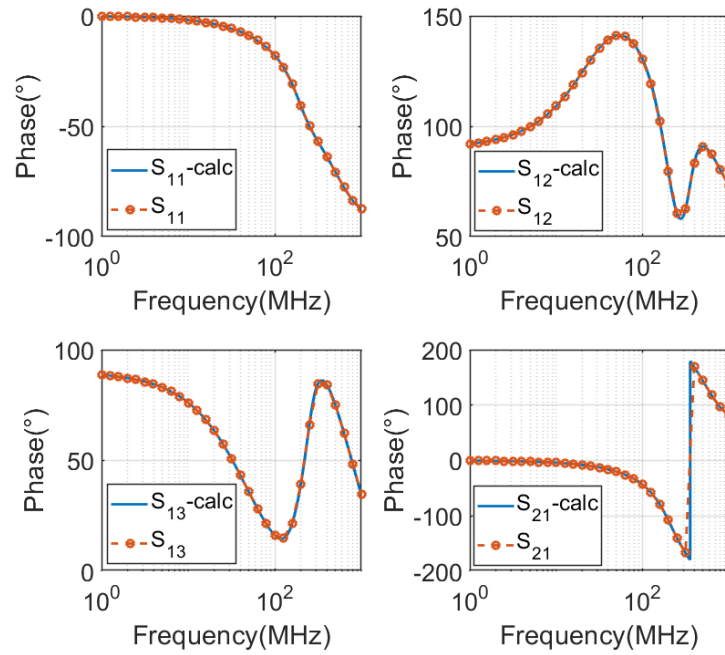
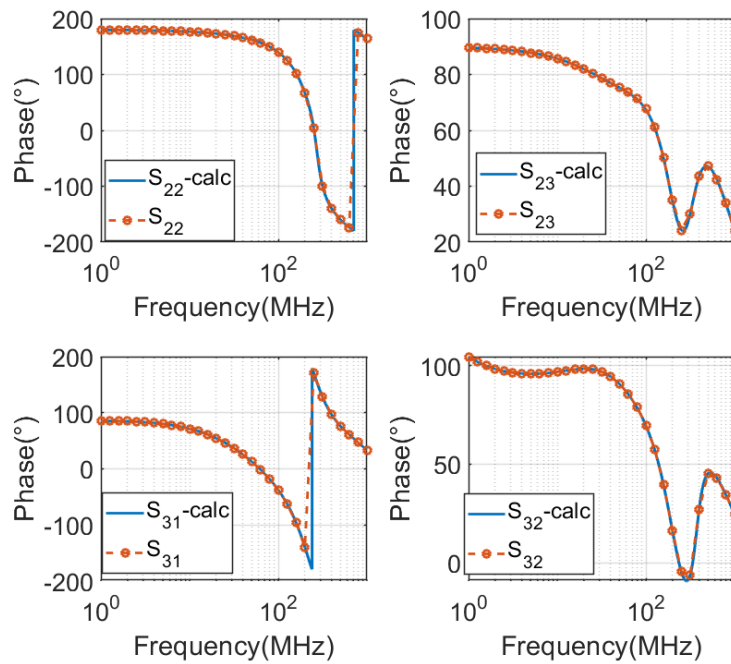


Figure 1.54: S-parameters of the DUT(2).



(a)



(b)

Figure 1.55: S-parameters of the DUT(3).

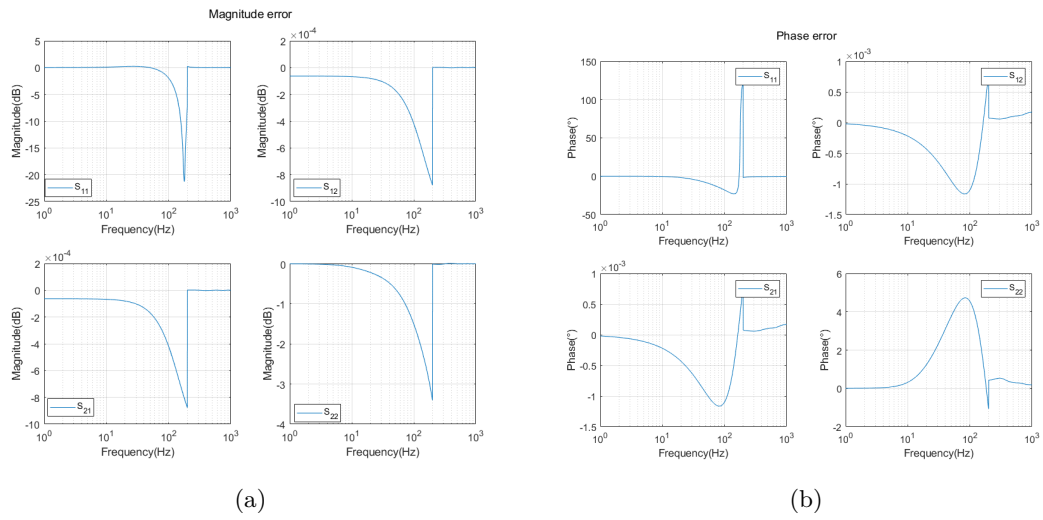


Figure 1.56: Error on the magnitude and phase for the fixture "2".



## Chapter 2

# De-embedding on real devices

### 2.1 Introduction

This chapter is dedicated to the application of the de-embedding algorithms proposed in chapter 1 to measurements made on real devices. The VNA at disposal is the *P9371A Keysight Streamline USB Vector Network Analyzer, 6.5 GHz* [47]. The instrument is calibrated with an *N7551A* electronic calibration (ECal) module. The frequency range was set from 300 kHz to 6.5 GHz.

### 2.2 Measurement on a 20 dB attenuator

The DUT is a characterized, stable 20 dB attenuator. The DUT is embedded within two test fixtures. Fixture "1" identifies the crimped 36 cm RG-58 cable, and fixture "2" identifies the cable of VNA kind of length 100 cm. To check the correctness of the de-embedding algorithm results, the attenuator is directly connected to the VNA cable ends where the SOLT calibration routine via an "ECal" module has been performed. This will provide the DUT S-parameters which will represent the expected results after the de-embedding application, shown in figure 2.1.

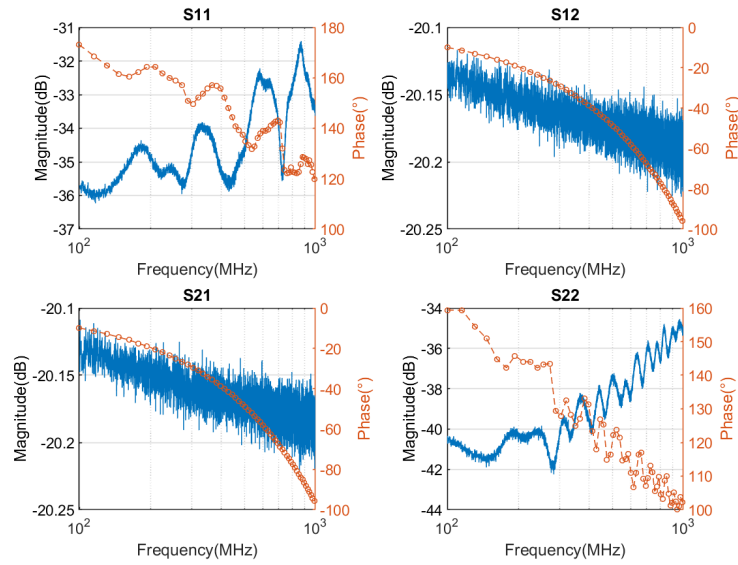


Figure 2.1: Measured S-parameters of the 20 dB attenuator.

The structures that are measured for the de-embedding are schematized in the block diagram of figure 2.2, where an emphasis is made on the different transitions required to connect each object with the others: their presence is inevitable and the error introduced on the S-parameters of the fixtures only will be considered. For the sake of clarity, each measure is provided with a unique alphabet letter as described in table 2.1.

<b>A</b>	Complete measurement of the fix1-DUT-fix2 structure
<b>B</b>	fix1 and fix2 closed on an SMA match termination
<b>C</b>	fix1 and fix2 closed on an SMA short termination
<b>D</b>	Thru connection between fix1 and fix2
<b>E</b>	Thru connection between fix2 and an equal structure

Table 2.1: Description of the measurements made for the TRM application.



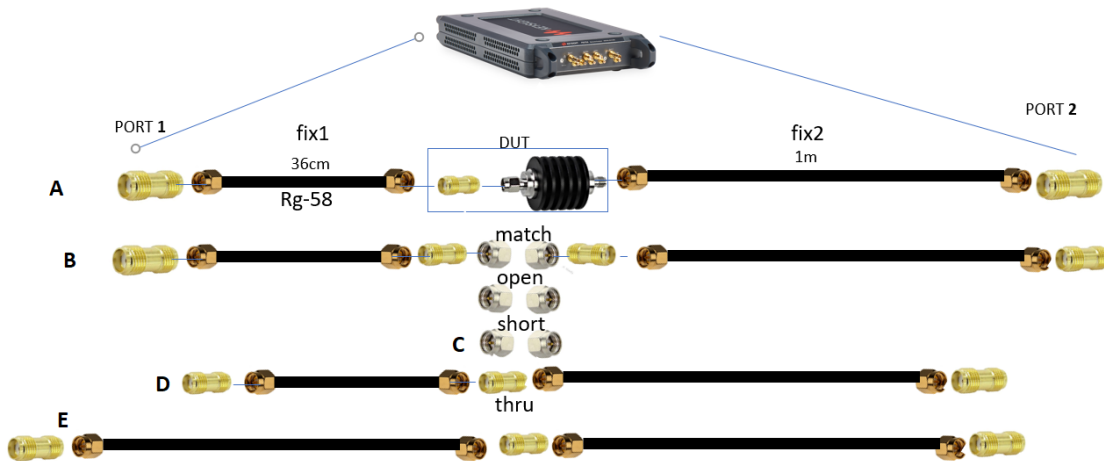


Figure 2.2: Schematic representation of the performed measurements.

For this set of measurements, the DUT S-parameters are obtained by applying the TRM in two different ways. The first one corresponds to the procedure described in appendix A.3, the second way is anticipating the de-embedding strategy for  $\geq 2$  port DUT with asymmetric test-fixtures developed in section 1.4, applied in the special case of a two-port DUT. In the first case, TRM is applied in the classical way. In the second one, the proposed strategy of left de-embedding to characterize both the two asymmetric error networks, required for multi-port DUTs, is used. Each strategy requires different measurements, which are reported in table below.

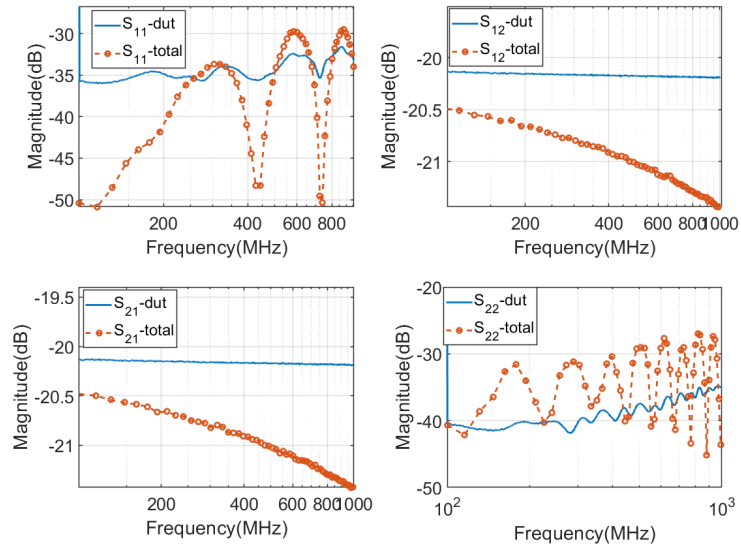
	A	B	C	D	E
Strategy 1	✓	✓	✓	✓	\
Strategy 2	✓	✓(fix2 only)	✓(fix2 only)	✓	✓

Table 2.2: List of the measurements required for each strategy.

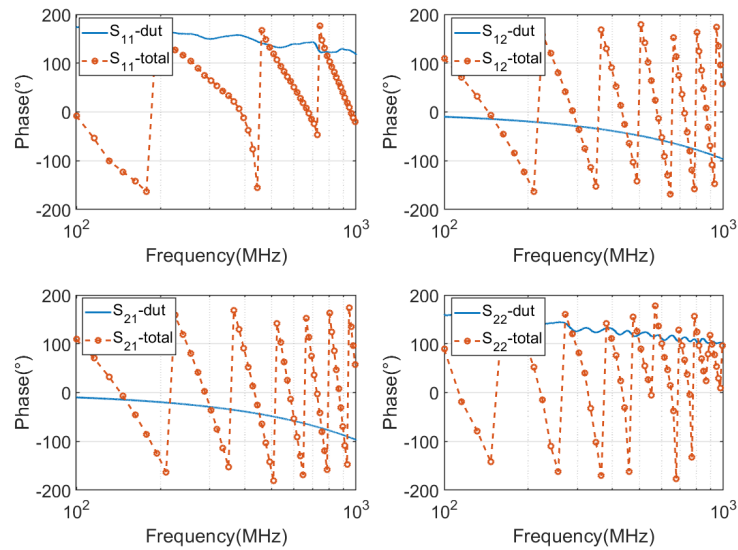
In the first strategy, TRM is applied once to fixture "1", fixture "2" and DUT, resulting in the S-parameters of the DUT only. In the second case, the TRM is applied first to fixture "2", then with an additional "thru" measurement and left de-embedding (as shown in section 1.4 and appendix A.4) also the fixture "1" S matrix is obtained, finally the DUT is de-embedded from the total measurements with left and right de-embedding. The fix-DUT-fix scattering matrix is compared with the DUT only one in figure 2.3.

An **important** point on the built standards has to be clarified. This is about the use of the SMA adapters, needed for connecting the fixtures with each other and to connect the VNA channels to them. In particular, the SMA-female/SMA-female adapter S-parameters have been directly measured, and are reported in figure 2.12. This adapter is behaving as a perfect "thru" (no reflection, all transmitted), apart from introducing a linear phase shift in the transmission parameters. The phase shift is measured and is equal to  $17^\circ$  at 1 GHz. The use of this connector will introduce an error in the de-embedding compatible with the effect of a finite length thru (which from a simulation perspective produces the

effects seen in section 1.3.7). This error will be better explained after the de-embedding is performed.



(a)



(b)

Figure 2.3: Total (A) and DUT only S-parameters.

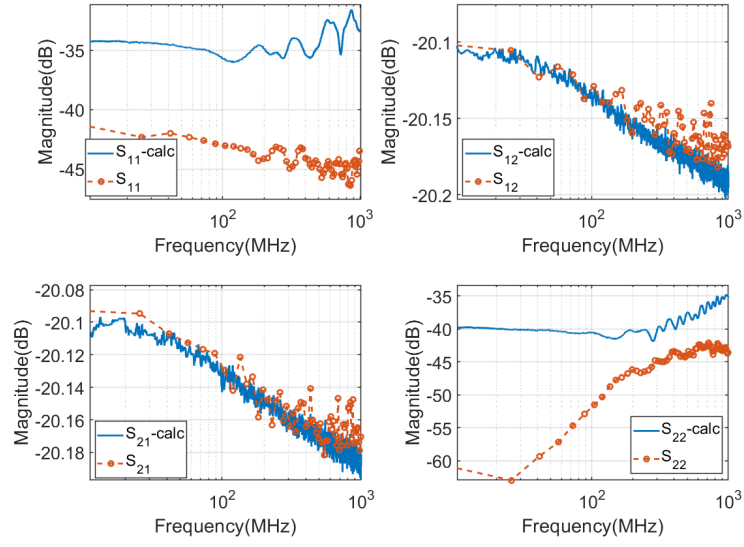
### 2.2.1 Strategy 1

In this case, only the DUT S-parameters can be obtained, by performing the measurements of the three TRM standards. The TRM procedure is applied and de-embedded DUT S-parameters are compared to the measured ones in figure 2.4. It can be seen that while there is a great difference in the  $s_{11}$  and  $s_{22}$ , a good matching is achieved in the transmission parameters ( $s_{12} = s_{21}$ ). The error on the return loss is due to the finite directivity of the VNA in the measurement bandwidth, which will be better explained in the "Strategy 2" case. Instead, the phase error on the DUT is clearly deriving from the effect of the finite THRU used in the de-embedding. The error matches exactly the measurement of the phase shift introduced by the SMA-female/SMA-female adapter (figure 2.12). In fact, the THRU standard is setting the position of the reference plane for the de-embedded results. This can be better described with illustration 2.5.

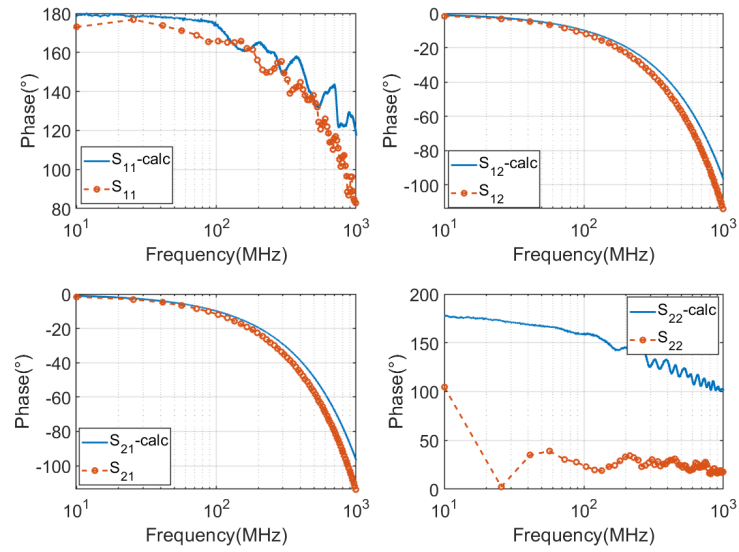
The green rectangle highlights the actual fixture that has to be removed from the complete fix-dut-fix measurement. The blue one is highlighting the actual one which is computed by the de-embedding. In fact, the first reference plane "1" is set at the first SMA-female, where the channel of the VNA is connected. The second reference plane "2" is set at the middle of the THRU standard. Thus, the mismatch between the *actual* and the *de-embedded* fixture is in the phase shift of an SMA-female adapter. Experimentally, this is confirmed in figure 2.4(b). The phase error on  $s_{21}$  and  $s_{12}$  is of  $\simeq 10^\circ$  and 500 MHz and of  $\simeq 20^\circ$  1 GHz, compatible with the phase shift of the SMA adapter.

In the next measurements, the phase shift introduced by the THRU of finite length is corrected. This is possible since for the successive arrangements considered, the fixtures scattering parameters can be fully characterized. A network representing half of the SMA-female can be modeled as a matched transmission line providing a  $\frac{17^\circ}{2}$  phase shift at 1 GHz, and can be left/right de-embedded from the obtained fixture S-parameters. This data is then used to de-embed the DUT.

This fact shows another advantage of de-embedding the DUT by fully characterizing the test fixtures: the finite length of the THRU can be taken into account and de-embedded.



(a)



(b)

Figure 2.4: Comparison between de-embedded DUT and actual one.

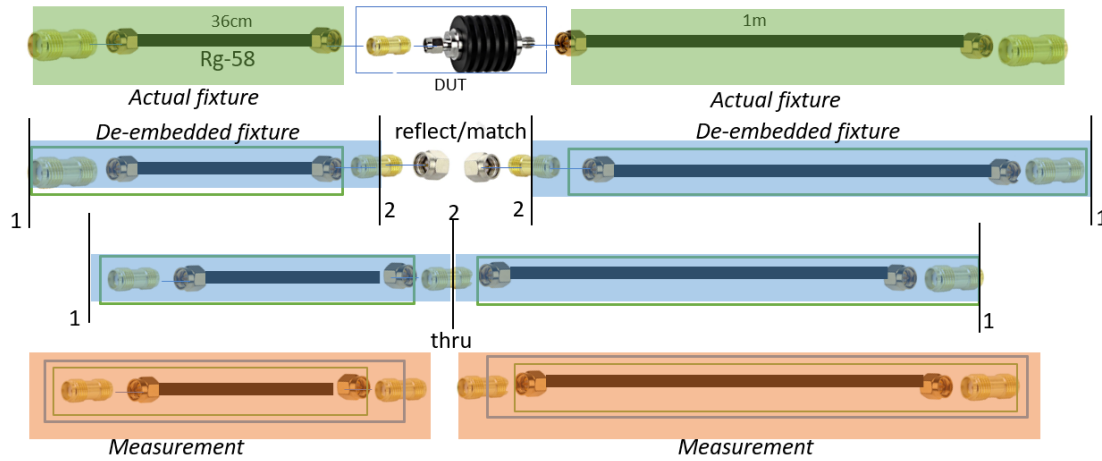
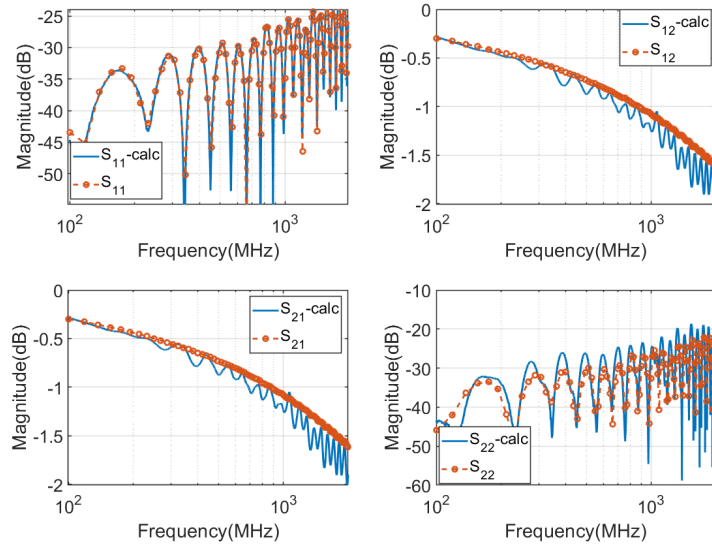


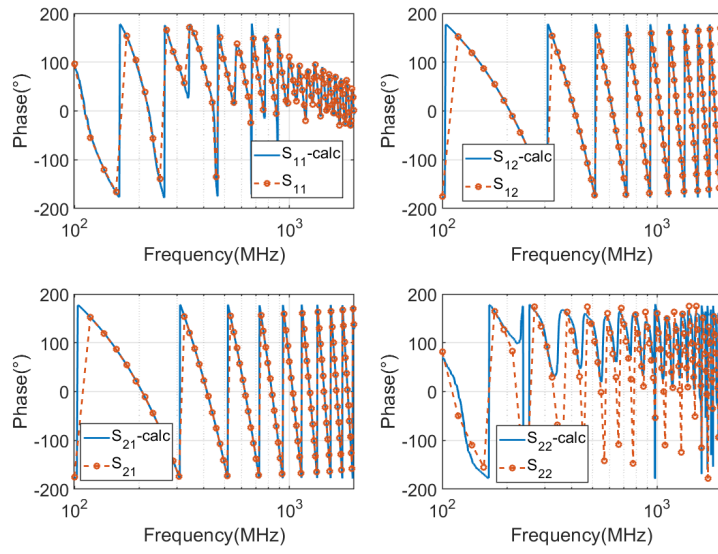
Figure 2.5: Difference between measured, de-embedded and actual fixtures.

### 2.2.2 Strategy 2

In this case, the S-parameters of the attenuator and both fixtures can be computed. The standard used for the "reflect" is of short type, but similar computation is performed for the open case. The TRM algorithm is then applied to this first set of values to extract the fixture "2" S-parameters. These are shown and compared to the ones from a direct measure of them with the VNA in figure 2.6. This information is then used to de-embed the fixture "2" contribution to the measurement of  $\mathbf{D}$ , obtaining the scattering matrix of fixture "1". The scattering parameters of the fixture "1" are obtained by realizing the "thru" connection (figure 2.7) and by right de-embedding the known fixture "1".



(a)



(b)

Figure 2.6: Fixture 2 de-embedded compared with the measurement.

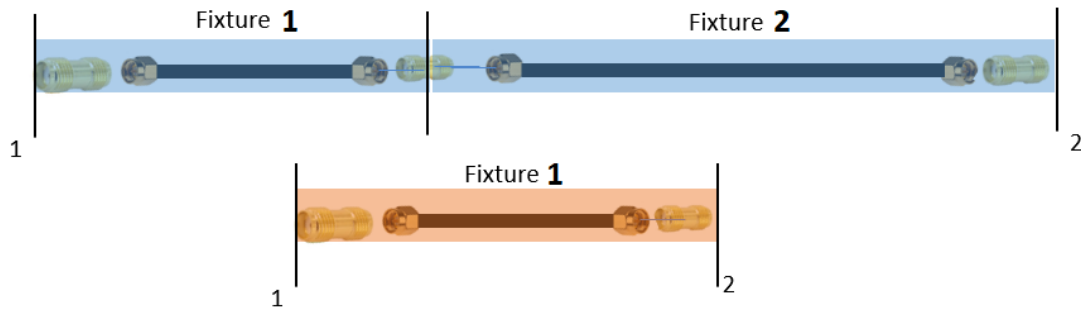


Figure 2.7: Schematic representation of the measurements for fixture 1.

The obtained fixture "1" is highlighted in *blue*. The VNA measures the *red* one: the half-I contribution can be removed and the resulting parameters are compared with the de-embedded ones in figure 2.8. Finally, the obtained fixture "1" and fixture "2" scattering parameters are left and right de-embedded from the complete (**A**) measure, respectively, using the equations of the appendix A.4 for the two-port case. The results is compared with the actual DUT in figure 2.10.

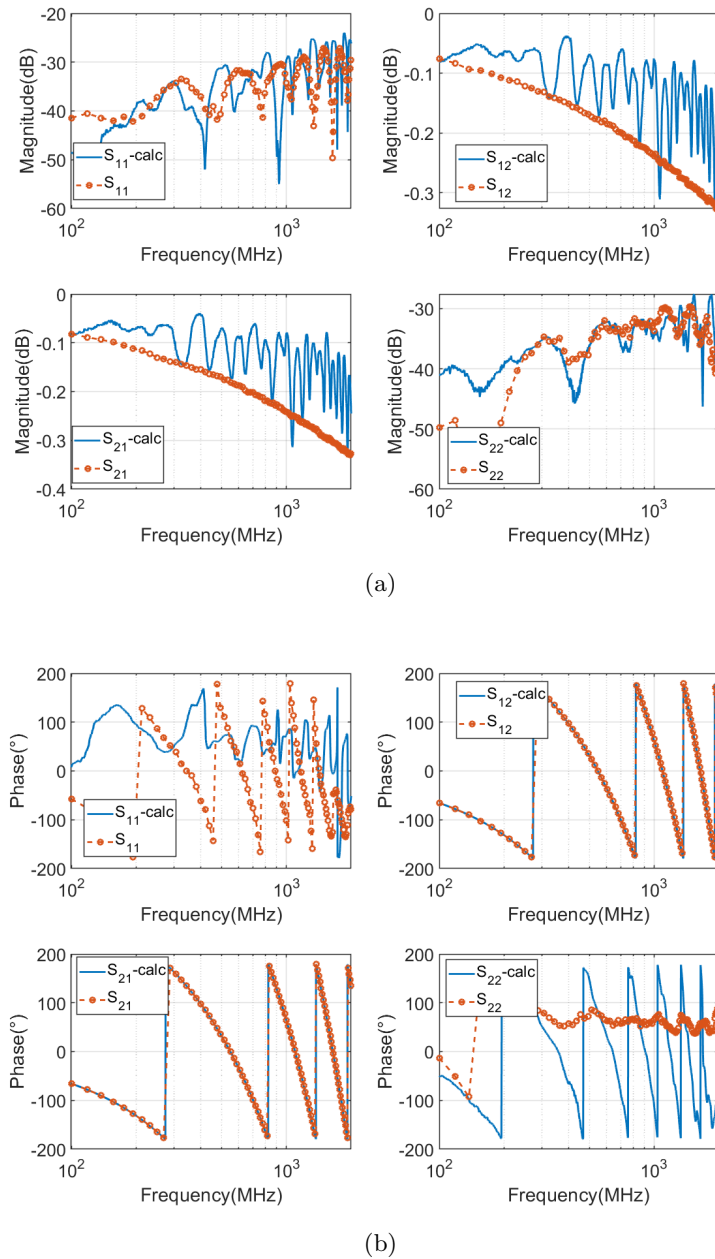


Figure 2.8: Fixture 1 de-embedded compared with the measurement.

The absolute error in dB for the magnitude and in phase for the phase of the reflection parameters  $s_{11}$  and  $s_{22}$  is due to the finite directivity (41 dB) of the VNA employed (figure 2.11). This is causing a significant error in the measurement of low values of return loss. For example, a quick computation of the error can be made according to the uncertainty graph from the datasheet. For an  $s_{11} = -30 \text{ dB} = 0.03$  the uncertainty is



close to 0.01, providing an  $s_{11,max} = 0.04 = -28 \text{ dB}$  and  $s_{11,min} = 0.02 = -34 \text{ dB}$ : the measurement is bounded within +2 dB and -4 dB of uncertainty. If the return loss of the fixture is even higher, as in the example case:  $s_{11} = -30 \text{ dB} = 0.01$ , the uncertainty close to 0.01 provides  $s_{11,max} = 0.02 = -34 \text{ dB}$  and  $s_{11,min} = 0.001 = -80 \text{ dB}$ , indicating that this measure is affected by great uncertainty. This problem is not affecting the measurement of small return losses (such as the reflection coefficient of the reflect standard) or the transmission parameters  $s_{21}$  and  $s_{12}$ . A detailed explanation of the error caused by the finite directivity of the VNA can be found in [48]. The phase error on the  $s_{21}$  and  $s_{12}$  of the DUT is much less than before (now  $3^\circ$  at 1 GHz), as the finite length thru has been taken into account before performing the de-embedding of the DUT. Ideally, the "thru" would be of zero length, however, the SMA-female is introducing a phase shift that becomes not negligible at higher frequencies. The measured S-parameters of the I-SMA are shown in figure 2.12. The phase shift introduced by this component has the same profile of the error made on the  $s_{21}$  of the DUT, in the right picture, when the effect of the finite length thru is not taken into account in the de-embedding. The glitches in the magnitude measurements are due to the different IF frequencies used in the measurement of the total structure and the two cables.

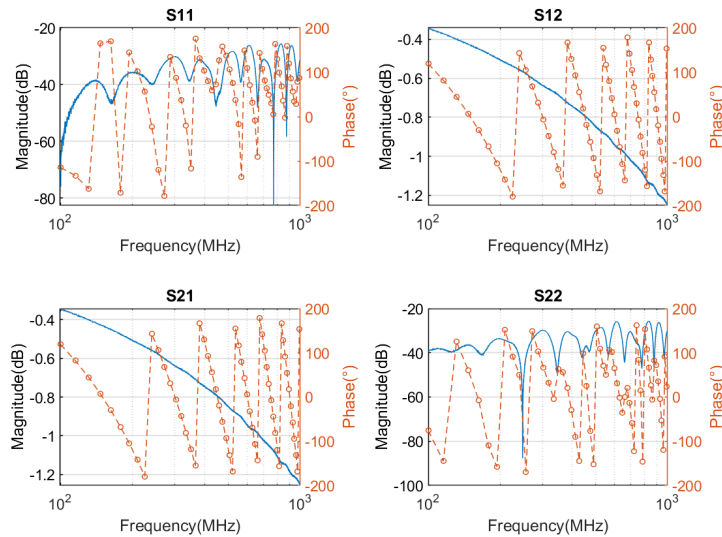
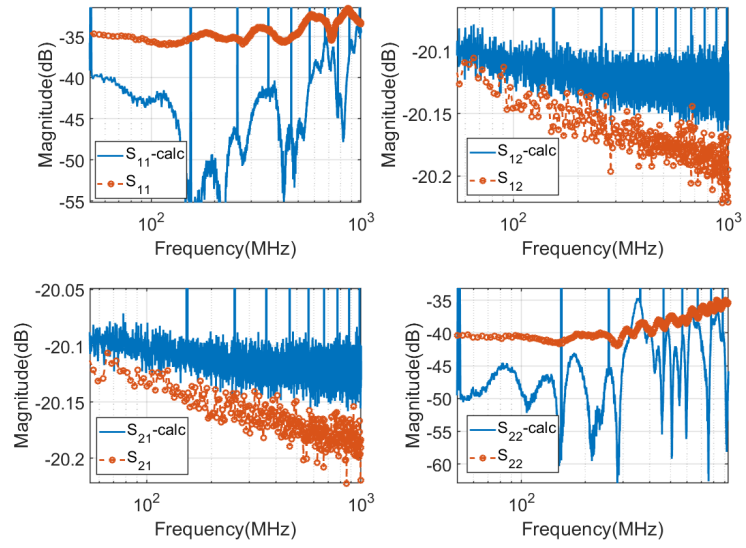
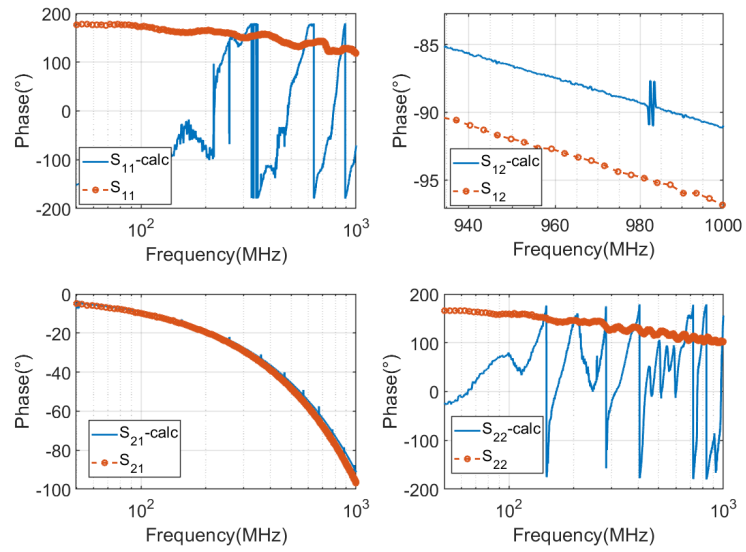


Figure 2.9: S-parameters of the thru connection between the fixtures **D**.



(a)



(b)

Figure 2.10: Magnitude and phase for the de-embedded DUT S-parameters compared to the actual ones.

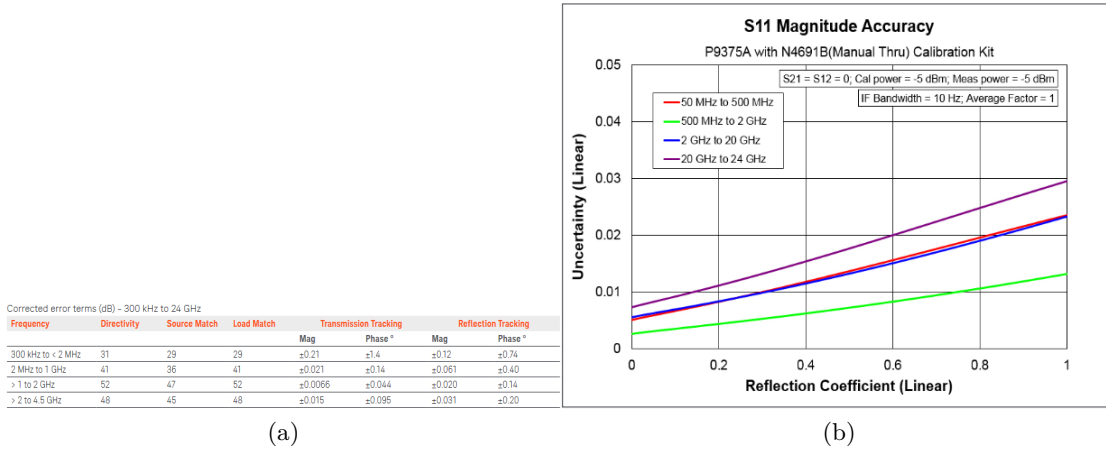


Figure 2.11: Table 3 from the datasheet of the VNA used. In the bandwidth up to 1 GHz the directivity is of 41 dB.

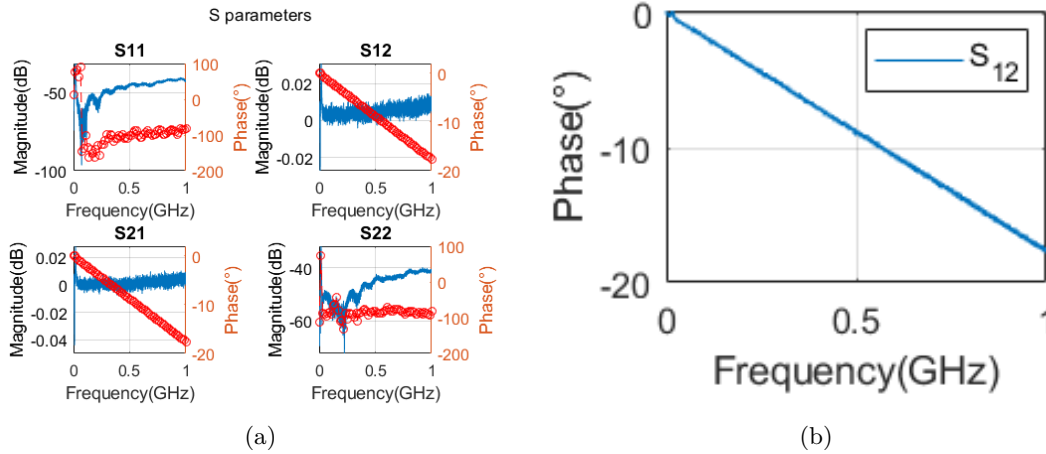


Figure 2.12: Measure of the I-SMA scattering parameters (left) and phase error on the  $s_{12}$  parameter between the measured and de-embedded DUT (right). The error is corresponding to the phase shift introduced by the I-SMA in the non-ideal thru connection.

### 2.3 De-embedding of a low return loss fixture

This simple measurement is made to demonstrate that the equations for left and right de-embedding of section 1.4 are valid regardless of the type of the fixture. In this example, a "thru" structure is realized connecting a capacitor soldered between two female SMA connectors (figure 2.13) between the two cables of the structure "E" from table 2.1. The built structure can be schematized as in figure 2.14.

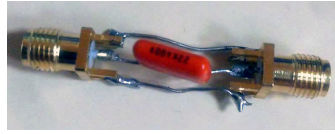


Figure 2.13: Capacitor soldered between two female SMA connectors.



Figure 2.14: Schematic representation of the thru between fixture "1" and the capacitor.

The measurements on this structure, compared with the capacitor only S-parameters, are shown below (figure 2.15).

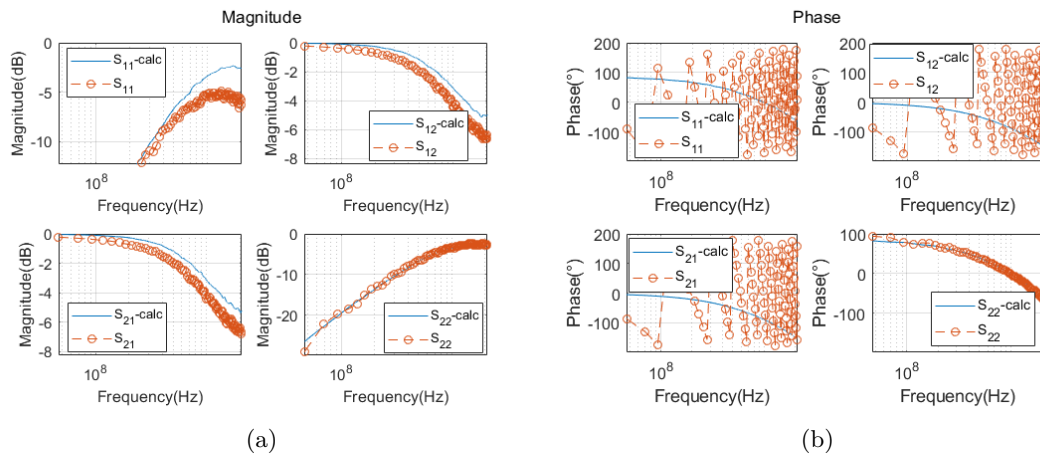
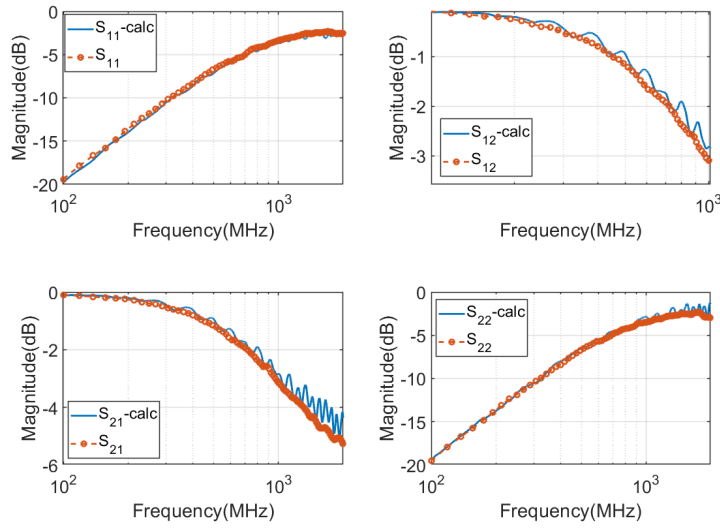
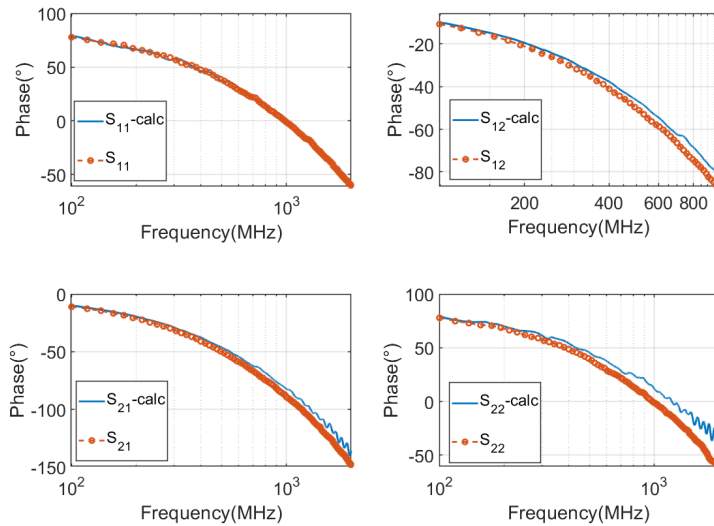


Figure 2.15: Capacitor (blue) and thru (red) scattering parameters.

The results of the de-embedding are reported in figure 2.16.



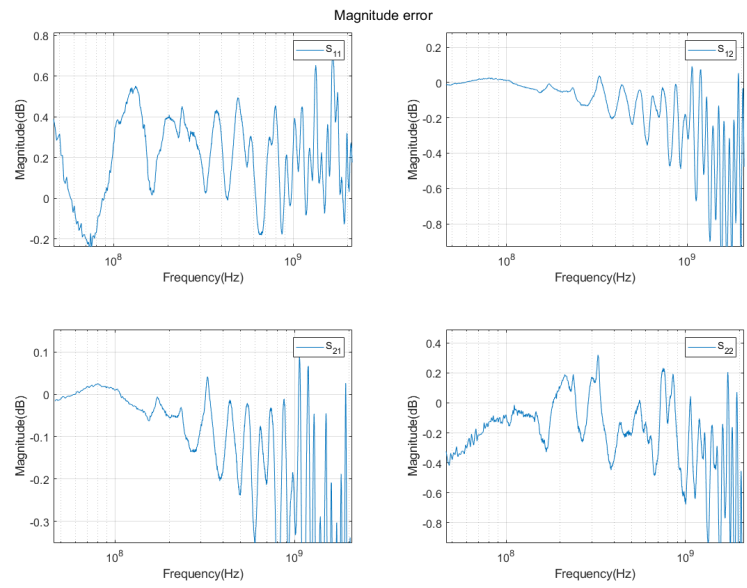
(a)



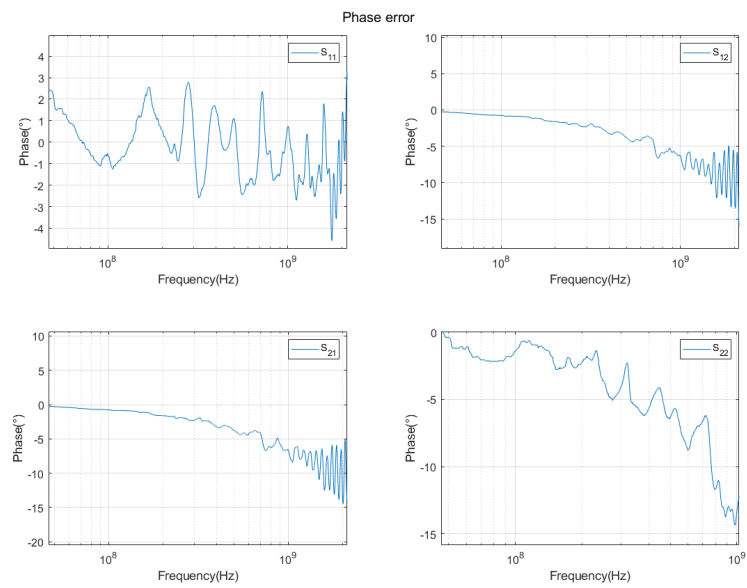
(b)

Figure 2.16: Comparison between actual and de-embedded capacitor scattering parameters.

It is noted that this time the measurements have a lower return loss: in this case the finite directivity of the VNA is not introducing uncertainty and there's little error (within  $\pm 1$  dB) on the S-parameters. The error of the de-embedding is reported below, in figure 2.17.



(a)



(b)

Figure 2.17: Error on the magnitude (a) and phase (b) on the de-embedded S-parameters of the capacitor.

## 2.4 Voltage follower test circuit

The DUT is a general-purpose opamp (TL081) connected in a voltage follower configuration. The schematic is shown in figure 2.18.

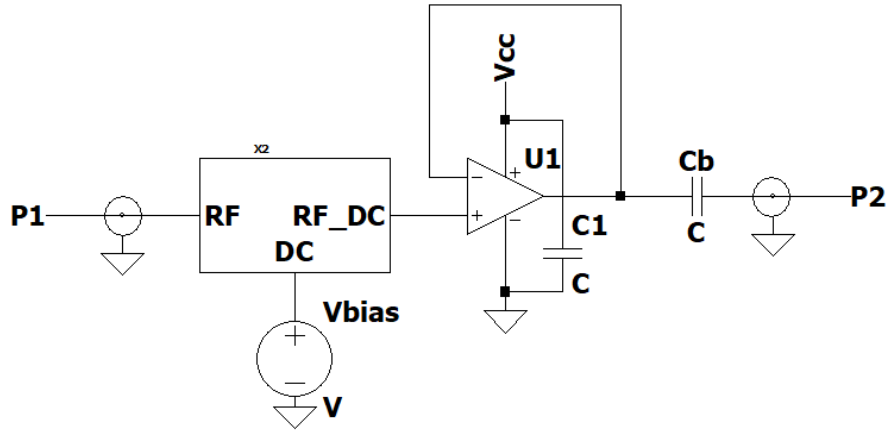


Figure 2.18: Schematic of the built prototype.

The opamp is powered by a single-supply voltage of  $V_{cc} = 6\text{ V}$ , the minimum required by the datasheet [49]. The noninverting input is connected to the bias tee designed in section 1.4.3. The RF port is connected to the VNA measurement system, the DC port is connected to a constant source  $V_{bias} = 3\text{ V}$ . These voltages are provided by a bench linear regulated power supply (Topward TPS-4000 [50]). The dc blocking capacitor at the output has a value of  $8.2\text{ nF}$  and a decoupling capacitor of  $C_1 = 100\text{ nF}$  is connected between the supply pins of the op-amp. The circuit was prototyped on a dual-side perfboard. To minimize the parasitics that would influence the measurement, the layout was made as much as compact as possible using SMD components. The ground plane was realized with adhesive copper tape.

### Asymmetric error network of 100 cm cable and 36 cm RG-58 cable

The setup is shown in figure 2.19. The fixtures "1" and "2" were already characterized.

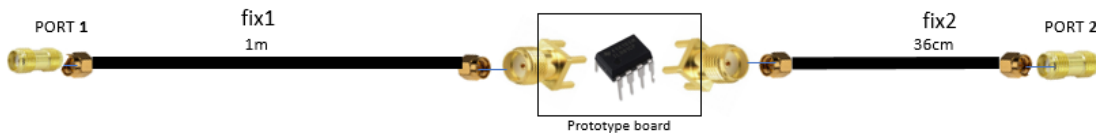
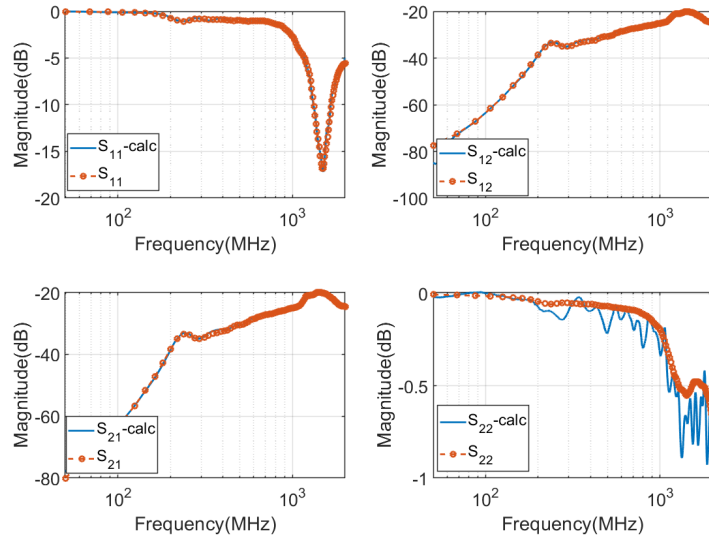
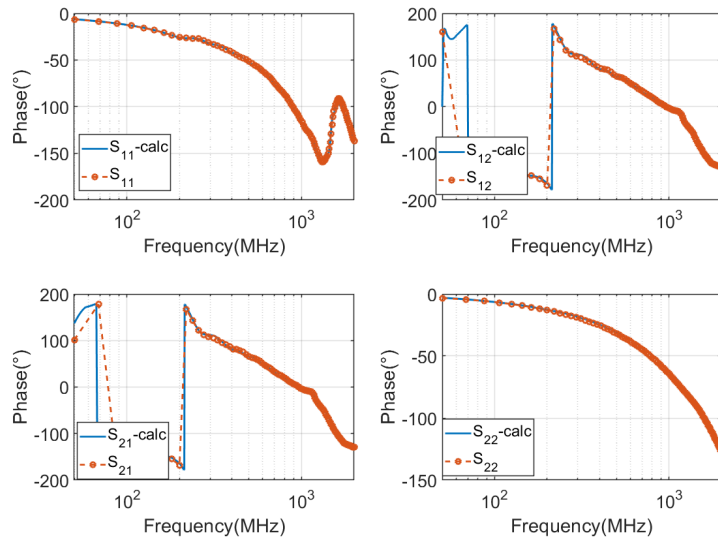


Figure 2.19: Second scenario.

The results follow in figure 2.20.



(a)



(b)

Figure 2.20: Comparison between de-embedded S-parameters (solid line) and measured one (circles).

The measurement of the total structure has been carried three times to ensure repeatability, and reported in figure 2.21.



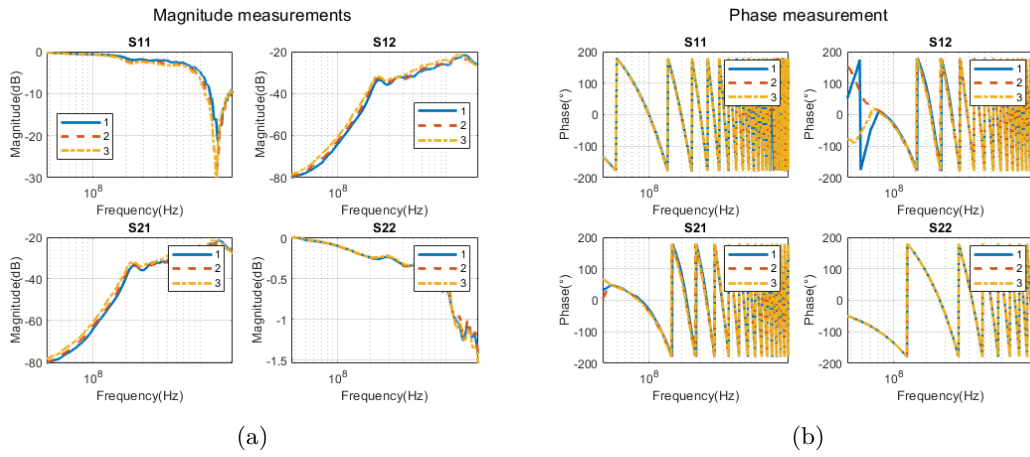


Figure 2.21: Plot of the acquisition of the S-parameters.

A comparison between the total measured S-parameters and the DUT one is provided in figure 2.22.

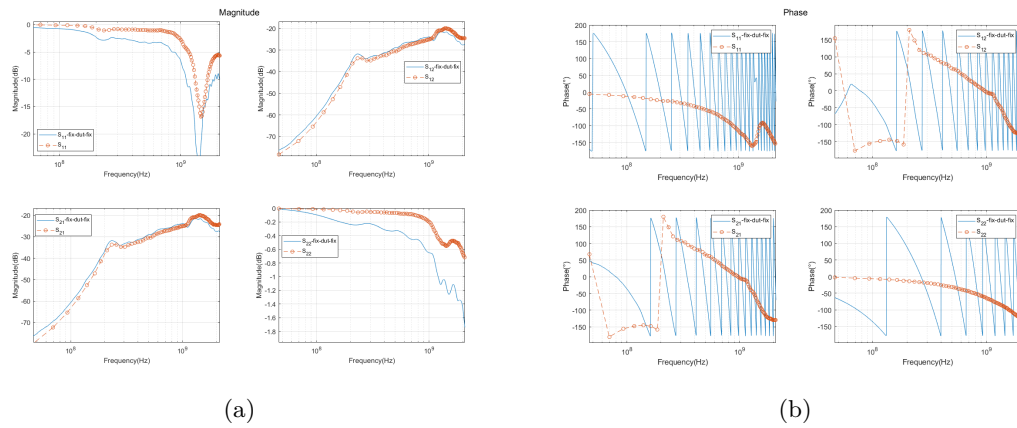


Figure 2.22: Comparison of the DUT s-parameters with the fix-dut-fix ones.

### Asymmetric error network of 36 cm cable and 100 cm RG-58 cable

To double-check the correctness of the results, the two fixtures are exchanged between port 1 and port 2. The setup is shown in figure 2.23.

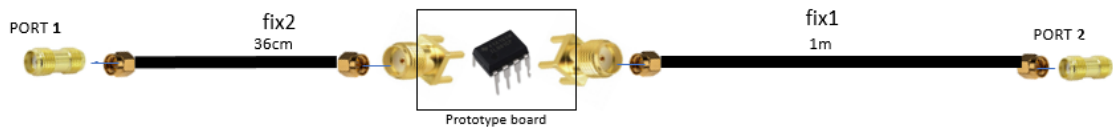
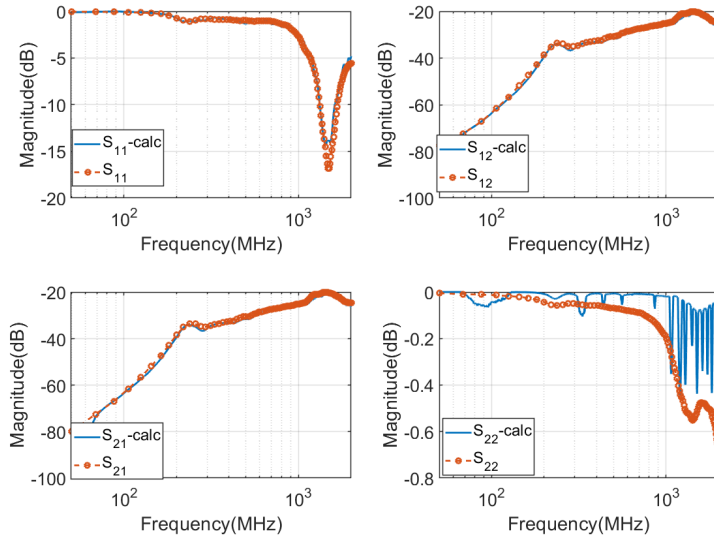
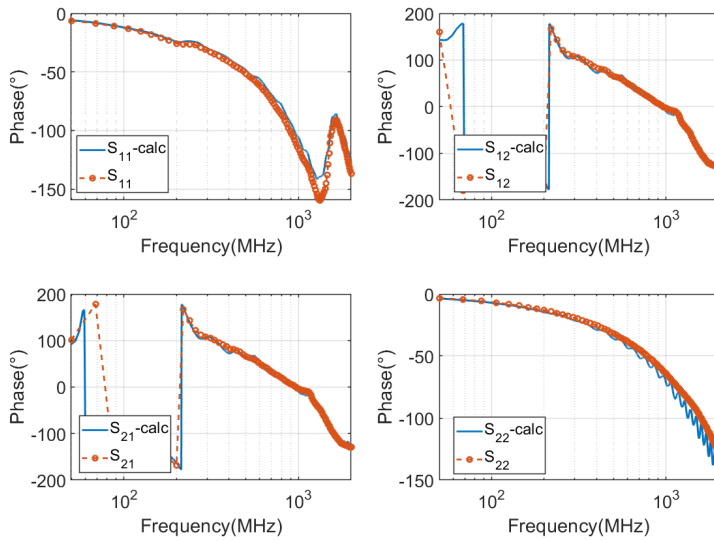


Figure 2.23: Third scenario.

The results follows in figure 2.24.



(a)



(b)

Figure 2.24: Comparison between de-embedded S-parameters (solid line) and measured one (circles).

The measurement of the total structure has been carried three times to ensure repeatability as the previous case, and reported in figure 2.25.

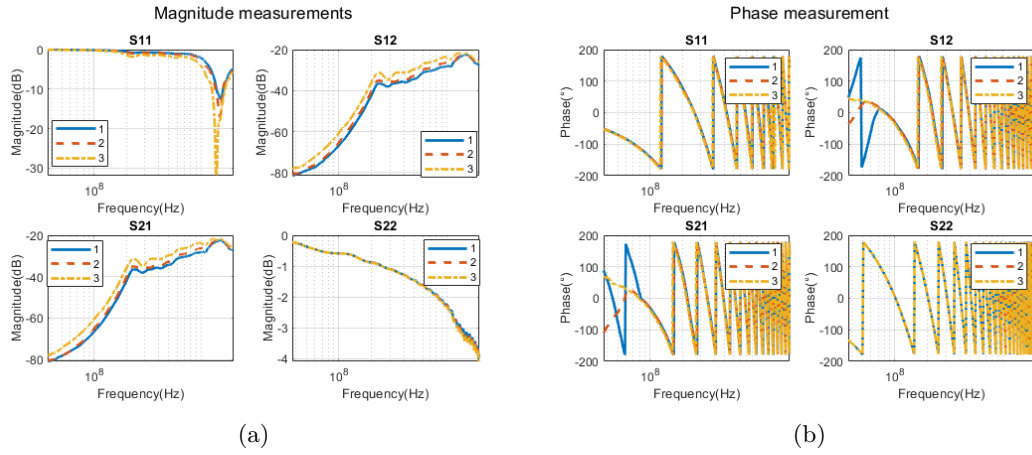


Figure 2.25: Plot of the acquisition of the S-parameters.

A comparison between the total measured S-parameters and the DUT one is provided in figure 2.26.

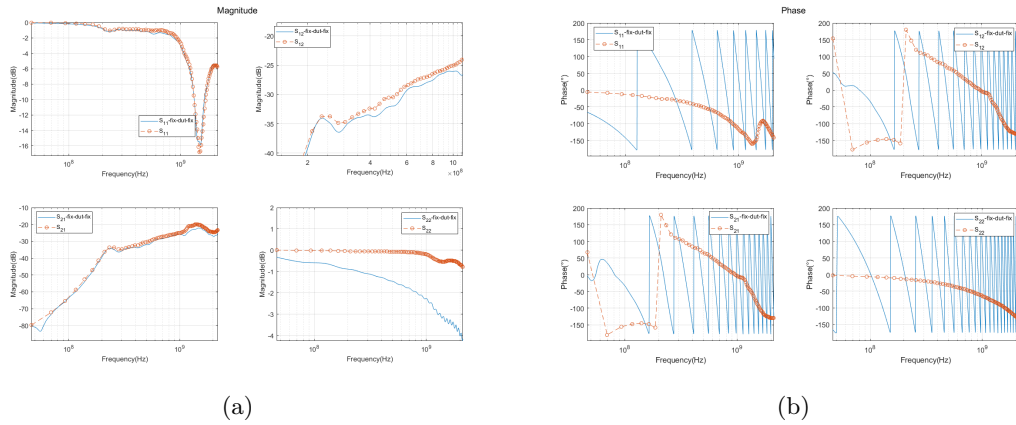


Figure 2.26: Comparison of the DUT s-parameters with the fix-dut-fix ones.

The error in dB and  $^{\circ}$  between measured and de-embedded DUT parameters are reported below (figures 2.27 and 2.28). For a larger part of the bandwidth, the error is below 1 dB and  $10^{\circ}$ .

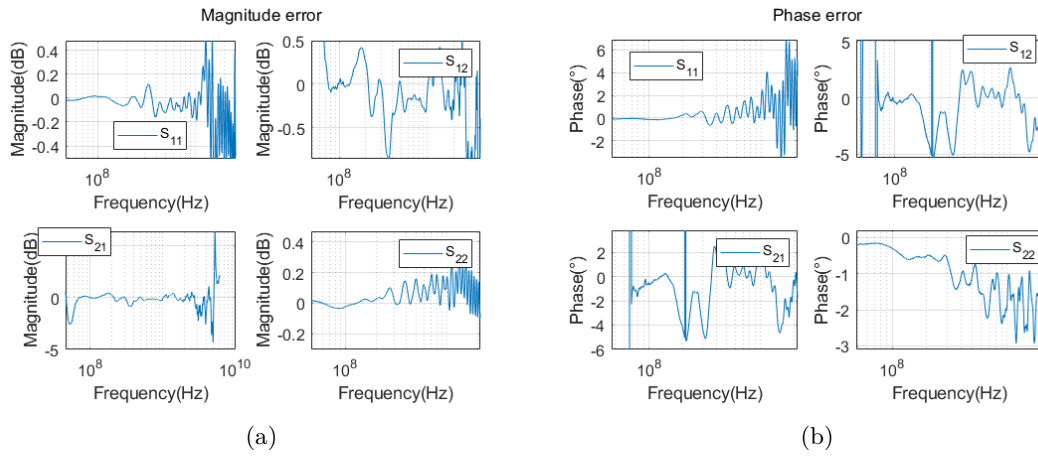


Figure 2.27: Error for the first scenario.

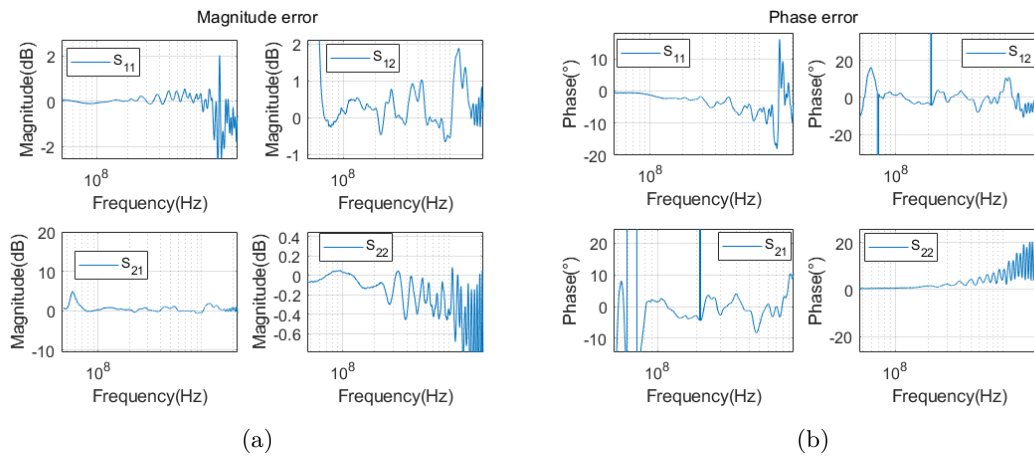


Figure 2.28: Error for the second scenario.



## Chapter 3

# Conclusions and future work

The main goal of this thesis was to develop a de-embedding procedure that applies to multi-port networks, with no hypothesis on their symmetry or type and applicable in a wide bandwidth. First, it were described the classical calibration strategies applied to the case of two-port networks. It was then explained how to deal with their limitations. The set goals were obtained first by using the two-port TRL/TRM to characterize a single error network, then by realizing  $N-1$  additional "thru" structures. After this characterization, multi-port de-embedding becomes possible.

The multi-port de-embedding strategy was validated in a SPICE environment. Measurements on real devices were made to validate the test-fixtures characterization using the proposed additional "thru" calibration structure. The results show that an accurate description of the error networks is obtained, and this can be used to de-embed the DUT. A two-port DUT was considered, but there is no reason to believe that the strategy wouldn't work for three or four-port devices, as confirmed by simulations. In fact, the theory shows how once a test-fixture is completely characterized, de-embedding can be carried out for two or multi-port devices.

Additional study is required when the calibration standards are not ideal. For example, a source of error is that the calibration structure is not the exact replica of the ones connected to the device. Other sources of errors are on the non-ideal "thru": the effect of the finite length have been studied, but when its characteristic impedance is different from the "line" one, an error is expected. In future works, the crosstalk between test-fixture could be included in the strategy. A multi-port LRL/LRM could be developed to consider the finite length "thru". Also, the extension of this strategy to differential structures could be studied.





# Appendix A

## Derivation of the de-embedding algorithms

### A.1 TRL line length computation

The bandwidth on which the de-embedding is applied is indicated as  $f_l - f_h$ . First, the ratio  $\frac{f_h}{f_l}$  is computed, allowing the choice of the number of line standard as in table 1.4. To have the best calibration, the line lengths and crossover points must ensure that their phase shift is as far as possible from  $0^\circ$  and  $180^\circ$  across the entire bandwidth. The geometric series proves useful to divide the bandwidth  $f_l - f_h$  identifying the crossover points, according to the following optimal criteria [51]. Each line can be used for a maximum bandwidth of 1:8. To ensure that the frequency range spanned by each line has the same ratio of upper to lower frequencies, guaranteeing the highest distance for each line from  $0^\circ$  and  $180^\circ$ , the ratio between the next crossover point and the previous one has to be kept constant over the entire bandwidth. The geometric sequence is of the form:

$$a, ar, ar^2, ar^3, \dots, ar^n \quad (\text{A.1})$$

Each term of the sequence corresponds to a frequency crossover point between the different line standards:

$$a, ar, ar^2, ar^3, \dots, ar^n = f_l, f_{t1}, f_{t2}, \dots, f_h \quad (\text{A.2})$$

In particular  $a = f_l$ ,  $ar^n = f_h$ . In the case of a single line,  $n = 1$ , the standard is used in the entire bandwidth resulting in  $f_{t1} = f_h$ . So it results  $a = f_l$  and  $r = \frac{f_h}{f_l}$ . In the two line case  $n = 2$ , as there are three terms in the series corresponding to  $f_l$ ,  $f_{t1}$  and  $f_h$ . It's possible to derive:

$$\frac{f_h}{f_l} = \frac{f_l r^2}{f_l}, r = \sqrt{\frac{f_h}{f_l}} \quad (\text{A.3})$$

Knowing  $r$ ,  $f_{t1} = ar = f_l \sqrt{\frac{f_h}{f_l}}$ . The bandwidth is divided in the range:

$$f_l, f_{t1} = f_l \sqrt{\frac{f_h}{f_l}}, f_h \quad (\text{A.4})$$

The longer line will be used in the range  $f_l - f_{t1}$  while the shorter one in the range  $f_{t1} - f_h$ . Thanks to the geometric sequence construction, the three points satisfy:

$$\frac{f_h}{f_t} = \frac{f_h}{f_l r} = \frac{f_t}{f_l} = \frac{f_l r}{f_l} = r \quad (\text{A.5})$$

Meaning that each line covers a frequency span of the same extension. To determine the line lengths, as explained, the optimal criteria is having them long  $l = \frac{\lambda}{4}$  at center frequency:

$$f_{c1} = \frac{f_l + f_{t1}}{2}, \lambda_{c1} = \frac{v_{eff}}{f_{c1}}, l_1 = \frac{\lambda_{c1}}{4} = \frac{1}{4} \frac{v_{eff}}{f_{c1}} \quad (\text{A.6})$$

$$f_{c2} = \frac{f_{t1} + f_h}{2}, \lambda_{c2} = \frac{v_{eff}}{f_{c2}}, l_2 = \frac{\lambda_{c2}}{4} = \frac{1}{4} \frac{v_{eff}}{f_{c2}} \quad (\text{A.7})$$

It's possible to compute the phase delay in  $^\circ$  of each line at the crossover points. This quantity at lower and upper frequency is the same for each line, verifying the initial requirement of optimal bandwidth division and line length.

$$\theta_{l1} = 90^\circ \frac{f_l}{f_{c1}}, \theta_{h1} = 90^\circ \frac{f_{t1}}{f_{c1}} \quad (\text{A.8})$$

$$\theta_{l2} = 90^\circ \frac{f_{t1}}{f_{c2}}, \theta_{h2} = 90^\circ \frac{f_h}{f_{c2}} \quad (\text{A.9})$$

And as stated above:

$$\frac{f_l}{f_{c1}} = \frac{2f_l}{f_l + f_{t1}} = \frac{2f_l}{f_l + rf_l} = \frac{2}{1+r}, \frac{f_{t1}}{f_{c2}} = \frac{2rf_l}{rf_l + f_h} = \frac{2r}{r+r^2} = \frac{2}{1+r} \quad (\text{A.10})$$

Providing as expected  $\theta_{l1} = \theta_{l2}$ . For the electrical length at the upper frequency:

$$\frac{f_{t1}}{f_{c1}} = \frac{2rf_l}{f_l + f_{t1}} = \frac{2r}{1+r}, \frac{f_h}{f_{c2}} = \frac{2f_h}{f_t + f_h} = \frac{2r^2}{r+r^2} = \frac{2r}{1+r} \quad (\text{A.11})$$

Providing  $\theta_{h1} = \theta_{h2}$ .

This addresses the cases of single line and two lines computation. The calculations for three and four line cases are below reported.

### A.1.1 Three lines

The bandwidth is divided in three intervals ( $n = 3$ ) indicated with:

$$f_l, f_{t1}, f_{t2}, f_h \quad (\text{A.12})$$

The ratio  $r$  of each point with the previous one is now computed as:

$$\frac{f_h}{f_l} = r^3, r = \sqrt[3]{\frac{f_h}{f_l}} \quad (\text{A.13})$$

Providing:

$$f_{t1} = r f_l, f_{t2} = r f_{t1} = r^2 f_l \quad (\text{A.14})$$

The center frequencies at which each line is long a quarter wavelength is:

$$f_{c1} = \frac{f_l + f_{t1}}{2}, f_{c2} = \frac{f_{t1} + f_{t2}}{2}, f_{c3} = \frac{f_{t2} + f_h}{2} \quad (\text{A.15})$$

The line lengths are computed using  $l_i = \frac{1}{4} \frac{v_{eff}}{f_{c,i}}$ , with  $v_{eff} = \frac{c_0}{\epsilon_{eff}}$ .

### A.1.2 Four lines

The bandwidth is divided in four intervals ( $n = 4$ ) indicated with:

$$f_l, f_{t1}, f_{t2}, f_{t3}, f_h \quad (\text{A.16})$$

The ratio  $r$  of each point with the previous one is now computed as:

$$\frac{f_h}{f_l} = r^4, r = \sqrt[4]{\frac{f_h}{f_l}} \quad (\text{A.17})$$

Providing:

$$f_{t1} = r f_l, f_{t2} = r f_{t1} = r^2 f_l, f_{t3} = r f_{t2} = r^3 f_l \quad (\text{A.18})$$

The center frequencies at which each line is long a quarter wavelength is:

$$f_{c1} = \frac{f_l + f_{t1}}{2}, f_{c2} = \frac{f_{t1} + f_{t2}}{2}, f_{c3} = \frac{f_{t2} + f_{t3}}{2}, f_{c4} = \frac{f_{t3} + f_h}{2} \quad (\text{A.19})$$

The line lengths are again computed using  $l_i = \frac{1}{4} \frac{v_{eff}}{f_{c,i}}$ , with  $v_{eff} = \frac{c_0}{\epsilon_{eff}}$ .

### A.1.3 Use of a higher number of line standards

For any ratio  $\frac{f_h}{f_l}$ , it's possible to choose a number of lines that is higher than the strictly required. This has the advantage of improving the de-embedding accuracy, as adding an additional line has the effect to move the phase shift at the crossover points farther from the limits of  $20^\circ$  and  $180^\circ$ . The disadvantage, in this case, is that the lines to be fabricated will be larger than the minimum number of lines case.

### A.1.4 Some numeric examples

This section is for providing insight on the required line standards to be fabricated.

#### FR4 board, TRL down to 10MHz

This example considers  $\epsilon_{eff} = 3.3$ ,  $f_l = 10 \text{ MHz}$ ,  $f_h = 1 \text{ GHz}$ . This results in  $\frac{f_h}{f_l} = 100$ , requiring three line standards (table A.1).

	$f_l$	$f_{c1}$	$f_{t1}$	$f_{c2}$	$f_{t2}$	$f_{c3}$	$f_h$
Frequency (GHz)	0.01	0.028	0.046	0.13	0.215	0.61	1
Line lengths(cm)		146.3		31.5		6.8	
$\theta_l$		32		32		32	
$\theta_h$		148		148		148	

Table A.1: Line standards required by the TRL.

The line lengths are unfeasible to be fabricated on a PCB. As said in section 1.3.3, the de-embedding at low frequencies is better performed with TRM.

#### Higher dielectric constant board

For circuit size reduction, a possibility is to fabricate a PCB with a higher dielectric constant. The "RT/duroid 6010LM laminate" from rogers corporation [52] has a dielectric constant of 10.2. Tables A.2 and A.3 compare the results between the two dielectrics. In the rogers case, the line lengths are nearly half of the FR4 case.

	$f_l$	$f_{c1}$	$f_{t1}$	$f_{c2}$	$f_h$
Frequency (GHz)	0.2	0.64	1.09	3.54	6
Line lengths(cm)		6.4		1.2	
$\theta_l$		27.8		27.8	
$\theta_h$		152.2		152.2	

Table A.2: Line standards required by the TRL,  $\epsilon_{eff} = 3.3$ .

	$f_l$	$f_{c1}$	$f_{t1}$	$f_{c2}$	$f_h$
Frequency (GHz)	0.2	0.64	1.09	3.54	6
Line lengths(cm)		3.6		0.6	
$\theta_l$		27.8		27.8	
$\theta_h$		152.2		152.2	

Table A.3: Line standards required by the TRL,  $\epsilon_{eff} = 10.2$ .

### Using an additional line to improve the accuracy

Considering the example above with  $\epsilon_{eff} = 3.3$  (FR4), the use of an additional line standard (for a total of three lines) will move the phase shifts farther from  $20^\circ$  and  $160^\circ$ , as shown in table A.4.

	$f_l$	$f_{c1}$	$f_{t1}$	$f_{c2}$	$f_{t2}$	$f_{c3}$	$f_h$
Frequency (GHz)	0.2	0.41	0.62	1.28	1.93	3.97	6
Line lengths(cm)		10		3.2		1	
$\theta_l$		43.8		43.8		43.8	
$\theta_h$		152.2		152.2		152.2	

Table A.4: Effect of an additional line standard.

## A.2 TRL for 2-port networks

The equations can be found in [53] and are reported below. Using R parameters, if:

$$b_1 = S_{11}a_1 + S_{12}a_2 \quad (\text{A.20})$$

$$b_2 = S_{21}a_1 + S_{22}a_2 \quad (\text{A.21})$$

$$\begin{bmatrix} b_1 \\ a_1 \end{bmatrix} = \frac{1}{S_{21}} \begin{bmatrix} -\Delta & S_{11} \\ -S_{22} & 1 \end{bmatrix} \begin{bmatrix} b_2 \\ a_2 \end{bmatrix} \quad (\text{A.22})$$

$$\Delta = S_{12}S_{21} - S_{11}S_{22} \quad (\text{A.23})$$

$$\mathbf{R} = \frac{1}{S_{21}} \begin{bmatrix} -\Delta & S_{11} \\ -S_{22} & 1 \end{bmatrix} \quad (\text{A.24})$$

The total measured matrix  $\mathbf{R}_M$  is the product of the matrices of the error boxes and the DUT:

$$\mathbf{R}_M = \mathbf{R}_A \mathbf{R} \mathbf{R}_B \quad (\text{A.25})$$

$$\mathbf{R} = \mathbf{R}_A^{-1} \mathbf{R}_M \mathbf{R}_B^{-1} \quad (\text{A.26})$$

$\mathbf{R}_A$  and  $\mathbf{R}_B$  can be written as follows:

$$\mathbf{R}_A = \begin{bmatrix} r_{11} & r_{12} \\ r_{21} & r_{22} \end{bmatrix} = r_{22} \begin{bmatrix} a & b \\ c & 1 \end{bmatrix} \quad (\text{A.27})$$

$$\mathbf{R}_B = \begin{bmatrix} \rho_{11} & \rho_{12} \\ \rho_{21} & \rho_{22} \end{bmatrix} = \rho_{22} \begin{bmatrix} \alpha & \beta \\ \gamma & 1 \end{bmatrix} \quad (\text{A.28})$$

The inverse of  $\mathbf{R}_A$  and  $\mathbf{R}_B$  can be derived:

$$\mathbf{R}_A^{-1} = \frac{1}{r_{22}} \frac{1}{a - bc} \begin{bmatrix} 1 & -b \\ -c & a \end{bmatrix} \quad (\text{A.29})$$

$$\mathbf{R}_B^{-1} = \frac{1}{\rho_{22}} \frac{1}{\alpha - \beta\gamma} \begin{bmatrix} 1 & -\beta \\ -\gamma & \alpha \end{bmatrix} \quad (\text{A.30})$$

The DUT matrix is expressed as:

$$\mathbf{R} = \frac{1}{r_{22}\rho_{22}} \frac{1}{a\alpha} \frac{1}{1 - b\frac{c}{a}} \frac{1}{1 - \gamma\frac{\beta}{\alpha}} \begin{bmatrix} 1 & -b \\ -c & a \end{bmatrix} \begin{bmatrix} 1 & -\beta \\ -\gamma & \alpha \end{bmatrix} \quad (\text{A.31})$$

Seven quantities are needed to find  $\mathbf{R}$  and de-embed the DUT, even if the error boxes, that are asymmetric, have 8 error terms. The needed quantities are  $a, b, c, \alpha, \beta, \gamma$  and  $r_{22}\rho_{22}$ . From THRU, REFLECT, LINE standard measurements, these quantities can be found and the solution can be provided. From the ideal through standard (represented as a 2x2 unit matrix) the measured  $\mathbf{R}$  matrix results:

$$\mathbf{R}_T = \mathbf{R}_A \mathbf{R}_B \quad (\text{A.32})$$

Where  $\mathbf{R}_A$  and  $\mathbf{R}_B$  are the  $\mathbf{R}$  matrices of the error boxes A and B. With the line standard connected, the measured  $\mathbf{R}$  matrix will be:

$$\mathbf{R}_D = \mathbf{R}_A \mathbf{R}_L \mathbf{R}_B \quad (\text{A.33})$$

Now, it's possible to write:

$$\mathbf{R}_B = \mathbf{R}_A^{-1} \mathbf{R}_T \quad (\text{A.34})$$

$$\mathbf{R}_D = \mathbf{R}_A \mathbf{R}_L \mathbf{R}_A^{-1} \mathbf{R}_T \quad (\text{A.35})$$

$$\mathbf{R}_D = \mathbf{R}_A \mathbf{R}_L \mathbf{R}_A^{-1} \quad (\text{A.36})$$

$$\mathbf{R}_D \mathbf{R}_T^{-1} \mathbf{R}_A = \mathbf{R}_A \mathbf{R}_L \quad (\text{A.37})$$

If we define  $\mathbf{T} = \mathbf{R}_D \mathbf{R}_T^{-1}$ , then substituting in the equation above we obtain:

$$\mathbf{T} \mathbf{R}_A = \mathbf{R}_A \mathbf{R}_L \quad (\text{A.38})$$

Where the  $\mathbf{T}$  matrix was defined above and it is known from measurements, while  $\mathbf{R}_A$  is the  $\mathbf{R}$  matrix of the fixture A and  $\mathbf{R}_L$  is the one of the line standard. The following equation holds:

$$\begin{bmatrix} t_{11} & t_{12} \\ t_{21} & t_{22} \end{bmatrix} \begin{bmatrix} a & b \\ c & 1 \end{bmatrix} = \begin{bmatrix} a & b \\ c & 1 \end{bmatrix} \begin{bmatrix} e^{-\gamma l} & 0 \\ 0 & e^{\gamma l} \end{bmatrix} \quad (\text{A.39})$$

Which can be expanded as:

$$\begin{cases} t_{11}a + t_{12}c = ae^{-\gamma l} \\ t_{21}a + t_{22}c = ce^{-\gamma l} \\ t_{11}b + t_{12} = be^{\gamma l} \\ t_{21}b + t_{22} = e^{\gamma l} \end{cases} .$$

Dividing the first by the second:

$$\frac{t_{11}a + t_{12}c}{t_{21}a + t_{22}c} = \frac{a}{c} = \frac{t_{11}\frac{a}{c} + t_{12}}{t_{21}\frac{a}{c} + t_{22}} \quad (\text{A.40})$$

That can be solved in terms of  $\frac{a}{c}$ :

$$t_{21} \left(\frac{a}{c}\right)^2 + (t_{22} - t_{11})\frac{a}{c} - t_{12} = 0 \quad (\text{A.41})$$

By dividing the third by the fourth:

$$\frac{t_{11}b + t_{12}}{t_{21}b + t_{22}} = b \quad (\text{A.42})$$

That can be solved in terms of  $b$ :

$$t_{21}b^2 + (t_{22} - t_{11})b - t_{12} = 0 \quad (\text{A.43})$$

And finally, by dividing the fourth by the second we obtain:

$$e^{2\gamma l} = c \frac{t_{21}b + t_{22}}{t_{21}a + t_{22}c} = \frac{t_{21}b + t_{22}}{t_{21}\frac{a}{c} + t_{22}} \quad (\text{A.44})$$

Since this ratio is not equal to unity (as  $e^{2\gamma l} \neq 1$ )  $b$  and  $\frac{a}{c}$  are two distinct roots of the quadratic equation, in which the same coefficients come into play. However, there's the need of a criteria for allowing the root choice, correctly identifying  $b$  and  $\frac{a}{c}$ . By writing:

$$\frac{a}{c} = \frac{r_{11}}{r_{21}} = S_{11} - \frac{S_{12}S_{21}}{S_{22}} \quad (\text{A.45})$$

Typically, the return loss of the fixture is very small ( $|S_{22}|, |S_{11}| < 1$ ) that yields  $|b| \ll 1$  and  $\left|\frac{a}{c}\right| \gg 1$ . The inequality  $|b| \ll \left|\frac{a}{c}\right|$  is used to determine the choice of the root. Now recalling that  $\mathbf{TR}_A = \mathbf{R}_A \mathbf{R}_L$ :

$$\det(\mathbf{T})\det(\mathbf{R}_A) = \det(\mathbf{R}_A)\det(\mathbf{R}_L) \quad (\text{A.46})$$

$$\det(\mathbf{T})\det(\mathbf{R}_L) = 1 \quad (\text{A.47})$$

So that it is possible to write:

$$t_{11}t_{22} - t_{12}t_{21} = 1 \quad (\text{A.48})$$

So only three terms out of four of the  $\mathbf{T}$  matrix are independent: by considering the previous system of equations, the  $t_{ij}$  terms are known once  $b$ ,  $\frac{a}{c}$  and  $e^{2\gamma l}$  are determined. What is left is to determine the other four quantities that are needed to de-embed the DUT.

$$r_{22}\rho_{22} \begin{bmatrix} a & b \\ c & 1 \end{bmatrix} \begin{bmatrix} \alpha & \beta \\ \gamma & 1 \end{bmatrix} = \mathbf{R}_A \mathbf{R}_B = \mathbf{R}_T = g \begin{bmatrix} d & e \\ f & 1 \end{bmatrix} \quad (\text{A.49})$$

Now computing:

$$\begin{bmatrix} a & b \\ c & 1 \end{bmatrix}^{-1} = \frac{1}{a-bc} \begin{bmatrix} 1 & -b \\ -c & a \end{bmatrix} \quad (\text{A.50})$$

$$r_{22}\rho_{22} \begin{bmatrix} a & b \\ c & 1 \end{bmatrix} = \frac{g}{a-bc} \begin{bmatrix} 1 & -b \\ -c & a \end{bmatrix} \begin{bmatrix} d & e \\ f & 1 \end{bmatrix} = \frac{g}{a-bc} \begin{bmatrix} d-bf & e-b \\ af-cd & a-ce \end{bmatrix} \quad (\text{A.51})$$

We extract:

$$r_{22}\rho_{22} = g \frac{a-ce}{a-bc} = g \frac{1 - e\frac{c}{a}}{1 - b\frac{c}{a}} \quad (\text{A.52})$$

And we also have:

$$\begin{bmatrix} \alpha & \beta \\ \gamma & 1 \end{bmatrix} = \frac{1}{a-ce} \begin{bmatrix} d-bf & e-b \\ af-cd & a-ce \end{bmatrix} \quad (\text{A.53})$$

From which the following three result:

$$\gamma = \frac{f - \frac{c}{a}d}{1 - \frac{c}{a}e} \quad (\text{A.54})$$

$$\frac{\beta}{\alpha} = \frac{e-b}{d-bf} \quad (\text{A.55})$$

$$\alpha a = \frac{d-bf}{1 - \frac{c}{a}e} \quad (\text{A.56})$$

At this point, the additional four quantities found are  $\frac{\beta}{\alpha}$ ,  $\gamma$ ,  $r_{22}\rho_{22}$  and  $\alpha a$ . In order to perform the de-embedding, we need to compute  $a$ . This can be done by considering the measurement of the return loss  $w_1$  of the reflect standard for the error box A:  $w_1 = \frac{a\Gamma_R + b}{c\Gamma_R + 1}$ . By solving for  $a$ , in terms of the known  $b$  and  $\frac{a}{c}$ :

$$a = \frac{w_1 - b}{\Gamma_R \left( 1 - w_1 \frac{c}{a} \right)} \quad (\text{A.57})$$



To determine  $a$ , since  $\Gamma_R$  is unknown, we also need the same measurement for the error box B:

$$w_2 = S_{22} + \frac{S_{12}S_{21}\Gamma_R}{1 - S_{11}\Gamma_R} = \frac{S_{22} - \Delta\Gamma_R}{1 - S_{11}\Gamma_R} \quad (\text{A.58})$$

$$w_2 = \frac{-\frac{\rho_{21}}{\rho_{22}} + \frac{\rho_{11}}{\rho_{22}}\Gamma_R}{1 - \frac{\rho_{12}}{\rho_{22}}\Gamma_R} \quad (\text{A.59})$$

$$w_2 = -\frac{\alpha\Gamma_R - \gamma}{\beta\Gamma_R - 1} \quad (\text{A.60})$$

Now  $\alpha$  can be found as follows:

$$\alpha = \frac{w_2 + \gamma}{\Gamma_R \left(1 + w_2 \frac{\beta}{\alpha}\right)} \quad (\text{A.61})$$

So that:

$$\frac{a}{\alpha} = \frac{w_1 - b}{w_2 + \gamma} \frac{1 + w_2 \frac{\beta}{\alpha}}{1 - w_1 \frac{c}{a}} \quad (\text{A.62})$$

And by multiplying the expression above by  $\alpha a$  found before:

$$a^2 = \frac{w_1 - b}{w_2 + \gamma} \frac{1 + w_2 \frac{\beta}{\alpha}}{1 - w_1 \frac{c}{a}} \frac{d - bf}{1 - \frac{c}{a}e} \quad (\text{A.63})$$

From which

$$a = \pm \left( \frac{w_1 - b}{w_2 + \gamma} \frac{1 + w_2 \frac{\beta}{\alpha}}{1 - w_1 \frac{c}{a}} \frac{d - bf}{1 - \frac{c}{a}e} \right)^{1/2} \quad (\text{A.64})$$

At this point  $a$  is determined within a  $\pm$  sign. To choose the correct root, the sign of the real part of the reflect standard employed has to be used:

$$\Gamma_R = \frac{w_1 - b}{a \left(1 - w_1 \frac{c}{a}\right)} \quad (\text{A.65})$$

The matrix of the DUT is now found as:

$$\mathbf{R} = \frac{1}{r_{22}\rho_{22}} \frac{1}{a\alpha} \frac{1}{1 - b\frac{c}{a}} \frac{1}{1 - \gamma\frac{\beta}{\alpha}} \begin{bmatrix} 1 & -b \\ -c & a \end{bmatrix} \begin{bmatrix} 1 & -\beta \\ -\gamma & \alpha \end{bmatrix} \quad (\text{A.66})$$

After the de-embedding algorithm is applied, also the product between the  $\mathbf{R}$  matrices of the two fixtures is known:

$$\mathbf{R}_A \mathbf{R}_B = r_{22}\rho_{22} \begin{bmatrix} a & b \\ c & 1 \end{bmatrix} \begin{bmatrix} \alpha & \beta \\ \gamma & 1 \end{bmatrix} \quad (\text{A.67})$$

While the terms inside the brackets are known, the fixture  $\mathbf{R}$  matrix (and so the  $\mathbf{S}$  one) is found only if the two are equal, as only the product  $r_{22}\rho_{22}$  is known, but not the two single terms. In the case of symmetrical test fixtures:

$$r_{22} = \rho_{22} = \sqrt{r_{22}\rho_{22}} \quad (\text{A.68})$$

### A.3 TRM for 2-port networks

As discussed in the de-embedding chapter, at low frequencies the "line" standard is replaced by the "match" one and the technique for obtaining the DUT-only scattering parameters is called "Thru-Reflect-Match" (TRM). The mathematical derivation for this technique can be addressed by treating it as a special case for the TRL method, explained in appendix A.2. Nevertheless, the mathematical procedure has to be handled with special attention, as the match standard is different from the line one.

The first step is to compute the transmission ( $\mathbf{R}$ ) matrix for the match standard. Figure A.1 shows the two-port network corresponding to the match standard.

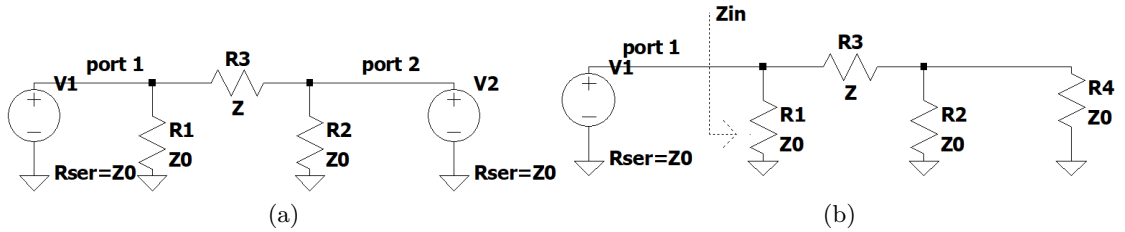


Figure A.1: Match standard (a) and set up for  $s_{11}$  computation (b).

The impedance  $Z$  is representing the isolation between ports 1 and 2: this will be taken into account in the computations but will not matter in the final results. The transmission matrix can be computed using equation A.24, after the S-parameters are known. First,  $s_{11}$  can be computed using 1.17.

$$Z_{in} = \frac{Z_0(Z + \frac{Z_0}{2})}{Z_0 + Z + Z_0/2} = \frac{Z_0(Z + Z_0/2)}{Z + \frac{3}{2}Z_0} \quad (\text{A.69})$$

$$\begin{aligned}
s_{11} &= \frac{Z_{in} - Z_0}{Z_{in} + Z_0} = \frac{\frac{Z_0 \left( Z + \frac{Z_0}{2} \right)}{Z + \frac{3}{2}Z_0} - Z_0}{\frac{Z_0 \left( Z + \frac{Z_0}{2} \right)}{Z + \frac{3}{2}Z_0} + Z_0} = \frac{Z_0 \left( Z + \frac{Z_0}{2} \right) - Z_0 \left( Z + \frac{3}{2}Z_0 \right)}{Z_0 \left( Z + \frac{Z_0}{2} \right) + Z_0 \left( Z + \frac{3}{2}Z_0 \right)} = \\
&= \frac{Z_0 Z + \frac{Z_0^2}{2} - Z_0 Z - \frac{3}{2}Z_0^2}{Z_0 Z + \frac{Z_0^2}{2} + Z_0 Z + \frac{3}{2}Z_0^2} = -\frac{1}{2} \frac{Z_0}{Z_0 + Z}
\end{aligned} \tag{A.70}$$

Due to the network symmetry,  $s_{22} = s_{11}$ . Then, it's possible to use 1.18 to find  $s_{21} = s_{12}$ , where  $V_{R4}$  is the voltage developed across  $R_4$ :

$$\begin{aligned}
s_{21} &= 2 \frac{2V_{R4}}{V_1} = \frac{\frac{Z_0}{2}}{Z + \frac{Z_0}{2}} \frac{\frac{Z_0 \left( Z + \frac{Z_0}{2} \right)}{Z + \frac{3}{2}Z_0}}{\frac{Z_0 \left( Z + \frac{Z_0}{2} \right)}{Z + \frac{3}{2}Z_0} + Z_0} = 2 \frac{\frac{Z_0}{2}}{Z + \frac{Z_0}{2}} \frac{Z_0 \left( Z + \frac{Z_0}{2} \right)}{Z_0 \left( Z + \frac{Z_0}{2} \right) + Z_0 Z + \frac{3}{2}Z_0^2} = \\
&= \frac{Z_0}{Z + \frac{Z_0}{2} + Z + \frac{3}{2}Z_0} = \frac{1}{2} \frac{Z_0}{Z_0 + Z}
\end{aligned} \tag{A.71}$$

The  $\mathbf{R}$  matrix can be computed with A.24:

$$r_{11} = -\frac{s_{11}s_{22} - s_{12}s_{21}}{s_{21}} = -\frac{\frac{1}{4} \frac{Z_0^2}{(Z + Z_0)^2} - \frac{1}{4} \frac{Z_0^2}{(Z + Z_0)^2}}{s_{21}} = 0 \tag{A.72}$$

$$r_{12} = \frac{s_{11}}{s_{21}} = \frac{-\frac{1}{2} \frac{Z_0}{Z + Z_0}}{\frac{1}{2} \frac{Z_0}{Z + Z_0}} = -1 \tag{A.73}$$

$$r_{21} = \frac{s_{11}}{s_{21}} = \frac{-\frac{1}{2} \frac{Z_0}{Z + Z_0}}{\frac{1}{2} \frac{Z_0}{Z + Z_0}} = -1 \tag{A.74}$$

$$r_{22} = \frac{1}{s_{21}} = \frac{2(Z_0 + Z)}{Z_0} \tag{A.75}$$

Let's consider now the equation that for TRL employs the measurement coming from the line-standard:

$$\mathbf{TR}_A = \mathbf{R}_A \mathbf{R}_L \quad (\text{A.76})$$

In this equivalence previously derived,  $\mathbf{T} = \mathbf{R}_D \mathbf{R}_T^{-1}$ ,  $\mathbf{R}_A$  is the  $\mathbf{R}$  matrix of the A fixture, while  $\mathbf{R}_L$  is the  $\mathbf{R}$  matrix for the line standard. In the TRM case, the  $\mathbf{R}_L$  matrix can be replaced by  $\mathbf{R}_M$ , that is corresponding to the  $\mathbf{R}$  matrix of a matched termination that has been just computed. In the TRM de-embedding, the value of the resistance of the "termination" (also called "match") standard employed will determine the reference impedance of the extracted DUT and fixture S-parameters, exactly in the same way as the TRL, where the "match" resistance is substituted by the characteristic impedance of the "line". If the impedance of the "match" is known, re-normalization to  $50\Omega$  is made as for the TRL. The  $\mathbf{R}_M$  matrix is expressed as follows:

$$\mathbf{R}_M = \begin{bmatrix} 0 & -1 \\ 1 & 2\frac{Z_0+Z}{Z_0} \end{bmatrix} \quad (\text{A.77})$$

It follows that:

$$\begin{bmatrix} t_{11} & t_{12} \\ t_{21} & t_{22} \end{bmatrix} \begin{bmatrix} a & b \\ c & 1 \end{bmatrix} = \begin{bmatrix} a & b \\ c & 1 \end{bmatrix} \begin{bmatrix} 0 & -1 \\ 1 & 2\frac{Z_0+Z}{Z_0} \end{bmatrix} \quad (\text{A.78})$$

Which can be expanded as:

$$\begin{cases} t_{11}a + t_{12}c = b \\ t_{21}a + t_{22}c = 1 \\ t_{11}b + t_{12} = -a + b \cdot 2\frac{Z_0+Z}{Z_0} \\ t_{21}b + t_{22} = -c + 2\frac{Z_0+Z}{Z_0} \end{cases} \quad (\text{A.79})$$

The same reasoning employed for the TRL can be applied here. In particular, it should be provided the equations that give  $b$  and  $\frac{a}{c}$ . The procedure is different from the TRL. First,  $b$  is obtained. In fact, considering the matrix  $\mathbf{R}_A$ :

$$\mathbf{R}_A = r_{22} \begin{bmatrix} a & b \\ c & 1 \end{bmatrix}$$

The  $\mathbf{R}_A$  matrix is the transmission matrix for fixture "A". It results from the conversion formulas [A.24](#):

$$b = s_{11} \quad (\text{A.80})$$

So  $b$  is equal to the input reflection coefficient of the fixture "A". In the TRM calibration, this is corresponding to the measured  $s_{11}$  of the match standard. So [A.80](#) is directly providing  $b$ . The other term is  $\frac{a}{c}$ . This can be obtained by dividing the first two of [A.79](#):

$$\frac{t_{11}a + t_{12}c}{t_{21}a + t_{22}c} = b$$

$$\frac{t_{11}\frac{a}{c} + t_{12}}{t_{21}\frac{a}{c} + t_{22}} = b$$

$$t_{11}\frac{a}{c} + t_{12} = t_{21}b\frac{a}{c} + t_{22}b$$

$$\frac{a}{c} = \frac{bt_{22} - t_{12}}{t_{11} - bt_{21}} \quad (\text{A.81})$$

From this point on, the equations are the same of the TRL (A.46 to A.68).

## A.4 multi-port de-embedding

The **right de-embedding** process consists of de-embed the known  $\mathbf{S}^{(2)}$  from the knowledge of  $\mathbf{S}$  and solving for  $\mathbf{S}^{(1)}$ . Let's start with the 1.66:

$$\mathbf{S}_{22} - \mathbf{S}_{22}^{(2)} = \mathbf{S}_{21}^{(2)}(\mathbf{I} - \mathbf{S}_{22}^{(1)}\mathbf{S}_{11}^{(2)})^{-1}\mathbf{S}_{22}^{(1)}\mathbf{S}_{12}^{(2)} \quad (\text{A.82})$$

$$(\mathbf{S}_{21}^{(2)})^{-1}(\mathbf{S}_{22} - \mathbf{S}_{22}^{(2)}) = (\mathbf{I} - \mathbf{S}_{22}^{(1)}\mathbf{S}_{11}^{(2)})^{-1}\mathbf{S}_{22}^{(1)}\mathbf{S}_{12}^{(2)} \quad (\text{A.83})$$

$$(\mathbf{I} - \mathbf{S}_{22}^{(1)}\mathbf{S}_{11}^{(2)})(\mathbf{S}_{21}^{(2)})^{-1}(\mathbf{S}_{22} - \mathbf{S}_{22}^{(2)}) = \mathbf{S}_{22}^{(1)}\mathbf{S}_{12}^{(2)} \quad (\text{A.84})$$

$$(\mathbf{S}_{21}^{(2)})^{-1}\mathbf{S}_{22} - (\mathbf{S}_{21}^{(2)})^{-1}\mathbf{S}_{22}^{(2)} - \mathbf{S}_{22}^{(1)}\mathbf{S}_{11}^{(2)}(\mathbf{S}_{21}^{(2)})^{-1}\mathbf{S}_{22} + \mathbf{S}_{22}^{(1)}\mathbf{S}_{11}^{(2)}(\mathbf{S}_{21}^{(2)})^{-1}\mathbf{S}_{22}^{(2)} = \mathbf{S}_{22}^{(1)}\mathbf{S}_{12}^{(2)} \quad (\text{A.85})$$

$$(\mathbf{S}_{21}^{(2)})^{-1}\mathbf{S}_{22} - (\mathbf{S}_{21}^{(2)})^{-1}\mathbf{S}_{22}^{(2)} = \mathbf{S}_{22}^{(1)}(\mathbf{S}_{11}^{(2)}(\mathbf{S}_{21}^{(2)})^{-1}\mathbf{S}_{22} - \mathbf{S}_{11}^{(2)}(\mathbf{S}_{21}^{(2)})^{-1}\mathbf{S}_{22}^{(2)}) + \mathbf{S}_{22}^{(1)}\mathbf{S}_{12}^{(2)} \quad (\text{A.86})$$

$$\begin{aligned} &(\mathbf{S}_{21}^{(2)})^{-1}\mathbf{S}_{22} - (\mathbf{S}_{21}^{(2)})^{-1}\mathbf{S}_{22}^{(2)} = \\ &= \mathbf{S}_{22}^{(1)}(\mathbf{S}_{11}^{(2)}(\mathbf{S}_{21}^{(2)})^{-1}\mathbf{S}_{22} - \mathbf{S}_{11}^{(2)}(\mathbf{S}_{21}^{(2)})^{-1}\mathbf{S}_{22}^{(2)} + \mathbf{S}_{12}^{(2)}) \end{aligned} \quad (\text{A.87})$$

$$\mathbf{S}_{22}^{(1)} = (\mathbf{S}_{21}^{(2)})^{-1}\mathbf{S}_{22} - (\mathbf{S}_{21}^{(2)})^{-1}\mathbf{S}_{22}^{(2)}(\mathbf{S}_{11}^{(2)}(\mathbf{S}_{21}^{(2)})^{-1}\mathbf{S}_{22} - \mathbf{S}_{11}^{(2)}) \quad (\text{A.88})$$

From the third equation:

$$(\mathbf{S}_{21}^{(1)}) = (\mathbf{I} - \mathbf{S}_{22}^{(1)}\mathbf{S}_{11}^{(2)})\mathbf{S}_{21}^{(2)} \quad (\text{A.89})$$

And similarly from the second one:

$$\mathbf{S}_{12}^{(1)} = \mathbf{S}_{12}(\mathbf{S}_{12}^{(2)})^{-1}(\mathbf{I} - \mathbf{S}_{11}^{(2)}\mathbf{S}_{22}^{(1)}) \quad (\text{A.90})$$

Finally from the first one:

$$\mathbf{S}_{11}^{(1)} = \mathbf{S}_{11} - \mathbf{S}_{12}^{(1)}\mathbf{S}_{11}^{(2)}(\mathbf{I} - \mathbf{S}_{22}^{(1)}\mathbf{S}_{11}^{(2)})^{-1}\mathbf{S}_{21}^{(1)} \quad (\text{A.91})$$

The **left de-embedding** process consists of de-embed the known  $\mathbf{S}^{(1)}$  from the knowledge of  $\mathbf{S}$  and solving for  $\mathbf{S}^{(2)}$ . Starting with the 1.63:

$$\mathbf{S}_{11} - \mathbf{S}_{11}^{(1)} = \mathbf{S}_{11}^{(1)} + \mathbf{S}_{12}^{(1)}\mathbf{S}_{11}^{(2)}(\mathbf{I} - \mathbf{S}_{22}^{(1)}\mathbf{S}_{11}^{(2)})^{-1}\mathbf{S}_{21}^{(1)} \quad (\text{A.92})$$

$$(\mathbf{S}_{12}^{(1)})^{-1}(\mathbf{S}_{11} - \mathbf{S}_{11}^{(1)})(\mathbf{S}_{21}^{(1)})^{-1} = \mathbf{S}_{11}^{(2)}(\mathbf{I} - \mathbf{S}_{22}^{(1)}\mathbf{S}_{11}^{(2)})^{-1} \quad (\text{A.93})$$

$$(\mathbf{S}_{12}^{(1)})^{-1}(\mathbf{S}_{11} - \mathbf{S}_{11}^{(1)})(\mathbf{S}_{21}^{(1)})^{-1}(\mathbf{I} - \mathbf{S}_{22}^{(1)}\mathbf{S}_{11}^{(2)}) = \mathbf{S}_{11}^{(2)} \quad (\text{A.94})$$

$$(\mathbf{S}_{12}^{(1)})^{-1}(\mathbf{S}_{11} - \mathbf{S}_{11}^{(1)})(\mathbf{S}_{21}^{(1)})^{-1} - ((\mathbf{S}_{12}^{(1)})^{-1}(\mathbf{S}_{11} - \mathbf{S}_{11}^{(1)})(\mathbf{S}_{21}^{(1)})^{-1})\mathbf{S}_{22}^{(1)}\mathbf{S}_{11}^{(2)} = \mathbf{I}\mathbf{S}_{11}^{(2)} \quad (\text{A.95})$$

$$(\mathbf{S}_{12}^{(1)})^{-1}(\mathbf{S}_{11} - \mathbf{S}_{11}^{(1)})(\mathbf{S}_{21}^{(1)})^{-1} = (\mathbf{S}_{11}^{(1)})(\mathbf{S}_{21}^{(1)})^{-1}\mathbf{S}_{22}^{(1)}\mathbf{S}_{11}^{(2)} + \mathbf{I}\mathbf{S}_{11}^{(2)} \quad (\text{A.96})$$

$$\mathbf{S}_{11}^{(2)} = (((\mathbf{S}_{12}^{(1)})^{-1}(\mathbf{S}_{11} - \mathbf{S}_{11}^{(1)})(\mathbf{S}_{21}^{(1)})^{-1})\mathbf{S}_{22}^{(1)} + \mathbf{I})^{-1}(\mathbf{S}_{12}^{(1)})^{-1}(\mathbf{S}_{11} - \mathbf{S}_{11}^{(1)})(\mathbf{S}_{21}^{(1)})^{-1} \quad (\text{A.97})$$

And in a similar way of before:

$$\mathbf{S}_{21}^{(2)} = \mathbf{S}_{21}(\mathbf{S}_{21}^{(1)})^{-1}(\mathbf{I} - \mathbf{S}_{22}^{(1)}\mathbf{S}_{11}^{(2)}) \quad (\text{A.98})$$

$$\mathbf{S}_{12}^{(2)} = (\mathbf{I} - \mathbf{S}_{11}^{(2)}\mathbf{S}_{22}^{(1)})(\mathbf{S}_{12}^{(1)})^{-1}\mathbf{S}_{12} \quad (\text{A.99})$$

$$\mathbf{S}_{22}^{(2)} = \mathbf{S}_{22} - \mathbf{S}_{21}^{(2)}(\mathbf{I} - \mathbf{S}_{22}^{(1)}\mathbf{S}_{11}^{(2)})^{-1}\mathbf{S}_{22}^{(1)}\mathbf{S}_{12}^{(2)} \quad (\text{A.100})$$

# Appendix B

## Matlab Code

In this appendix, it is provided the Matlab code used for the de-embedding. The main script allows the choice of two-port de-embedding or multi-port de-embedding.

```
1 %Main file for calling the de-embedding scripts. Can be used by
   following
2 %the prompts in the command window.
3 % Other m-files required: multiline.m, TRM_TRL_calibration.m,
4 % f_thru_de_embedding_left.m, f_multiport_de_embedding.m
5 % Subfunctions: select_match(),select_line(number), symmetrize(
   standard,symm)
6 disp("Insert choice"); disp("1: two-port de-embedding or two-
   port fixture characterization"); disp("2: multi-port de-
   embedding")
7 choice1 = input("");
8 switch(choice1)
9     case 1
10         disp("1: TRM");disp("2: TRM + TRL");disp("3: TRL")
11         choice2 = input("");
12         disp("Select thru measurement");[file_thru , path_thru] =
           uigetfile('*.s2p'); thru = sparameters(strcat(
           path_thru,file_thru));
13         calibration.frequencies = thru.Frequencies; res = length
           (calibration.frequencies);
14         disp("Select reflect measurement");[file_reflect ,
           path_reflect] = uigetfile('*.s2p'); reflect =
           sparameters(strcat(path_reflect ,file_reflect));
15         disp("Enter 1 for open, -1 for short"); reflection=input
           ("");
16         disp("Enter 1 if only reflect s11 is present in the
           measurement, enter 2 if s11 and s22 are present");
           symmetry = input("");
```

```

17     reflect = symmetrize(reflect ,symmetry);
18     disp("Enter 1 if fix-dut-fix two-port measurement is
19         present, enter 2 if not"); symmetry = input("");
20     if(symmetry ==1)
21     disp("Select fix-dut-fix measurement"); [file_total ,
22         path_total] = uigetfile('*.s2p'); total = sparameters
23         (strcat(path_total, file_total));
24     else
25     total = sparameters(zeros(2,2,res), calibration.
26         frequencies);
27     end
28     switch(choice2)
29     case 1
30         path_match = select_match(); match = sparameters
31             (path_match);
32         disp("Enter 1 if only match s11 is present in
33             the measurement, enter 2 if s11 and s22 are
34             present"); symmetry = input("");
35         match = symmetrize(match,symmetry); path_line =
36             0;
37         line_number = 0; only_TRL = 0; e_eff=1; fl=
38             calibration.frequencies(end)/1e9; fh =
39             calibration.frequencies(end)/1e9;
40     case 2
41         path_match = select_match(); match = sparameters
42             (path_match);
43         disp("Enter 1 only match s11 is present, enter 2
44             if s11 and s22 are present"); symmetry =
45             input("");
46         match = symmetrize(match,symmetry); only_TRL =
47             0;
48         disp("Enter lowest frequency (GHz) from which
49             apply the TRL"); fl = input("");
50         disp("Enter the upper frequency (GHz) to which
51             apply the TRL"); fh = input("");
52         disp("Enter line number"); line_number = input
53             (""); path_line = select_line(line_number);
54         disp("Enter line epsilon")
55         e_eff = input("");
56     case 3
57         disp("Enter line number")
58         line_number = input("");
59         path_line = select_line(line_number);
60         only_TRL = 1;
61     end

```



---

```

44 [line1, line2, line3, line4] = line_struct(line_number,
      path_line, calibration.frequencies);
45 disp("Enter the vector (Ohm) [R_match, Z0_line1, Z0_line2,
      Z0_line3, Z0_line4] for impedance correction")
46 z0_correction = input("");
47 %build the calibration input
48 calibration.line_number = line_number;
49 calibration.thru = thru; calibration.reflect = reflect;
      calibration.match = match; calibration.total = total;
50 calibration.line1 = line1; calibration.line2 = line2;
      calibration.line3 = line3; calibration.line4 = line4;
51 %Compute the transition frequencies of each line standard and
      build the
52 %matrix of the match/line standard.
53 [line_p, index_fl, index_1, index_2, index_3] = multiline(
      calibration, only_TRL, e_eff, fl, fh);
54 calibration.line = sparameters(line_p, calibration.frequencies
      );
55 z0=50;
56 [fix1, fix2, dut, cal] = TRM_TRL_calibration(z0, calibration,
      symmetry, reflection, z0_correction, index_fl, index_1,
      index_2, index_3, line_number);

57
58 case 2
59 disp("Enter the number of DUT ports"); Num = input("");
60 disp("Enter the port number of the characterized fixture");
      first = input(""); entered(1) = first;
61 disp("Enter the fixture"); [file_fix, path_fix] = uigetfile('*.*
      s2p'); fix = sparameters(strcat(path_fix, file_fix));
62 Fix{first} = fix;
63 for k=2:Num
64 disp("Enter the port number of the fixture in the thru
      connection"); Id = input("");
65 disp("Enter the known fixture of the thru"); [file_fix, path_fix
      ] = uigetfile('*.*s2p'); fix = sparameters(strcat(path_fix,
      file_fix));
66 disp("Select thru of the known fixture with fixture connected to
      port " + Id ); [file_thru, path_thru] = uigetfile('*.*s2p');
      thru_2 = sparameters(strcat(path_thru, file_thru));
67 Fix{Id} = f_thru_de_embedding_left(thru_2, fix, 1);
68 rfwrite(Fix{Id}, "fix" + Id + ".s2p"); entered(k) = Id;
69 disp("Already entered "); entered
70 end

```

```
71 disp("Enter the total fix-dut-fix measurement"); [file_tot ,  
    path_tot] = uigetfile('*.s2p'); tot = sparameters(strcat(  
    path_tot, file_tot));  
72 [dut] = f_multiport_de_embedding(tot, Fix);  
73 end  
74  
75  
76 function path_match = select_match()  
77 disp("Select match file")  
78 [file_match, path_match1] = uigetfile('*.s2p');  
79 path_match = strcat(path_match1, file_match);  
80 end  
81  
82 function path_line = select_line(number)  
83 disp("Select line measurement, starting from low frequency ones  
    ")  
84 for k=1:number  
85 disp("Select line "+ k + " file")  
86 [file_line, path_line1] = uigetfile('*.s2p');  
87 path_line{k} = strcat(path_line1, file_line);  
88 end  
89 end  
90  
91 function [line1, line2, line3, line4] = line_struct(line_number,  
    Path_tot_line, freq)  
92 res = length(freq);  
93 switch line_number  
94     case 0  
95         line1 = sparameters(zeros(2,2,res), freq); line2 =  
            sparameters(zeros(2,2,res), freq);  
96         line3 = sparameters(zeros(2,2,res), freq); line4 =  
            sparameters(zeros(2,2,res), freq);  
97     case 1  
98         line1 = sparameters(Path_tot_line{1}); line2 =  
            sparameters(zeros(2,2,res), freq);  
99         line3 = sparameters(zeros(2,2,res), freq); line4 =  
            sparameters(zeros(2,2,res), freq);  
100    case 2  
101        line1 = sparameters(Path_tot_line{1}); line2 =  
            sparameters(Path_tot_line{2});  
102        line3 = sparameters(zeros(2,2,res), freq); line4 =  
            sparameters(zeros(2,2,res), freq);  
103    case 3  
104        line1 = sparameters(Path_tot_line{1}); line2 =  
            sparameters(Path_tot_line{2});
```

---

```

105         line3 = sparameters(Path_tot_line{3}); line4 =
           sparameters(zeros(2,2,res), freq);
106     case 4
107         line1 = sparameters(Path_tot_line{1}); line2 =
           sparameters(Path_tot_line{2});
108         line3 = sparameters(Path_tot_line{3}); line4 =
           sparameters(Path_tot_line{4});
109     end
110 end
111 function S_obj = symmetrize(standard,symm) %build the match and
           reflect matrices
112 S_obj_p = standard.Parameters;
113 S_obj_p(1,2,:) = 0.000001; %set transmission to -120dB
114 S_obj_p(2,1,:) = S_obj_p(1,2,:);
115 if(symm == 1)
116     S_obj_p(2,2,:) = S_obj_p(1,1,:);
117 end
118 S_obj = sparameters(S_obj_p,standard.Frequencies);
119 end

1 function [one, two, three, four, number] = f_TRL_line_calc(fl,fh
           ,e_eff, drawPlot)
2 %% HEADER
3 %TRL_line_calc - Computation of the line standards to fabricate
           required to perform a TRL de embedding.
4 %
5 % Syntax: [one, two, three, four, number] = TRL_line_calc(fl,fh
           ,e_eff)
6 %
7 % Inputs:
8 %     fl - Lower frequency (GHz) from which apply the TRL.
9 %     fh - Upper frequency (GHz) to which apply the TRL.
10 %     e_eff - Effective dielectric constant of the PCB.
11 %
12 % Outputs:
13 %     one, two, three, four - Line standard characteristics for
           each corresponding number of lines.
14 %     | physical length(mm) | transition frequency (GHz) | center
           frequency (GHz) | phase at lowest frequency (deg) | phase at
           highest frequency (deg) |
15 %     each row i represent the i-th line to fabricate.
16 %     number - minimum number of lines to be used such that
           lowest and upper
17 %     phase delay is between 20deg and 160deg.
18 %

```

---

```

19 % Example: [one, two, three, four, number] = TRL_line_calc(fl, fh
    , e_eff)
20 %
21 % Other m-files required: none
22 % Subfunctions: none
23 % MAT-files required: none
24 %
25 % See also: https://www.microwaves101.com/encyclopedias/trl-
    calibration
26 % Author: Ivan Porcelli
27 % Politecnico di torino
28 % email address: s277252@studenti.polito.it
29 % Website:
30 % December 2021
31 %% Declare the variables
32 lines = zeros(4,3);
33 fh_fl = fh/fl;
34 fc1 = 0; ft1 = 0; fc2 = 0; ft2 = 0; fc3 = 0; ft3 = 0; fc4 = 0;
    ft4=0; l1 =0; l2 = 0; l3 = 0; l4 = 0; number= 0;
35 phi_l1 =0; phi_h1 = 0; phi_l2 =0; phi_h2 = 0; phi_l3 =0; phi_h3
    = 0; phi_l4 =0; phi_h4 = 0;
36
37 %% Compute the line lengths and frequency ranges
38 %one line solution
39 ft1 = fh; %GHz
40 fc1 = fl + (fh-fl)/2; %GHz
41 l1 = (1/4)*300/(sqrt(e_eff)*fc1); %mm
42 phi_l1 = l1*360/(300/fl/sqrt(e_eff));
43 phi_h1 = l1*360/(300/fh/sqrt(e_eff));
44 one(1,1) = l1; one(1,2) = ft1; one(1,3) = fc1; one(1,4) = phi_l1
    ; one(1,5) = phi_h1;
45 one(2,1) = l2; one(2,2) = ft2; one(2,3) = fc2; one(2,4) = phi_l2
    ; one(2,5) = phi_h2;
46 one(3,1) = l3; one(3,2) = ft3; one(3,3) = fc3; one(3,4) = phi_l3
    ; one(3,5) = phi_h3;
47 one(4,1) = l4; one(4,2) = ft4; one(4,3) = fc4; one(4,4) = phi_l4
    ; one(4,5) = phi_h4;
48 if(fh_fl<=8)
49     number = 1;
50 end
51 frequencies = linspace(fl*1e9, fh*1e9*1.1, 1000);
52
53 y1 = l1*360./(300./frequencies./sqrt(e_eff))/1e9;
54
55 if(drawPlot)

```

```

56 figure
57 semilogx(frequencies , y1, 'LineWidth',2.1);
58     xlabel('Frequency(Hz)')
59     ylabel('Electrical length(deg)')
60     grid on; set(gca, 'fontsize',20);
61     xline(ft1*1e9)
62         title("One line solution")
63         legend("Line 1")
64 end
65 %two line solution
66 ft1 = fl*sqrt(fh/fl); %GHz
67 ft2 = fh;
68 fc1 = fl + (ft1-fl)/2; %GHz
69 l1 = (1/4)*300/(sqrt(e_eff)*fc1); %mm
70 fc2 = ft1 + (fh - ft1)/2; %GHz
71 l2 = (1/4)*300/(sqrt(e_eff)*fc2); %mm
72 phi_l1 = l1*360/(300/fl/sqrt(e_eff));
73 phi_h1 = l1*360/(300/ft1/sqrt(e_eff));
74 phi_l2 = l2*360/(300/ft1/sqrt(e_eff));
75 phi_h2 = l2*360/(300/fh/sqrt(e_eff));
76 two(1,1) = l1; two(1,2) = ft1; two(1,3) = fc1; two(1,4) = phi_l1
77     ; two(1,5) = phi_h1;
78 two(2,1) = l2; two(2,2) = ft2; two(2,3) = fc2; two(2,4) = phi_l2
79     ; two(2,5) = phi_h2;
80 two(3,1) = l3; two(3,2) = ft3; two(3,3) = fc3; two(3,4) = phi_l3
81     ; two(3,5) = phi_h3;
82 two(4,1) = l4; two(4,2) = ft4; two(4,3) = fc4; two(4,4) = phi_l4
83     ; two(4,5) = phi_h4;
84 if (fh_fl>8 && fh_fl <=64)
85 number = 2;
86 end
87 y = [l1*360./(300./frequencies./sqrt(e_eff))/1e9; l2
88     *360./(300./frequencies./sqrt(e_eff))/1e9];
89 if (drawPlot)
90 figure
91 for k=1:2
92
93 semilogx(frequencies , y(k,:), 'LineWidth',2.1);
94 hold on
95     xlabel('Frequency(Hz)')
96     ylabel('Electrical length(deg)')
97
98     grid on; set(gca, 'fontsize',20);
99     title("Two lines solution")
100 end

```

```

96     xline(ft1*1e9);           xline(ft2*1e9)
97
98     legend("Line 1", "Line 2")
99     end
100    %three line solution
101    ft1 = fl*10^(log10(fh/fl)/3); %GHz
102    fc1 = fl + (ft1-fl)/2; %GHz
103    l1 = (1/4)*300/(sqrt(e_eff)*fc1); %mm
104    ft2 = fl*10^(log10(fh/fl)*(2/3)); %GHz
105    ft3=fh;
106    fc2 = (ft1 + ft2)/2; %GHz
107    l2 = (1/4)*300/(sqrt(e_eff)*fc2); %mm
108    fc3 = (ft2 + fh)/2;
109    l3 = (1/4)*300/(sqrt(e_eff)*fc3); %mm
110    phi_l1 = l1*360/(300/fl/sqrt(e_eff));
111    phi_h1 = l1*360/(300/ft1/sqrt(e_eff));
112    phi_l2 = l2*360/(300/ft1/sqrt(e_eff));
113    phi_h2 = l2*360/(300/ft2/sqrt(e_eff));
114    phi_l3 = l3*360/(300/ft2/sqrt(e_eff));
115    phi_h3 = l3*360/(300/fh/sqrt(e_eff));
116    three(1,1) = l1; three(1,2) = ft1; three(1,3) = fc1; three(1,4)
        = phi_l1; three(1,5) = phi_h1;
117    three(2,1) = l2; three(2,2) = ft2; three(2,3) = fc2; three(2,4)
        = phi_l2; three(2,5) = phi_h2;
118    three(3,1) = l3; three(3,2) = ft3; three(3,3) = fc3; three(3,4)
        = phi_l3; three(3,5) = phi_h3;
119    three(4,1) = l4; three(4,2) = ft4; three(4,3) = fc4; three(4,4)
        = phi_l4; three(4,5) = phi_h4;
120    if(fh_fl>64 && fh_fl <=512)
121        number = 3;
122
123    end
124    y = [l1*360./(300./frequencies./sqrt(e_eff))/1e9; l2
        *360./(300./frequencies./sqrt(e_eff))/1e9; l3*360./(300./
        frequencies./sqrt(e_eff))/1e9];
125    if (drawPlot)
126        figure
127        for k=1:3
128
129            semilogx(frequencies , y(k,:), 'LineWidth',2.1);
130            hold on
131                xlabel('Frequency(Hz)')
132                ylabel('Electrical length(deg)')
133
134                grid on; set(gca, 'fontsize',20);

```

```

135         title("Three lines solution")
136     end
137     xline(ft1*1e9);           xline(ft2*1e9);   xline(fh*1e9);
138
139     legend("Line 1", "Line 2", "Line 3")
140 end
141 %four line solution
142 ft1 = fl*10^(log10(fh/fl)/4); %GHz
143 fc1 = fl + (ft1-fl)/2; %GHz
144 l1 = (1/4)*300/(sqrt(e_eff)*fc1); %mm
145 ft2 = fl*10^(log10(fh/fl)*2/4); %GHz
146 fc2 = (ft1 + ft2)/2; %GHz
147 l2 = (1/4)*300/(sqrt(e_eff)*fc2); %mm
148 ft3 = fl*10^(log10(fh/fl)*3/4); %GHz
149 fc3 = (ft2 + ft3)/2;
150 l3 = (1/4)*300/(sqrt(e_eff)*fc3); %mm
151 fc4 = (ft3 + fh)/2;
152 ft4 = fh;
153 l4 = (1/4)*300/(sqrt(e_eff)*fc4); %mm
154 phi_l1 = l1*360/(300/fl/sqrt(e_eff));
155 phi_h1 = l1*360/(300/ft1/sqrt(e_eff));
156 phi_l2 = l2*360/(300/ft1/sqrt(e_eff));
157 phi_h2 = l2*360/(300/ft2/sqrt(e_eff));
158 phi_l3 = l3*360/(300/ft2/sqrt(e_eff));
159 phi_h3 = l3*360/(300/ft3/sqrt(e_eff));
160 phi_l4 = l4*360/(300/ft3/sqrt(e_eff));
161 phi_h4 = l4*360/(300/fh/sqrt(e_eff));
162 four(1,1) = l1; four(1,2) = ft1; four(1,3) = fc1; four(1,4) =
    phi_l1; four(1,5) = phi_h1;
163 four(2,1) = l2; four(2,2) = ft2; four(2,3) = fc2; four(2,4) =
    phi_l2; four(2,5) = phi_h2;
164 four(3,1) = l3; four(3,2) = ft3; four(3,3) = fc3; four(3,4) =
    phi_l3; four(3,5) = phi_h3;
165 four(4,1) = l4; four(4,2) = ft4; four(4,3) = fc4; four(4,4) =
    phi_l4; four(4,5) = phi_h4;
166 if(fh_fl>512)
167     number = 4;
168 end
169 y = [l1*360./(300./frequencies./sqrt(e_eff))/1e9; l2
    *360./(300./frequencies./sqrt(e_eff))/1e9; l3*360./(300./
    frequencies./sqrt(e_eff))/1e9; l4*360./(300./frequencies./
    sqrt(e_eff))/1e9];
170 if (drawPlot)
171     figure
172     for k=1:4

```

```

173
174 semilogx(frequencies , y(k,:), 'LineWidth',2.1);
175 hold on
176     xlabel('Frequency(Hz)')
177     ylabel('Electrical length(deg)')
178
179     grid on; set(gca,'fontsize',20);
180     title("Four lines solution")
181 end
182     xline(ft1*1e9);           xline(ft2*1e9);   xline(ft3*1e9); xline
    (fh*1e9);
183
184 legend("Line 1", "Line 2", "Line 3", "Line 4")
185 end
186
187 end

1 function [line_p, index_fl,index_1, index_2, index_3] =
    multiline(calibration,only_TRL, e_eff, fl, fh)
2 %% HEADER
3 %multiline – This function is called by the main function
4 %"f_TRM_TRL_multiline_de_embedding.m". It computes the matrix
    that contains
5 %the match and line standards data considering the transition
    frequency
6 %between each standard.
7 %
8 % Syntax: [line_p, index_fl,index_1, index_2, index_3] =
    multiline(calibration,only_TRL, e_eff, fl, fh)
9 %
10 % Inputs:
11 %     calibration – Struct containing the fields:
12 %         line_number: number of line stadnards
13 %         freq: frequency vector of the measurements
14 %         match, line1, line2, line3, line4: Corresponding
    measurements
15 %
16 %     only_TRL – 1: Only TRL is used.
17 %               – 0: Use TRM if the specified line number is 0,
    otherwise
18 %               uses a combination of TRM/TRL..
19 %
20 %     fl – Lower frequency (GHz) from which apply the TRL. From
    the lowest
21 %     measured frequency to fl TRM will be used.

```



```
22 %
23 %   fh – Upper frequency (GHz) to which apply the TRL.
24 %
25 %   e_eff – Effective dielectric constant of the line standards
26 %
27 % Outputs:
28 %   line_p – matrix that contains the match and line standards
           data
29 %   index_fl – Frequency vector index up to which use match
           standard. When
30 %   just TRL is used, index_fl = 0
31 %   index_1, index_2, index_3 – Transition frequencies indexes
           for the line
32 %   measurements. Line 1 used between index_fl + 1 and index_1,
           Line 2 used
33 %   between index_1 + 1 and index_2 ...
34 % Example:
35 %
36 % Other m-files required: TRL_line_calc.m,
           f_TRM_TRL_multiline_de_embedding.m,
37 % Subfunctions: none
38 % MAT-files required: none
39 %
40 % See also: /
41 % Author: Ivan Porcelli
42 % Politecnico di torino
43 % email address: s277252@studenti.polito.it
44 % Website:
45 % March 2022
46 %————— BEGIN CODE —————
47
48 line_number = calibration.line_number;
49 match = calibration.match; line1 = calibration.line1; line2 =
           calibration.line2;
50 line3 = calibration.line3; line4 = calibration.line4; freq =
           calibration.frequencies;
51
52 [~, two, three, four, number] = f_TRL_line_calc(fl, fh, e_eff);
53
54 line_p = zeros(2,2,length(freq));
55
56 switch line_number
57     case 0
58         line_p(:, :, 1:end) = match.Parameters(:, :, 1:end);
```

```

59     disp("Match from " + freq(1)/1e6 + " MHz to " + freq(end
        )/1e6 + " MHz")
60     disp("Only match standard used")
61     index_fl = length(freq); index_1 = length(freq); index_2
        = length(freq); index_3 = length(freq);
62     case 1
63         [~, index_fl] = min(abs(freq-1e9*f1)); %From min freq to
            fl match is used
64         index_fl = ~only_TRL*index_fl;
65         line_p(:, :, 1:index_fl) = match.Parameters(:, :, 1:index_fl
            );
66         line_p(:, :, ((index_fl+1):end)) = line1.Parameters(:, :, ((
            index_fl+1):end));
67         disp("Match from " + freq(1)/1e6 + " MHz to " + freq(max
            (1, index_fl))/1e6 + " MHz")
68         disp("Line 1 from " + freq(max(1, index_fl))/1e6 + " MHz
            to " + freq(end)/1e6 + " MHz")
69         index_1 = length(freq); index_2 = length(freq); index_3
            = length(freq);
70     case 2
71         [~, index_fl] = min(abs(freq-1e9*f1)); %From min freq to
            fl match is used
72         index_fl = ~only_TRL*index_fl;
73         [~, index_1] = min(abs(freq-1e9*two(1,2)));
74         line_p(:, :, 1:index_fl) = match.Parameters(:, :, 1:index_fl
            );
75         line_p(:, :, ((index_fl+1):index_1)) = line1.Parameters
            (:, :, ((index_fl+1):index_1));
76         line_p(:, :, ((index_1+1):end)) = line2.Parameters(:, :, ((
            index_1+1):end));
77         disp("Match from " + freq(1)/1e6 + " MHz to " + freq(max
            (1, index_fl))/1e6 + " MHz")
78         disp("Line 1 from " + freq(max(1, index_fl))/1e6 + " MHz
            to " + freq(index_1)/1e6 + " MHz")
79         disp("Line 2 from " + freq(index_1)/1e6 + " MHz to " +
            freq(end)/1e6 + " MHz")
80         index_2 = length(freq); index_3 = length(freq);
81
82     case 3
83         [~, index_fl] = min(abs(freq-1e9*f1)); %From min freq to
            fl match is used
84         index_fl = ~only_TRL*index_fl;
85         [~, index_1] = min(abs(freq-1e9*three(1,2)));
86         [~, index_2] = min(abs(freq-1e9*three(2,2)));

```

```

87     line_p(:, :, 1:index_fl) = match.Parameters(:, :, 1:index_fl
88         );
89     line_p(:, :, ((index_fl+1):index_1))= line1.Parameters
90         (:, :, ((index_fl+1):index_1));
91     line_p(:, :, ((index_1+1):index_2))= line2.Parameters
92         (:, :, ((index_1+1):index_2));
93     line_p(:, :, ((index_2+1):end))= line3.Parameters(:, :, ((
94         index_2+1):end));
95     disp("Match from " + freq(1)/1e6 + " MHz to " + freq(max
96         (1,index_fl))/1e6 + " MHz")
97     disp("Line 1 from " + freq(max(1,index_fl))/1e6 + " MHz
98         to " + freq(index_1)/1e6 + " MHz")
99     disp("Line 2 from " + freq(index_1)/1e6 + " MHz to " +
100         freq(index_2)/1e6 + " MHz")
101     disp("Line 3 from " + freq(index_2)/1e6 + " MHz to " +
102         freq(end)/1e6 + " MHz")
103     index_3 = length(freq);
104 otherwise
105     [~, index_fl] = min(abs(freq-1e9*f1)); %From min freq to
106         fl match is used
107     index_fl = ~only_TRL*index_fl;
108     [~, index_1] = min(abs(freq-1e9*four(1,2)));
109     [~, index_2] = min(abs(freq-1e9*four(2,2)));
110     [~, index_3] = min(abs(freq-1e9*four(3,2)));
111     line_p(:, :, 1:index_fl) = match.Parameters(:, :, 1:index_fl
112         );
113     line_p(:, :, ((index_fl+1):index_1))= line1.Parameters
114         (:, :, ((index_fl+1):index_1));
115     line_p(:, :, ((index_1+1):index_2))= line2.Parameters
116         (:, :, ((index_1+1):index_2));
117     line_p(:, :, ((index_2+1):index_3))= line3.Parameters
118         (:, :, ((index_2+1):index_3));
119     line_p(:, :, ((index_3+1):end))= line4.Parameters(:, :, ((
120         index_3+1):end));
121     disp("Match from " + freq(1)/1e6 + " MHz to " + freq(max
122         (1,index_fl))/1e6 + " MHz")
123     disp("Line 1 from " + freq(max(1,index_fl))/1e6 + " MHz
124         to " + freq(index_1)/1e6 + " MHz")
125     disp("Line 2 from " + freq(index_1)/1e6 + " MHz to " +
126         freq(index_2)/1e6 + " MHz")
127     disp("Line 3 from " + freq(index_2)/1e6 + " MHz to " +
128         freq(index_3)/1e6 + " MHz")
129     disp("Line 4 from " + freq(index_3)/1e6 + " MHz to " +
130         freq(end)/1e6 + " MHz")
131 end

```

```
113 %————— END OF CODE —————

1 function [fix1,fix2,dut,cal] = TRM_TRL_calibration(z0,
    calibration, symmetry, reflection, z0_renorm, index_fl,
    index_1, index_2, index_3,line_number)
2 %% HEADER
3 %%TRM_TRL_calibration – This function is called by the main
    function
4 %"f_TRM_TRL_multiline_de_embedding.m". It implements the de-
    embedding
5 %mathematics.
6 %
7 % Syntax: [fix1,fix2,dut] = TRM_TRL_calibration(z0, calibration
    , symmetry, reflection, z0_renorm, index_fl,index_1, index_2,
    index_3,line_number)
8 %
9 % Inputs: see functions "f_TRM_TRL_multiline_de_embedding.m" and
    "multiline.m"
10 %
11 % Outputs:
12 %     dut – Dut scattering parameters
13 %     fix1 – Left fixture scattering parameters
14 %     fix2 – Right fixture scattering parameters (equal to fix1,
    but reversed ports)
15 %
16 % Example:
17 %
18 % Other m-files required: TRL_line_calc.m,
    f_TRM_TRL_multiline_de_embedding.m, multiline.m
19 % Subfunctions: none
20 % MAT-files required: none
21 %
22 % See also: /
23 % Author: Ivan Porcelli
24 % Politecnico di torino
25 % email address: s277252@studenti.polito.it
26 % Website:
27 % March 2022
28 %————— BEGIN CODE —————
29 %extract the s matrix of the standards
30 thru_s = calibration.thru.Parameters;
31 reflect_s = calibration.reflect.Parameters;
32 line_s = calibration.line.Parameters;
33 total_s = calibration.total.Parameters;
34 freq = calibration.frequencies;
```

```

35 res = length(freq);
36
37 %Renormalization of the s parameters of the measured standards
38 line_s = re_normalize(line_s,0);
39 reflect_s = re_normalize(reflect_s,0);
40 thru_s = re_normalize(thru_s,0);
41 total_s = re_normalize(total_s,0);
42
43 %calculate trasmission matrices
44 line_T = s2t(line_s);
45 thru_T= s2t(thru_s);
46 total_T = s2t(total_s);
47
48 %define dut and fixture transmission matrices
49 R = zeros(2,2,res);
50 fix_tr = zeros(2,2,res);
51
52 %de embedding for each frequency
53 for k=1:res
54     line_t = line_T(:, :, k);
55     thru_t = thru_T(:, :, k);
56     total_t = total_T(:, :, k);
57
58     line_t([1 4]) = line_t([4 1]);
59     line_t([3 2]) = line_t([2 3]);
60
61     thru_t([1 4]) = thru_t([4 1]);
62     thru_t([3 2]) = thru_t([2 3]);
63
64     total_t([1 4]) = total_t([4 1]);
65     total_t([3 2]) = total_t([2 3]);
66
67     T = line_t*inv(thru_t);
68     [x] = roots([T(2,1), T(2,2) - T(1,1), -T(1,2)]);
69     if(k > index_fl) %use trl expression
70     if(abs(x(1))>abs(x(2)))
71         a_c = x(1); %a/c
72         b = x(2); %b
73     else
74         a_c = x(2); %a/c
75         b = x(1); %b
76     end
77     %use trm expression
78     b = line_s(1,1,k);
79     c = (1-(T(2,1)/T(1,2))*b)/(T(2,2)-T(1,2)*T(2,1)/T(1,1));

```

```

80     a = (b-T(1,2)*c)/T(1,1);
81     a_c = a/c;
82     end
83     %g d e f
84     g = thru_t(2,2);
85     thru_t = thru_t./g;
86     d = thru_t(1,1);
87     e = thru_t(1,2);
88     f = thru_t(2,1);
89     %compute the 4 parameters
90     gamma = (f - d/a_c)/(1 - e/a_c);
91     beta_alpha = (e - b)/(d - b*f);
92     r22rho22 = g*(1-e/a_c)/(1 - b/a_c);
93     alphaa = (d - b*f)/(1 - e/a_c);
94     %compute a
95     w1 = reflect_s(1,1,k);
96     w2 = reflect_s(2,2,k);
97
98     term1 = (w1 - b)/(w2 + gamma);
99     term2 = (1+w2*beta_alpha)/(1 - w1/a_c);
100    term3 = (d - b*f)/(1-e/a_c);
101
102    a = sqrt(term1*term2*term3);
103    gamma_reflect =(w1 - b)/(a*(1-w1/a_c));
104
105    if (sign(real(gamma_reflect))~=reflection)
106        a = -sqrt(term1*term2*term3);
107        gamma_reflect =(w1 - b)/(a*(1-w1/a_c));
108
109    end
110
111    %dut direct computation
112    coeff = (1/r22rho22)*(1/alphaa)*(1/(1-b/a_c))*(1/(1-gamma*
        beta_alpha));
113    m1 = [1 -b; -a/a_c a];
114    m2 = [1 -beta_alpha*alphaa/a; -gamma alphaa/a];
115
116    %matrice dut
117    R_p = coeff*m1*total_t*m2;
118    R_p([1 4]) = R_p([4 1]);
119    R_p([3 2]) = R_p([2 3]);
120    R(:, :, k) = R_p;
121
122    %fixture matrix (only if symmetric)
123    fix_tr_tmp = (1/sqrt(r22rho22))*(1/(a - b*a/a_c ))*m1;

```

---

```

124     fix_tr_tmp = inv(fix_tr_tmp);
125     fix_2_tmp = fix_tr_tmp;
126     fix_tr_tmp([1 4]) = fix_tr_tmp([4 1]);
127     fix_tr_tmp([3 2]) = fix_tr_tmp([2 3]);
128     fix_tr(:, :, k) = fix_tr_tmp;
129     fix_2(:, :, k) = fix_2_tmp;
130 end
131 %Left fixture scattering matrix
132 fix1_p = t2s(fix_tr);
133
134 %Right fixture scattering matrix
135 fix2_p = fix1_p;
136 for k=1:res
137     tmp = fix2_p(1,1,k);
138     fix2_p(1,1,k) = fix2_p(2,2,k);
139     fix2_p(2,2,k) = tmp;
140 end
141
142 %renormalize fix s-parameters
143 fix1_p = re_normalize(fix1_p,1);
144 fix2_p = re_normalize(fix2_p,1);
145 fix1_p(1,2,:) = angle_corr(fix1_p(1,2,:)); fix1_p(2,1,:) =
    angle_corr(fix1_p(2,1,:));
146 fix2_p(1,2,:) = angle_corr(fix2_p(1,2,:)); fix2_p(2,1,:) =
    angle_corr(fix2_p(2,1,:));
147 fix1 = sparameters(fix1_p, freq);
148 fix2 = sparameters(fix2_p, freq);
149
150 %compute dut s-parameters
151 if (~isnan(R)) %total is provided
152     dut = t2s(R);
153     dut = re_normalize(dut,1);
154     dut = sparameters(dut, freq);
155 else
156     dut = [];
157 end
158
159 cal = deembedsparams(calibration.thru, fix1, fix2);
160
161
162 if (~symmetry)
163     fix1.Parameters = zeros(2,2,res);
164     fix2.Parameters = zeros(2,2,res);
165 end
166

```

```

167 function s = angle_corr(Sp)
168 Sp_angle = angle(Sp);
169 Sp_diff = squeeze(diff(Sp_angle));
170 index = find(abs(Sp_diff) > pi*0.98);
171 counter = length(index);
172 i = 1; %keep track of the index
173 for kk=1:res
174 if(i<=counter)
175 if (kk==index(i))
176     i = i+1;
177 end
178 end
179 if(mod(i,2) == 0)
180 Sp(kk) = -(1)*Sp(kk);
181 end
182 end
183 s = Sp;
184 end
185 function y = re_normalize(S_param, opposite)
186     if(opposite)
187         z1 = z0_renorm;
188         z1_renorm = z0*ones(1,5);
189     else
190         z1 = z0*ones(1,5);
191         z1_renorm = z0_renorm;
192     end
193     %match freq re-normalization
194
195     %line freq re-normalization
196     switch line_number
197     case 0
198         S_param_m = s2s(S_param(:, :, 1:max(1, index_fl)), z1(1)
199             , z1_renorm(1));
200         S_param(:, :, 1:index_fl) = S_param_m;
201         disp("renorm from "+z1(1) + " to " + z1_renorm(1));
202     case 1
203         S_param_m = s2s(S_param(:, :, 1:max(1, index_fl)), z1(1)
204             , z1_renorm(1));
205         S_param(:, :, 1:max(1, index_fl)) = S_param_m;
206         S_param_1 = s2s(S_param(:, :, (index_fl+1):end), z1(2)
207             , z1_renorm(2));
208         S_param(:, :, (index_fl+1):end) = S_param_1;
209     case 2
210         S_param_m = s2s(S_param(:, :, 1:max(1, index_fl)), z1(1)
211             , z1_renorm(1));

```



```

208     S_param(:, :, 1:max(1, index_fl)) = S_param_m;
209     S_param_1 = s2s(S_param(:, :, (index_fl+1):index_1), z1
    (2), z1_renorm(2));
210     S_param(:, :, (index_fl+1):index_1) = S_param_1;
211     S_param_2 = s2s(S_param(:, :, (index_1+1):end), z1(3),
    z1_renorm(3));
212     S_param(:, :, (index_1+1):end) = S_param_2;
213     case 3
214         S_param_m = s2s(S_param(:, :, 1:max(1, index_fl)), z1(1)
    , z1_renorm(1));
215         S_param(:, :, 1:max(1, index_fl)) = S_param_m;
216         S_param_1 = s2s(S_param(:, :, (index_fl+1):index_1), z1
    (2), z1_renorm(2));
217         S_param(:, :, (index_fl+1):index_1) = S_param_1;
218         S_param_2 = s2s(S_param(:, :, (index_1+1):index_2), z1
    (3), z1_renorm(3));
219         S_param(:, :, (index_1+1):index_2) = S_param_2;
220         S_param_3 = s2s(S_param(:, :, (index_2+1):end), z1(4),
    z1_renorm(4));
221         S_param(:, :, (index_2+1):end) = S_param_3;
222     otherwise
223         S_param_m = s2s(S_param(:, :, 1:max(1, index_fl)), z1(1)
    , z1_renorm(1));
224         S_param(:, :, 1:max(1, index_fl)) = S_param_m;
225         S_param_1 = s2s(S_param(:, :, (index_fl+1):index_1), z1
    (2), z1_renorm(2));
226         S_param(:, :, (index_fl+1):index_1) = S_param_1;
227         S_param_2 = s2s(S_param(:, :, (index_1+1):index_2), z1
    (3), z1_renorm(3));
228         S_param(:, :, (index_1+1):index_2) = S_param_2;
229         S_param_3 = s2s(S_param(:, :, (index_2+1):index_3), z1
    (4), z1_renorm(4));
230         S_param(:, :, (index_2+1):index_3) = S_param_3;
231         S_param_4 = s2s(S_param(:, :, (index_3+1):end), z1(5),
    z1_renorm(5));
232         S_param(:, :, (index_3+1):end) = S_param_4;
233     end
234     y = S_param;
235     end
236
237 end
238
239 %————— END OF CODE —————

1 function [dut] = f_multiport_de_embedding(total, Fix)

```

```
2 %% HEADER
3 %f_multiport_de_embedding – This function can perform de-
  embedding on
4 %networks with an even or odd number of ports. The S-parameters
  of the
5 %fixtures attached to the DUT have to be provided.
6 %
7 % Syntax: [dut] = f_multiport_de_embedding(path)
8 %
9 % Inputs:
10 % total = sparameters object of the fix-dut-fix measurement
11 % Fix = struct containing the fixture s-parameters
12 %
13 % Outputs:
14 % dut – Dut scattering parameters
15 %
16 % Example:
17 %
18 % Other m-files required: f_thru_de_embedding_right.m,
  f_thru_de_embedding_left.m
19 % Subfunctions: diagonalize(Fixture, N, left_right)
20 % MAT-files required: none
21 %
22 % See also: /
23 % Author: Ivan Porcelli
24 % Politecnico di torino
25 % email address: s277252@studenti.polito.it
26 % Website:
27 % March 2022
28 %% ————— BEGIN CODE —————
29
30 %acquire the Nport
31 Nport = total.NumPorts;
32
33 %check if even or odd. If odd, add a fictitious thru port to the
  DUT.
34 if(mod(Nport,2) == 0)
35     %is even
36     even = 1;
37     N = Nport; %N is the number of actual ports
38 else
39     %is odd
40     even = 0;
41     N = Nport + 1; %Add a fictitious port (ideal thru) to make N
      even
```

---

```

42     Fix{N} = sparameters(ones(2,2,length(Fix{1}.Frequencies))
43         ...
         .* flip(eye(2)), Fix{1}.Frequencies); %The fixture added
         is an ideal thru
44 end
45
46 %get total scattering parameters
47 S_fdf = total.Parameters; %fixture-dut-fixture parameters
48 freq = total.Frequencies;
49 Nfreq = length(freq);
50
51 %build the S_t matrix for the algorithm (total measurement)
52 S_t = zeros(N,N, Nfreq);
53 for k=1:N
54     for j = 1:N
55         if(~even) %if odd, make even by adding a fictitious port
56             .
57             % Reflection is = 1 and transmission from/to other
58             ports is 0.
59             % The other parameters are untouched.
60             if (j==N || k == N)
61                 S_t(k,j,:) = 0; %transmission is 0 from/to the
62                 fictitious port
63             else
64                 S_t(k,j,:) = S_fdf(k,j,:);
65             end
66             if(k == N && j == N)
67                 S_t(k,j,:) = 1; %reflection is 1 from the
68                 fictitious port
69             end
70             else %if even, no modification
71                 S_t(k,j,:) = S_fdf(k,j,:);
72             end
73         end
74     end
75 end
76 left = diagonalize(Fix, N, 1); %build the matrix of the N/2
77     ports left-fixture
78 right = diagonalize(Fix, N, 0); %build the matrix of the N/2
79     ports right-fixture
80
81 %multiport right de embedding
82 S_1 = f_thru_de_embedding_right(sparameters(S_t, freq),
83     sparameters(right, freq), 0).Parameters;
84
85

```

```

78 %multiport left de embedding
79 S_dut = f_thru_de_embedding_left(sparameters(S_1, freq),
    sparameters(left, freq), 0).Parameters;
80
81 if(even)
82 dut = sparameters(S_dut, freq);
83 else %discard the parameters of the fictitious port
84 dut = sparameters(S_dut(1:(N-1), 1:(N-1), :), freq);
85 end
86
87 end
88
89 function diagonal = diagonalize(Fixture, N, left_right)
90 %This subfunctions builds the matrix of the left and right
    fixtures.
91 %For two port de-embedding, S11 S12 S21 S22 are scalar
    parameters. For N
92 %port de-embedding, they are matrices of dimension N/2.
93 res = length(Fixture{1}.Frequencies);
94 s_11 = zeros(res, N/2); s_12 = zeros(res, N/2);
95 s_21 = zeros(res, N/2); s_22 = zeros(res, N/2);
96 if(left_right == 1)
97 start = 0; %left fixture uses fix1, fix2, ... fix(N/2) data
98 else
99 start = N/2; %right fixture uses fix(N/2+1), ... fixN data
100 end
101 for k=1:(N/2)
102     s_11(:, k) = squeeze(Fixture{start + k}.Parameters(1, 1, :));
        s_12(:, k) = squeeze(Fixture{start + k}.Parameters(1, 2, :));
103     s_21(:, k) = squeeze(Fixture{start + k}.Parameters(2, 1, :));
        s_22(:, k) = squeeze(Fixture{start + k}.Parameters(2, 2, :));
104 end
105 s_11_diag = zeros(N/2, N/2, k); s_12_diag = zeros(N/2, N/2, k);
106 s_21_diag = zeros(N/2, N/2, k); s_22_diag = zeros(N/2, N/2, k);
107 diagonal = zeros(N, N, k);
108 for k=1:res
109     s_11_diag(:, :, k) = diag(s_11(k, :)); s_12_diag(:, :, k) = diag(
        s_12(k, :));
110     s_21_diag(:, :, k) = diag(s_21(k, :)); s_22_diag(:, :, k) = diag(
        s_22(k, :));
111     if(left_right)
112 diagonal(:, :, k) = [s_11_diag(:, :, k), s_12_diag(:, :, k);
        s_21_diag(:, :, k), s_22_diag(:, :, k) ];
113     else

```

---

```

114     diagonal(:, :, k) = [s_22_diag(:, :, k), s_12_diag(:, :, k);
115         s_21_diag(:, :, k), s_11_diag(:, :, k) ]; %right
116     % fixture has exchanged reflection parameters.
117     end
118
119 end
120 %% ----- END OF CODE -----

1 function [right] = f_thru_de_embedding_left(thru, left, twoport)
2 %% HEADER
3 %f_thru_de_embedding_left - De-embeds the S-matrix of a known
4   left fixture
5 %from a thru connection with a right one. The right fixture
6   matrix is
7 %obtained as output.
8 %
9 % Syntax: [right] = f_thru_de_embedding_left(thru, left,
10   twoport)
11 %
12 % Inputs:
13 %   thru - S parameter object of the thru fix_l - fix_r
14 %   left - S parameter object of the left fixture fix_r
15 %   twoport - 1: set when this function is directly called as a
16 %   main
17 %   function, to compute the two-port right fixture S
18 %   -parameters.
19 %   Port numbers of left, right, thru S-parameters
20 %   are
21 %   reported below:
22 %           1   1'''\_____/'''2| |2'''\_____/'''1   2
23 %           port 2 is the one closer to the DUT and the port
24 %           1 is to farthest one.
25 %           - 0: when called by "f_multiport_de_embedding.m".
26 % Outputs:
27 %   right - S parameter object of the right fixture
28 %
29 % Example:
30 %
31 % Other m-files required: none
32 % Subfunctions: none
33 % MAT-files required: none
34 %
35 % See also: (1) Tsiklauri, M., and N. Dikhaminjia. ...

```

---

```

29 % ..."De-embedding algorithm for odd port network parameters."
    IEEE Electromagnetic Compatibility Magazine 8.2 (2019):
    75-80.
30 % Author: Ivan Porcelli
31 % Politecnico di torino
32 % email address: s277252@studenti.polito.it
33 % Website:
34 % March 2022
35 %% ----- BEGIN CODE -----
36
37 S_1 = thru.Parameters;
38 N = left.NumPorts;
39 Nfreq = length(thru.Frequencies);
40
41 %left de embedding
42 S_2_11 = zeros(N/2,N/2,Nfreq); S_2_12 = zeros(N/2,N/2,Nfreq);
43 S_2_21 = zeros(N/2,N/2,Nfreq); S_2_22 = zeros(N/2,N/2,Nfreq);
44
45 for k=1:Nfreq
46     S111 = squeeze(left.Parameters(1:N/2,1:N/2,k)); S112 =
        squeeze(left.Parameters(1:N/2,(N/2+1):N,k));
47     S121 = squeeze(left.Parameters((N/2+1):N,1:N/2,k)); S122 =
        squeeze(left.Parameters((N/2+1):N,(N/2+1):N,k));
48
49     St11 = squeeze(S_1(1:N/2,1:N/2,k)); St12 = squeeze(S_1(1:N
        /2,(N/2+1):N,k));
50     St21 = squeeze(S_1((N/2+1):N,1:N/2,k)); St22 = squeeze(S_1((
        N/2+1):N,(N/2+1):N,k));
51
52     A = ((S112)\(St11-S111))/(S121);
53
54     S211 = (A*S122+eye(N/2,N/2))\A;
55     S221 = (St21/(S121))*(eye(N/2,N/2)-S122*S211);
56     S212 = (eye(N/2,N/2)-S211*S122)*((S112)\St12);
57     S222 = St22 - (S221/(eye(N/2,N/2)-S122*S211))*S122*S212;
58
59     S_2_11(:, :, k) = S211; S_2_12(:, :, k) = S212;
60     S_2_21(:, :, k) = S221; S_2_22(:, :, k) = S222;
61     if (twoport)
62         S_2_11(:, :, k) = S222; S_2_22(:, :, k) = S211;
63     end
64 end
65
66 S_right = [S_2_11, S_2_12; S_2_21, S_2_22];
67 right = sparameters(S_right, thru.Frequencies);

```

---

```

68 end
69 %% ----- END OF CODE -----

1 function [left] = f_thru_de_embedding_right(thru, right, twoport
   )
2 %% HEADER
3 %f_thru_de_embedding_right - De-embeds the S-matrix of a known
   right fixture
4 %from a thru connection with a left one. The left fixture matrix
   is
5 %obtained as output.
6 %
7 % Syntax: [left] = f_thru_de_embedding_right(thru, right,
   twoport)
8 %
9 % Inputs:
10 % thru - S parameter object of the thru fix_l - fix_r
11 % right - S parameter object of the right fixture fix_r
12 % twoport - 1: set when this function is directly called as a
   main
13 % function, to compute the two-port left fixture S-
   parameters.
14 % Port numbers of left, right, thru S-parameters
   are
15 % reported below:
16 %          1 1'''\_____/'''2| |2'''\_____/'''1 2
17 %          port 2 is the one closer to the DUT and the port
   1 is to farthest one.
18 %          - 0: when called by "f_multiport_de_embedding.m".
19 % Outputs:
20 % left - S parameter object of the left fixture
21 %
22 % Example:
23 %
24 % Other m-files required: none
25 % Subfunctions: none
26 % MAT-files required: none
27 %
28 % See also: (1) Tsiklauri, M., and N. Dikhaminjia. ...
29 % ..."De-embedding algorithm for odd port network parameters."
   IEEE Electromagnetic Compatibility Magazine 8.2 (2019):
   75-80.
30 % Author: Ivan Porcelli
31 % Politecnico di torino
32 % email address: s277252@studenti.polito.it

```

---

```

33 % Website:
34 % March 2022
35 %% ----- BEGIN CODE -----
36
37 S_t = thru.Parameters;
38 N = right.NumPorts;
39 Nfreq = length(thru.Frequencies);
40
41 %right de embedding
42 S_1_11 = zeros(N/2,N/2,Nfreq); S_1_12 = zeros(N/2,N/2,Nfreq);
43 S_1_21 = zeros(N/2,N/2,Nfreq); S_1_22 = zeros(N/2,N/2,Nfreq);
44
45 for k=1:Nfreq
46     Sr11 = squeeze(right.Parameters(1:N/2,1:N/2,k)); Sr12 =
47         squeeze(right.Parameters(1:N/2,(N/2+1):N,k));
48     Sr21 = squeeze(right.Parameters((N/2+1):N,1:N/2,k)); Sr22 =
49         squeeze(right.Parameters((N/2+1):N,(N/2+1):N,k));
50     if(twoport)
51         tmp = Sr11; Sr11 = Sr22; Sr22 = tmp;
52     end
53     St11 = squeeze(S_t(1:N/2,1:N/2,k)); St12 = squeeze(S_t(1:N
54         /2,(N/2+1):N,k));
55     St21 = squeeze(S_t((N/2+1):N,1:N/2,k)); St22 = squeeze(S_t((
56         N/2+1):N,(N/2+1):N,k));
57
58     A = (Sr21)\St22 - (Sr21)\Sr22;
59     B = Sr11*((Sr21)\St22) - Sr11*((Sr21)\Sr22);
60
61     S122 = A/(B+Sr12);
62     S121 = (eye(N/2,N/2)-S122*Sr11)*((Sr21)\St21);
63     S112 = (St12/(Sr12))*(eye(N/2,N/2)-Sr11*S122);
64     S111 = St11 - S112*Sr11*((eye(N/2,N/2)-S122*Sr11)\S121);
65
66     S_1_11(:, :, k) = S111; S_1_12(:, :, k) = S112;
67     S_1_21(:, :, k) = S121; S_1_22(:, :, k) = S122;
68
69 end
70 S_1 = [S_1_11, S_1_12; S_1_21, S_1_22];
71 left = sparameters(S_1, thru.Frequencies);
72 end
73 %% ----- END OF CODE -----

```



# Bibliography

- [1] «370-2020 - IEEE Standard for Electrical Characterization of Printed Circuit Board and Related Interconnects at Frequencies up to 50 GHz». In: (2021).
- [2] David M. Pozar. *Microwave Engineering, 4th Edition*. 2012.
- [3] *The Evolution of RF/Microwave Network Analyzers | Keysight Technical Backgrounder*. url: <https://about.keysight.com/en/newsroom/backgrounders/na/>.
- [4] Valeria Teppati, Andrea Ferrero, and Mohamed Sayed. *Modern RF and microwave measurement techniques*. Vol. 9781107036413. 2007. doi: [10.1017/CB09781107036413](https://doi.org/10.1017/CB09781107036413).
- [5] Andrej Rumiantsev and Nick Ridler. «VNA calibration». In: *IEEE Microwave Magazine* 9 (3 2008). issn: 15273342. doi: [10.1109/MMM.2008.919925](https://doi.org/10.1109/MMM.2008.919925).
- [6] Joel P. Dunsmore. *Handbook of Microwave Component Measurements*. 2020. doi: [10.1002/9781119477167](https://doi.org/10.1002/9781119477167).
- [7] *4.3: Calibration - Engineering LibreTexts*. url: [https://eng.libretexts.org/Bookshelves/Electrical\\_Engineering/Electronics/Microwave\\_and\\_RF\\_Design\\_III\\_-\\_Networks\\_\(Steer\)/04%3A\\_Chapter\\_4/4.03%3A\\_Section\\_3-](https://eng.libretexts.org/Bookshelves/Electrical_Engineering/Electronics/Microwave_and_RF_Design_III_-_Networks_(Steer)/04%3A_Chapter_4/4.03%3A_Section_3-).
- [8] Richard A Hackborn. «An automatic network analyzer system». In: *The Micro Wave Jour* 11 (1968), pp. 45–52.
- [9] B. P. Hand. «Developing accuracy specifications for automatic network analyzer systems». In: *Hewlett-Packard Journal* February (1970), p. 16.
- [10] James G. Evans. «Measuring Frequency Characteristics of Linear Two-Port Networks Automatically». In: *Bell System Technical Journal* 48 (5 1969), pp. 1313–1338. issn: 15387305. doi: [10.1002/J.1538-7305.1969.TB04270.X](https://doi.org/10.1002/J.1538-7305.1969.TB04270.X).
- [11] W. Kruppa and Kenneth F. Sodomsy. «An explicit solution for the scattering parameters of a linear two-port measured with an imperfect test set». In: *IEEE Transactions on Microwave Theory and Techniques* 19 (1 1971), pp. 122–123. issn: 15579670. doi: [10.1109/TMTT.1971.1127466](https://doi.org/10.1109/TMTT.1971.1127466).
- [12] I. KÁsa. «Closed-Form Mathematical Solutions to Some Network Analyzer Calibration Equations». In: *IEEE Transactions on Instrumentation and Measurement* 23 (4 1974), pp. 399–402. issn: 15579662. doi: [10.1109/TIM.1974.4314321](https://doi.org/10.1109/TIM.1974.4314321).
- [13] Stig Rehnmark. «On the Calibration Process of Automatic Network Analyzer Systems». In: *IEEE Transactions on Microwave Theory and Techniques* 22 (4 1974), pp. 457–458. issn: 15579670. doi: [10.1109/TMTT.1974.1128250](https://doi.org/10.1109/TMTT.1974.1128250).

- 
- [14] Nikola Janjusevic. *UVNA-63 Application Note Error Correction*. url: <https://www.minicircuits.com/app/AN49-016.pdf>.
- [15] Norman R. Franzen and Ross A. Speciale. «A New Procedure for System Calibration and Error Removal in Automated S-Parameter Measurements». In: (Nov. 1975), pp. 69–73. doi: [10.1109/EUMA.1975.332155](https://doi.org/10.1109/EUMA.1975.332155).
- [16] Glenn F. Engen. «Calibration Technique for Automated Network Analyzers with Application to Adapter Evaluation». In: *IEEE Transactions on Microwave Theory and Techniques* 22 (12 1974), pp. 1255–1259. issn: 15579670. doi: [10.1109/TMTT.1974.1128472](https://doi.org/10.1109/TMTT.1974.1128472).
- [17] *Agilent PN 8720-2 In-fixture Microstrip Device Measurements Using TRL\* Calibration*. url: <http://anlage.umd.edu/Microwave%20Measurements%20for%20Personal%20Web%20Site/5091-1943E.pdf>.
- [18] Roger B. Marks. «Formulations of the Basic Vector Network Analyzer Error Model including Switch-Terms». In: *50th ARFTG Conference Digest - Fall 1997: Measurement Techniques for Digital Wireless Applications* (1997), pp. 115–126. doi: [10.1109/ARFTG.1997.327265](https://doi.org/10.1109/ARFTG.1997.327265).
- [19] Thomas G Ruttan et al. «Multiport VNA measurement». In: *IEEE Microwave Magazine* 9.3 (2008), pp. 56–69.
- [20] Keysight Technologies. *De-Embedding and Embedding S-Parameter Networks Using a Vector Network Analyzer*. url: [www.keysight.com](http://www.keysight.com).
- [21] «Agilent AN 1287-9 In-Fixture Measurements Using Vector Network Analyzers Application Note». In: (). url: <https://icmicrowave.com/wp-content/uploads/2020/11/AN-1287-9.pdf>.
- [22] Robert Schaefer and Agilent Technologies. «Challenges and Solutions for Removing Fixture Effects in Multi-port Measurements». In: (2008). url: [http://www.magazines007.com/pdf/DesignCon\\_08\\_Schaefer.pdf](http://www.magazines007.com/pdf/DesignCon_08_Schaefer.pdf).
- [23] *Using the TRL Calibration Board for the F0480 Matched Broadband RF VGA*. url: <https://www.renesas.com/eu/en/document/apn/874-using-trl-calibration-board-f0480-matched-broadband-rf-vga?language=en>.
- [24] Nils Nazoa. *S-PARAMETER MEASUREMENT OF SMT COMPONENTS USING THE LA19-13-03 VNA*. url: <https://www.minicircuits.com/app/AN49-016.pdf>.
- [25] *FABRICATING AND USING A PCB-BASED TRL PATTERN WITH A CMT VNA*. url: <https://coppermountaintech.com/wp-content/uploads/2018/05/Design-and-Fabrication-of-a-TRL-Calibration-Kit.pdf>.
- [26] Nils Nazoa. «S-PARAMETER MEASUREMENT OF SMT COMPONENTS USING THE LA19-13-03 VNA». In: (2013).

- [27] Jason Ellison, Stephen B. Smith, and Sedig Agili. «Using a 2x-thru standard to achieve accurate de-embedding of measurements». In: *Microwave and Optical Technology Letters* 62 (2 Feb. 2020), pp. 675–682. issn: 1098-2760. doi: [10.1002/MOP.32098](https://onlinelibrary.wiley.com/doi/full/10.1002/MOP.32098). url: <https://onlinelibrary.wiley.com/doi/full/10.1002/mop.32098>  
<https://onlinelibrary.wiley.com/doi/abs/10.1002/mop.32098>  
<https://onlinelibrary.wiley.com/doi/10.1002/mop.32098>.
- [28] Changwook Yoon et al. «Design criteria of automatic fixture removal (AFR) for asymmetric fixture de-embedding». In: *IEEE International Symposium on Electromagnetic Compatibility* 2014-September (September Sept. 2014), pp. 654–659. issn: 21581118. doi: [10.1109/ISEMC.2014.6899051](https://doi.org/10.1109/ISEMC.2014.6899051).
- [29] M. Tsiklauri and N. Dikhaminjia. «De-embedding algorithm for odd port network parameters». In: *IEEE Electromagnetic Compatibility Magazine* 8 (2 Apr. 2019), pp. 75–80. issn: 21622272. doi: [10.1109/MEMC.2019.8753449](https://doi.org/10.1109/MEMC.2019.8753449).
- [30] Guillermo Gonzalez. *Microwave transistor amplifiers : analysis and design*. Prentice-Hall, 1984, p. 245. isbn: 9780135816462.
- [31] Roberto Sorrentino and Giovanni Bianchi. *Microwave and RF Engineering*. 2010. doi: [10.1002/9780470660201](https://doi.org/10.1002/9780470660201).
- [32] Ananjan Basu. *An Introduction to Microwave Measurements*. 2014. doi: [10.1201/b17964](https://doi.org/10.1201/b17964).
- [33] *Vector Network Analyzer Error Correction and Calibration Techniques | Keysight*. url: <https://www.keysight.com/it/en/assets/7018-06761/application-notes/5965-7709.pdf>.
- [34] Errikos Lourandakis. *On-wafer Microwave Measurements and De-embedding*. Artech House, 2016.
- [35] Agilent Application Note 1364-1. *De-embedding and Embedding S-Parameter Networks Using a Vector Network Analyzer*. 2001.
- [36] *Agilent Network Analysis Applying the 8510 TRL Calibration for Non-Coaxial Measurements*. url: [http://emlab.uiuc.edu/ece451/appnotes/TRL\\_2.pdf](http://emlab.uiuc.edu/ece451/appnotes/TRL_2.pdf).
- [37] H. J. Eul and B. Schiek. «Thru-match reflect: one result of a rigorous theory for de-embedding and network analyzer calibration». In: *Conference Proceedings - European Microwave Conference* (18 1988), pp. 909–914. doi: [10.1109/EUMA.1988.333924](https://doi.org/10.1109/EUMA.1988.333924).
- [38] William Jeffrey Highton. *Measuring Characteristic Impedance of PCB tracks using a Vector Network Analyser*. 2005. url: <https://chemandy.com/technical-articles/measuring-track-characteristic-impedance/measuring-track-characteristic-impedance-article1.htm>.
- [39] Walter Johnson. *Transmission lines and networks*. McGraw-Hill, 1950.
- [40] «Help File - User Manual for E5080A ENA Network Analyzer (Operation and Programming) | Keysight». In: (). url: <https://www.keysight.com/it/en/lib/resources/help-files/help-file--user-manual-for-e5080a-ena-network-analyzer-operation-and-programming-2574092.html>.

- [41] Dae Han Kwon et al. «Characterization and modeling of a new via structure in multilayered printed circuit boards». In: *IEEE Transactions on Components and Packaging Technologies* 26 (2 June 2003), pp. 483–489. issn: 15213331. doi: [10.1109/TCAPT.2003.815119](https://doi.org/10.1109/TCAPT.2003.815119).
- [42] Glenn F. Engen and Cletus A. Hoer. «Thru-Reflect-Line: An Improved Technique for Calibrating the Dual Six-Port Automatic Network Analyzer». In: *IEEE Transactions on Microwave Theory and Techniques* 27 (12 1979). issn: 15579670. doi: [10.1109/TMTT.1979.1129778](https://doi.org/10.1109/TMTT.1979.1129778).
- [43] Clayton R Paul. *Introduction to electromagnetic compatibility*. Vol. 184. John Wiley & Sons, 2006.
- [44] Gary W. Johnson. *Wideband Bias Tee*.
- [45] Charles Baylis, Lawrence Dunleavy, and William Clausen. «Design of bias tees for a pulsed-bias, pulsed-RF test system using accurate component models». In: *Microwave Journal* 49 (10 2006). issn: 01926225.
- [46] Matteo Vincenzo Quitadamo and Franco Fiori. «A SPICE Model of Operational Amplifiers for Electromagnetic Susceptibility Analysis». In: *IEEE Transactions on Electromagnetic Compatibility* (2022), pp. 1–11. issn: 0018-9375. doi: [10.1109/TEMC.2021.3135114](https://doi.org/10.1109/TEMC.2021.3135114). url: <https://ieeexplore.ieee.org/document/9680689/>.
- [47] *P9371A Keysight Streamline USB Vector Network Analyzer, 6.5 GHz* | Keysight. url: <https://www.keysight.com/it/en/product/P9371A/streamline-usb-vector-network-analyzer-6-5-ghz.html>.
- [48] *Understanding Directivity* | Anritsu America. url: <https://www.anritsu.com/en-us/test-measurement/solutions/en-us/understanding-directivity>.
- [49] *TL081 datasheet*. url: <https://www.ti.com/lit/ds/symlink/tl082h.pdf>.
- [50] «RigPix Database - Power supplies - Topward TPS-4000 Model 4303». In: (). url: [https://www.rigpix.com/psu/topward\\_tps4303.htm](https://www.rigpix.com/psu/topward_tps4303.htm).
- [51] *TRL calibration*. url: <https://www.microwaves101.com/encyclopedias/trl-calibration>.
- [52] *RT/duroid® 6006/6010LM High Frequency Laminates*. url: <http://www.rogerscorp.com/acm..>
- [53] Jose E Schutt-Aine. *ECE 451-Jose Schutt-Aine ECE 451 Automated Microwave Measurements TRL Calibration*. url: <http://emlab.uiuc.edu/ece451/notes/TRL.pdf>.